SOURCES AND FATE OF CHROMOPHORIC DISSOLVED ORGANIC MATTER IN THE ARCTIC OCEAN AND SURROUNDING WATERSHEDS

A Dissertation

by

SALLY ANNETTE WALKER

Submitted to the Office of Graduate Studies of
Texas A&M University
in partial fulfillment of the requirements for the degree of

DOCTOR OF PHILOSOPHY

August 2012

Major Subject: Oceanography

Sources and Fate of Chromophoric Dissolved Organic Matter in the Arctic Ocean and Surrounding Watersheds

SOURCES AND FATE OF CHROMOPHORIC DISSOLVED ORGANIC MATTER IN THE ARCTIC OCEAN AND SURROUNDING WATERSHEDS

A Dissertation

by

SALLY ANNETTE WALKER

Submitted to the Office of Graduate Studies of
Texas A&M University
in partial fulfillment of the requirements for the degree of

DOCTOR OF PHILOSOPHY

Approved by:

Chair of Committee,	Rainer Amon
Committee Members,	Thomas Bianchi
	Patrick Louchouarn
	Alejandro Orsi
Head of Department,	Piers Chapman

August 2012

Major Subject: Oceanography

ABSTRACT

Sources and Fate of Chromophoric Dissolved Organic Matter in the Arctic Ocean and Surrounding Watersheds. (August 2012)

Sally Annette Walker, B.A., Texas A&M University

Chair of Advisory Committee: Dr. Rainer Amon

Given the pace of climate change in the Arctic, it is vital to better constrain terrigenous dissolved organic matter (tDOM) fluctuations in large Arctic Rivers and the role that climate change may bring to tDOM inputs into the Arctic Ocean and to the global carbon cycle. This project uses the optical properties of chromophoric dissolved organic matter (CDOM) to investigate the quality, quantity and fate of dissolved organic matter (DOM) in large Arctic Rivers and the interior Arctic Basin. In large rivers surrounding the Arctic, peak discharge CDOM is largely derived from fresh terrestrial plant material whereas during base flow the CDOM pool has a greater microbial imprint, particularly in the Mackenzie. The higher microbial imprint in the Mackenzie can be explained by longer water residence times, which may be important in a warming climate where increased precipitation rates will likely lead to increased hydrological connectivity and therefore longer water residence times. In surface waters of the Canadian Archipelago, 17 % of the DOM pool is of terrestrial origin, even though waters are diluted with sea ice melt, suggesting the likelihood of a subsurface plume of tDOM entrained within river runoff from Arctic Rivers. In the interior Arctic, an

elevated terrestrial CDOM signal in the Eurasian Basin (EB) points to the presence of Eurasian river CDOM entrained within river runoff in the Transpolar Drift. In contrast, autochthonous/microbial CDOM sources become more important the Canadian Basin (CB) and the terrestrial CDOM signal is much lower relative to the EB.

A good constraint on the nature and distributions of freshwater (FW) in the Arctic Ocean is paramount to understand the role climate change may play for the Arctic's hydrological cycle. During this study, we used the spatial patterns of terrestrially derived CDOM to better understand the distribution and nature of river runoff across the upper Arctic Basin. This study illustrates the usefulness of CDOM to finger-print water masses within the Arctic Ocean and shows promise to improve our understanding of upper Arctic Ocean ventilation patterns.

To my Mother, who by example has taught me the true meaning of courage and without her none of this would have been possible and to my Dad, who always had faith in me.

ACKNOWLEDGEMENTS

I would first like to thank my committee chair, Dr. Rainer Amon, who has not only taught me how to become a strong and successful scientist, but for teaching me to believe in myself. Without him, none of this would have been possible. I would also like to thank my committee members, Dr. Thomas Bianchi, Dr. Patrick Louchouarn, and Dr. Alejandro Orsi for their guidance and support throughout the course of this research. I am grateful to Dr. Colin Stedmon for his training on PARAFAC analysis and the meaningful conversations he has taken the time to share, Dr. Louchouarn and Dr. Duan Shwang for lignin analysis, Amanda Rinehart for her help collecting samples, Stephanie Smith for her work on DOM fractionation during sea ice formation, and Kerestin Goodman for her help with sample analysis. I would also like to thank the captain, scientists and crew of the Oden for logistical assistance during Beringia and AOS 2005 and TAMUG, TAMU, and the National Science Foundation for the funding (OPP-0229302, ARC-0425582, ARC-0713991). And, last but definitely not least, I would like to thank my family (and friends) for all the support and faith they have put in me over the years.

NOMENCLATURE

ACIA	The Arctic Climate Impact Assessment
AMOC	Atlantic meridional overturning circulation
AOS	Arctic Ocean Section
AOS	Apparent oxygen utilization
Atl	Atlantic
BIX	Biological/autochthonous index
CB	Canadian Basin
CDOM	Chromophoric Dissolved Organic Matter
DIC	Dissolved inorganic carbon
DOC	Dissolved organic carbon
DOM	Dissolved Organic Matter
EB	Eurasian Basin
EEM	Excitation Emission Matrix
EGC	East Greenland Current
FDOM	Fluorescent dissolved organic matter
FI	Fluorescence Index
FW	Freshwater
GC/MS	Gas chromatography-mass spectrometry
HTC	High temperature combustion
HWL	Halocline water layer

IPCC	Intergovernmental Panel on Climate Change
LHW	Lower halocline water layer
LOP	Lignin oxidation products
OC	Organic carbon
PARAFAC	Parallel Factor Analysis
PARTNERS	Pan-Arctic River Transport of Nutrients, Organic Matter, and Suspended Sediments
PSW	Polar surface water
R.U.	Raman units
SUVA	Specific UV absorbance at 254 nm
tDOM	Terrestrial dissolved organic matter
TPD	Transpolar Drift
UHW	Upper halocline water layer
WGC	West Greenland Current

TABLE OF CONTENTS

LIST OF FIGURES

FIGURE Page

FIGURE Page

FIGURE Page

LIST OF TABLES

CHAPTER I

INTRODUCTION: THE ROLE OF CLIMATE CHANGE ON CARBON STORAGE IN LARGE ARCTIC RIVERS AND THE HYDROLOGICAL CYCLE OF THE ARCTIC OCEAN AND NORDIC SEAS

Terrestrial carbon export and freshwater fluxes to the Arctic Ocean are disproportionately large compared to other ocean basins and are much more susceptible to climate change. In conjunction with this, average Arctic temperatures have increased over the last century at nearly twice the global average [*IPCC Fourth Assessment report*]. As a result the response of the Arctic to changes in climate is a major issue of global concern, yet its sensitivity to warming is not entirely clear. In conjunction, it is not entirely clear if the Arctic will represent a positive or negative feedback loop for the global climate system [*The Arctic Climate Impact Assessment (ACIA)*].

Large watersheds surrounding the Arctic basin contain roughly 50% of the global soil organic carbon (OC) [*Tarnocai et al.*, 2009]. The vast majority of this soil OC is stored in permafrost within Siberia, where current models project a particularly pronounced temperature increase [*Prowse et al.*, 2006]. As a result, dramatic changes have been observed in the Arctic over the last century in regards to the storage and cycling of carbon in large Arctic Rivers. Current models predict that climate-induced permafrost disintegration during the next 100 years could potentially release as much as 25% of the carbon stored in Arctic soils [*Gruber et al.*, 2004]. As warming in the Arctic

---

This dissertation follows the style of *Journal of Geophysical Research*.

region continues, carbon released from permafrost erosion could have significant impact on the biogeochemical cycling of organic carbon within large Arctic rivers and shelf seas and potentially influence atmospheric CO_2 concentrations [*Bates et al.*, 2010; *Fabry et al.*, 2009] as well as the amount of terrestrial carbon delivered to the North Atlantic [*Amon et al.*, 2003; *Benner et al.*, 2005; *Hansell et al.*, 2004]. Given the projected warming rates and the large amount of carbon stored in permafrost regions surrounding the Arctic basin, it is therefore vital that we gain a better understanding of the nature of carbon within large Arctic rivers and to determine its variability over the annual hydrograph.

Climate change in the Arctic is especially important due to the Arctic's prominent role in the global hydrological cycle. Dramatic changes have been observed in the Arctic over the last century in regards to the storage and cycling of freshwater (FW) and the volume of freshwater export to the North Atlantic where deep water is formed. Such changes are expected to continue, and perhaps accelerate in the coming century. This is important because increased FW discharge to the Arctic has the potential to influence halocline formation in the interior basin, thereby influencing sea ice formation, and deepwater formation in the North Atlantic.

In the interior Arctic Basin, halocline formation is critical to sea ice dynamics because it effectively traps heat within Atlantic origin waters from sea ice at the surface. The halocline is sustained by winter convection in the interior basin [*Rudels et al.*, 2004; *Rudels, et al.*, 1996] and through large scale lateral advection from the shelf [*Aagaard et al.*, 1981]. During winter months, sea ice formation results in salt injection into the

underlying waters, causing it to become denser, sink and subsequently haline convection into the pycnocline occurs [*Rudels et al.,* 2004]. *Rudels et al.* [2004] suggests this process removes the polar surface water (PSW) layer below the ice cover at the surface and forms the halocline layer (HWL). In addition, brine release during ice formation along the extensive shelf creates a dense, "shelf-derived" water mass that sinks below FW inputs. These shelf-derived waters are advected into the interior Arctic and also help to maintain the halocline layer throughout the central basin [*Aagaard et al.*, 1981]. The annual rate of dense shelf water injection into the halocline is estimated to be ~ 2.5 x 10^6 m^3 s^{-1} [*Aagaard et al.*, 1981]. This is similar to the inflow of waters from the Atlantic [*Aagaard et al.*, 1981], indicating that Atlantic waters are also linked to the formation of dense shelf waters. Therefore, fluctuations in Atlantic inflow waters, coupled with a massive river diversion, could potentially cause a thinning of the halocline layer, placing warm Atlantic water in more direct contact with sea ice at the surface [*Aagaard et al.*, 1981; *Rudels et al.*, 2004; *Rudels, et al.*, 1996].

The Beaufort Gyre is the largest FW reservoir in the Arctic Ocean [*Yamamoto-Kawai et al.*, 2005] and, depending on atmospheric circulation patterns, it could release significant amounts of FW to the North Atlantic via the East Greenland Current and/or the Canadian Archipelago [*Yamamoto-Kawai et al.*, 2005]. Such a FW release was believed to be the source of the Great Salinity Anomaly [*Dickson et al.*, 1988], which influenced the entire North Atlantic sub polar gyre and inhibited deep convection in the Labrador Sea [*Lazier*, 1980]. Since 2003, the Beaufort Gyre has accumulated more than 5000 km^3 of FW (an increase of ~25%; [*Proshutinsky et al.,* 2009]) and appears ready to

release another massive FW pulse toward the North Atlantic deep convection sites. This, together with the enhanced delivery of FW to the Nordic Seas via runoff and ice melt, has the potential to impact the production of dense water [*Ohno and Bro*, 2006], and thereby influence the Atlantic meridional overturning circulation (AMOC) and global climate patterns. It is therefore critical we can accurately identify the different FW components contributing to the surface layers of the Arctic Ocean.

River runoff is one of the dominant FW components in the upper Arctic Ocean [*Jones et al.*, 2008a; *Yamamoto-Kawai et al.*, 2008] and Nordic Seas [*Amon et al.*, 2003; *Jones et al.*, 2008b] and contributes to the ventilation of the cold halocline layer across the Arctic Ocean. While recent work has shed light on some of the physical aspects of river runoff distributions, the nature, source, and quantity of runoff being fluxed into the Arctic interior remains poorly understood, especially in the Canadian Basin (CB) during this time of climate warming. If we are to understand how river runoff is stored then released from the Arctic, how it emanates from the Arctic into the Nordic Seas, and how it might impact halocline ventilation and convection in the sub-polar Atlantic, we need to determine the composition and sources of runoff waters within the Arctic Ocean and coastal seas.

To better understand the quality and fate of dissolved organic carbon (DOC) in the Arctic Ocean and its surrounding watersheds as well as river runoff distributions within the Arctic Ocean the optical properties of chromophoric dissolved organic matter were investigated using Excitation/Emission Matrix Spectroscopy (EEM's) coupled to a new technique, Parallel Factor Analysis (PARAFAC). EEM's spectroscopic analysis

collects excitation and emission over a broad wavelength rage, with intensity on the z-axis, resulting in a fluorescence landscape. The use of EEM's spectroscopy is limited in that it only allows for a qualitative identification of various CDOM fractions. This is because the fluorescence spectra tend to be dominated by the more concentrated fluorophores and by fluorophores exhibiting longer fluorescence lifetimes. More recently, EEM spectroscopy coupled with PARAFAC, a multivariate technique, has enabled researchers to mathematically decompose the combined CDOM fluorescence signal into fluorescent components that correspond to a chemical analyte, or group of strongly co-varying analytes [*Murphy et al.*, 2007; *Stedmon and Bro*, 2008; *Stedmon et al.*, 2003]. A model is derived by the process of minimizing the sum of squared residuals, where the mixtures of the signals are mathematically separated into unique constituents similar to traditional chromatographic separations. PARAFAC decomposes the fluorescent data matrix into a set of trilinear terms and a residual array using the following equation [*Stedmon et al.*, 2003]:

$$x_{ijk} = \sum_{f=1}^{F} a_{if} b_{if} c_{kf} + \varepsilon_{ijk}$$

$$i = 1,\ldots, I; \quad j = 1,\ldots,J; \quad k = 1,\ldots,K$$

where x_{ijk} is the intensity of the fluorescence for any given sample (i) at emission wavelength j and excitation wavelength k, a_{if} is directly proportional to the concentration of an analyte in the sample (i), b_{if} is an estimate of the emission spectrum of the analyte,

c_{kf} is an estimate of the excitation spectrum of the analyte, F is the number of components (analytes) defined by the model, and ε_{ijk} is the residual matrix and represents the variability not accounted for by the model. The benefit of using PARAFAC over other statistical approaches (i.e. Principal Component Analysis; PCA) is that the solutions are uniquely identified without adding mathematical constraints and therefore requires no assumptions on spectral shape, the number of fluorescent components, or to statistical assumptions on the structure of the noise [*Stedmon et al.*, 2003]. With that said, very little spectroscopic information exists regarding CDOM inputs to the Arctic region and even less is understood regarding the structures of the underlying fluorophores.

The optical properties of CDOM were investigated during three independent studies. The first study (Chapter II) includes river data collected from 2004 – 2006 as part of the Pan-Arctic River Transport of Nutrients, Organic Matter, and Suspended Sediments (PARTNERS) project and includes the Mackenzie, Lena, Kolyma, Ob, and Yenisei. The objectives of this study were to identify sources and seasonal differences of CDOM quality within large Arctic rivers, to link watershed characteristics to differences in CDOM quality between the rivers, and to explore the usefulness of PARAFAC as a means to trace CDOM during transport and mixing within the Arctic Ocean. The second study (Chapter III) includes a sample set collected within Canadian Archipelago surface waters and the Mackenzie River plume during 2005 (Beringia 2005). The objectives of this study were to determine how the behavior of PARAFAC components compares to lignin phenol trends as a circulation tracer in the Arctic Ocean and to analyze what

additional chemical information can be deduced from their spectral character. The third study (Chapter IV) includes samples collected from across the Arctic Basin during the 2005 Arctic Ocean Section (AOS 2005). The objectives of this study were to determine PARAFAC component sources and distributions across the upper Arctic Ocean, to investigate the underlying factors controlling PARAFAC component speciation during transport and mixing, to determine if PARAFAC components can be used to trace river runoff across the upper Arctic Ocean, and to compare and contrast PARAFAC runoff distribution estimates to estimates based on traditional tracer techniques.

This study illustrates how fluorescence paired with PARAFAC can be used to describe the nature of DOM in large Arctic rivers and within the Arctic Ocean and demonstrates its potential to characterize runoff distributions within the upper Arctic Ocean. The ability to differentiate and qualitatively trace the different sources of fluorescent components and determine the underlying factors controlling CDOM speciation during transport and mixing opens new possibilities for the use of CDOM as a more specific tracer in oceanography.

CHAPTER II

SEASONAL CHANGES IN ARCTIC RIVER CHROMOPHORIC DISSOLVED ORGANIC MATTER (CDOM) QUALITY: A COMPARISON OF LARGE ARCTIC RIVERS

2.1 Overview

Arctic rivers deliver over 10 % of the annual global river discharge to the ocean yet little is known about the seasonal fluctuations in the quantity and quality of terrigenous dissolved organic matter (tDOM) over the annual hydrograph. A good constraint on such fluctuations is paramount to understand the role that climate change may bring to tDOM inputs into the Arctic Ocean and to the global carbon budget. To better understand such changes the optical properties of colored DOM (CDOM) were studied in five large Arctic rivers, including the Mackenzie, Lena, Kolyma, Ob and Yenisei rivers. Samples were collected over several seasonal cycles as part of the PARTNERS project and were analyzed using the absorption coefficient at 350 nm (a_{350}), spectral slope ($S_{(275-295)}$), specific UV absorbance at 254 nm (SUVA), biological/autochthonous index (BIX), fluorescence index (FI), and Parallel Factor Analysis (PARAFAC). Environmental dynamics of individual PARAFAC components were evaluated and compared to discharge, total dissolved organic carbon (DOC) concentrations, lignin phenol and p-hydroxybenzene compositions, and the ^{14}C-DOC age. Three components were terrestrially derived, but could not be associated with a

specific source, and two were characteristic of a microbially altered CDOM pool. Based on these optical parameters, peak discharge CDOM is largely derived from fresh terrestrial plant material, has a higher molecular weight, and is predominately aromatic in nature. During base flow the CDOM pool shifts to a lower molecular weight, is less aromatic, and fresh terrestrial sources become less important, particularly in the Mackenzie. Differences in CDOM quality between the rivers could be explained by differences in their individual watershed characteristics and help to explain the relatively different quality of CDOM in the Mackenzie River.

2.2 Introduction

Large Arctic Rivers are a unique environment to study the fate of terrestrially derived DOM (tDOM) because their watersheds contain roughly 50% of the global soil organic carbon (OC), with ~ 67 % of that amount located in the Eurasian watersheds [*Tarnocai et al.*, 2009]. Recent estimates suggest that 1400 - 1850 Pg C are stored within Arctic soils, with ~ 88 % located in vast permafrost regions surrounding the Arctic basin [*Tarnocai et al.*, 2009], particularly in Siberia. Perennial permafrost is critical to the global carbon budget because of its capacity to act as a long term storage for organic carbon, isolating it from UV and microbial degradation, and because it is highly susceptible to climate change [*Tarnocai et al.*, 2009].

While a substantial increase in global air temperatures have been observed since ~ 1980 [*McGuire et al.*, 2009], the Arctic region is currently warming faster than the

global warming rate. Surface air temperatures north of 62° N have increased by an average of 0.6 °C since 1985 [*Polyakov et al.*, 2002] and models project that the mean annual temperature will increase by 3.7 °C between the 1981 – 2090, or approximately twice the projected increase in global mean annual temperatures [*Kattsov et al.,* 2005]. Given the large pool of soil OC stored within watersheds surrounding the Arctic, recent warming trends in high latitudes have the potential to cause rapid changes in the Earth system [*McGuire et al.,* 2009]. As a result the response of the Arctic's carbon cycle to changes in climate is a major issue of global concern, yet its sensitivity to warming during the remainder of the 21st century remains highly uncertain [*McGuire et al.,* 2009]. Recent studies suggest substantial permafrost degradation, with a loss of 6 – 11 X 10^6 km^2 of near surface permafrost by 2100 [*Euskirchen et al.*, 2009; *Lawrence and Slater*, 2008]. Further, *Gruber et al.* [2004] estimated that climate induced permafrost disintegration during the next 100 years will release as much as 25% of carbon stored in Arctic soils. As warming in the Arctic region continues, permafrost erosion combined with increased river discharge [*Peterson et al.*, 2002] will likely have a significant impact on the biogeochemical cycling of organic carbon within large Arctic rivers and shelf seas and potentially influence atmospheric CO_2 concentrations [*Bates and Mathis*, 2009; *Fabry et al.*, 2009] and the amount of terrestrial carbon delivered to the North Atlantic [*Amon et al.,* 2003, *Hansell et al.,* 2004].

Due to extreme seasonal changes in snow cover and air temperature there is a large annual variability in runoff from large Arctic rivers. During winter months low precipitation and air temperatures result in low runoff rates. In contrast, during spring

months warming temperatures, increasing precipitation, and extensive snowmelt create a pronounced peak in discharge, which is referred to as the spring freshet. Associated with these fluctuations are large changes in the characteristics of the tDOM exported to the Arctic Ocean. Based on lignin and p-hydroxybenzene compositions and ^{14}C-DOC ages of Arctic tDOM, ~75 % of lignin discharged to the Arctic occurs during spring freshet and is predominantly derived from an abundance of young, boreal-forest vegetation derived leachates [*Amon et al.,* 2012; *Neff et al.,* 2006; *Spencer et al.,* 2009]. During base flow, older, soil and peat derived DOC transported by ground water becomes more significant [*Amon et al.,* 2012; *Neff et al.,* 2006; *Spencer et al.,* 2009].

If we are to predict how the Arctic's carbon cycle will respond to a warming climate, it is imperative to understand both qualitative and quantitative changes in Arctic tDOM over the annual hydrograph. To identify sources and seasonal differences of DOM quality within large Arctic Rivers we focus on the light absorbing constituent of the DOM pool, referred to as chromophoric dissolved organic matter (CDOM) and its fluorescent sub fraction (FDOM). CDOM absorbs light in the UV and visible wavelength range (240-600 nm), and FDOM emits a fluorescence between 300 and 600 nm. Characteristics of the absorption and fluorescence spectra vary as a function of the chemical nature of the organic matter present and these measurements have become a convenient proxy to determine sources, nature, and fate of DOM in natural environments [*Coble*, 2007; *Stedmon et al.*, 2011; *Walker et al.*, 2009]. The optical properties of CDOM have previously been used to predict DOC concentrations, distinguish compositional characteristics and discriminate between terrestrial versus marine DOM

sources [*Coble*, 1996; *Ferrari and Dowell*, 1998; *Walker et al.*, 2009]. The optical parameters used in this study include the absorption coefficient at 350 nm (a_{350}), the spectral slope ($S_{(275-295)}$), the specific UV absorbance at 254 nm (SUVA), the biological/autochthonous index (BIX), the fluorescence index (FI), and Excitation/Emission Matrix Spectroscopy (EEM's) coupled to a new technique, Parallel Factor Analysis (PARAFAC). PARAFAC is a multivariate technique capable of decomposing the combined CDOM fluorescence signal into specific components that can be traced to a source [*Cory and McKnight*, 2005; *Stedmon and Bro*, 2008; *Stedmon et al.*, 2003; *Walker et al.*, 2009].

The objectives of this study were to: 1) identify sources and seasonal differences of CDOM quality within large Arctic rivers, 2) to link watershed characteristics to differences in CDOM quality between the rivers, and 3) explore the usefulness of PARAFAC as a means to trace CDOM during transport and mixing.

2.3 Methods

2.3.1 Sample Collection

River data presented here were collected as part of the Pan-Arctic River Transport of Nutrients, Organic Matter, and Suspended Sediments (PARTNERS) project and include the Mackenzie, Lena, Kolyma, Ob, and Yenisei. Samples were collected from 2004-2006 near the river mouth at discharge gauging stations at the following locations (Fig. 2.1); Tsiigehtchic for the Mackenzie River (~ 300 km upstream from the

Arctic Ocean), Zhigansk for the Lena (~ 850 km upstream from the Arctic Ocean), Cherskiy for the Kolyma (~ 100 km upstream from the Arctic Ocean), Salekhard for the Ob (~ 1000 km upstream from the Arctic Ocean), and Dudinka for the Yenisei (~ 600 km upstream from the Arctic Ocean). To represent surface to bottom and cross channel chemistry, river water samples were collected at five different locations along a cross-channel transect using a torpedo shaped, Teflon coated, 60 kg, depth integrated sampler (US D-96). During winter, water samples were collected through a hole drilled into the ice. Individual samples collected to represent one location were homogenized using a Teflon churn. Water samples were filtered (0.45 μm Pall Aquaprep 600 capsule filters) into acid washed 1 liter polycarbonate bottles and kept frozen until analysis in the lab. Optical samples presented for this study were collected at various times of the year, reflecting the changing seasonal hydrograph, and are presented here as averages from three flow regimes (peak, mid, and base flow conditions) within each river.

2.3.2 Dissolved Organic Carbon (DOC)

DOC and ^{14}C-DOC ages were measured in parallel to this optical sample set and are presented in previous studies. ^{14}C-DOC measurements were made and presented by *Raymond et al.* [2007] and are therefore not discussed. DOC concentrations were measured on a MQ-1001 TOC analyzer (MQ-Scientific) according to *Qian and Mopper* [1996] and *Peterson et al.* [2003] using the high temperature combustion (HTC) method as described in *Amon et al.* [2012].

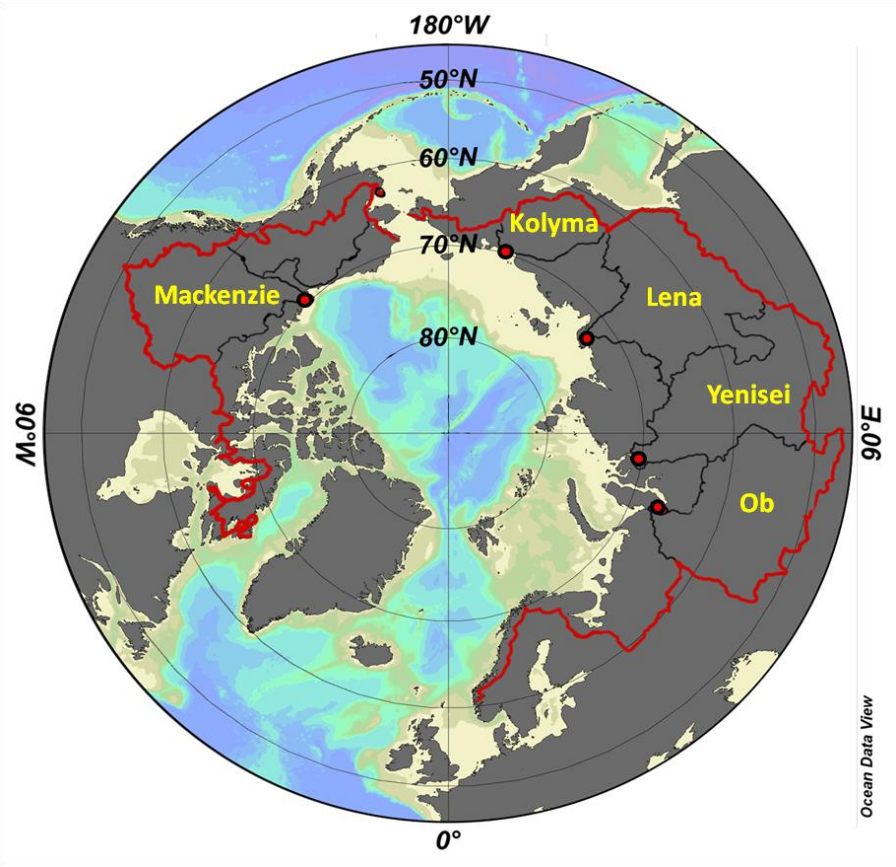

Figure 2.1. Map of discharge gauging stations where samples were collected in the Mackenzie, Lena, Kolyma, Ob, and Yenisei watersheds.

2.3.3 Optical Measurements

Samples were warmed to room temperature prior to optical analysis. Absorbance measurements were recorded on a Shimadzu UV-2401PC/2501PC using a 5 cm quartz cuvette. Absorbance spectra were measured from 200-800 nm at 0.5 nm increments and were blank corrected using Milli-Q water as a reference. Absorbance values for some of these samples were very high and data below 240 nm was often beyond the linear range of the spectrophotometer and therefore discarded. In order to avoid inner filter effects,

samples were diluted with Milli-Q water to an absorbance value of 0.10 at 240 nm in a 1 cm cell before fluorescence was measured. Dilution to this level ensures absorption coefficients were low enough to not influence the excitation and emission light in the cuvette [*Ohno and Bro*, 2006].

Fluorescence measurements were made on a Photon Technologies International Fluorometer (Quanta Master-4 SE) using a 1 cm quartz cuvette with excitation and emission slit widths set to 5 nm. Excitation emission matrix scans (EEMs) for each sample were obtained by collecting a series of emission spectra ranging from 230 to 600 nm (2 nm increments) at excitation wavelengths ranging from 220 to 450 nm (5 nm increments). To account for fluctuations in light source characteristics the fluorescence signal was normalized to that from a reference detector during measurement; emission and excitation correction files generated by the manufacturer were applied to each sample EEM to correct for instrument specific biases. Post acquisition, raw EEM's were exported to Matlab, Raman calibrated, corrected for Rayleigh and Raman scatter, and organized for the modeling process according to *Walker et al.* [2009] (Chapter III).

2.3.4 Calculations: Optical Indices

Using absorbance measurements we calculated absorption coefficients, the spectral slope ($S_{(275\text{-}295)}$), and the specific UV absorbance at 254 nm (SUVA). Absorption coefficients (a, m^{-1}) were calculated by equation (2.1):

$$a_{\lambda}(m^{-1}) = (2.303 * A_{\lambda})/L \qquad (2.1)$$

where A is absorbance at a specific excitation wavelength and L is the cuvette path length in meters. The shape of the absorption spectra (ranging from 275 nm to 295 nm) was characterized by determining the exponential spectral slope coefficient ($S_{(275-295)}$) according to [*Helms et al.*, 2008]. The spectral slope is derived by fitting the absorption data to equation (2.2):

$$a_\lambda = a_{\lambda ref} e^{-S(\lambda - \lambda ref)}, \quad (2.2)$$

where a is the Napierian absorption coefficient (m^{-1}), λ is the wavelength (nm), and λ_{ref} is a reference wavelength. SUVA was calculated *Weishaar et al.,* [2003] by equation (2.3):

$$SUVA = (A_{254} / L) / [DOC], \quad (2.3)$$

where A_{254} is the absorbance at 254 nm measured in the 1 cm cuvette , L is the cuvette path length in m (0.01 m), and the concentration of DOC is measured in milligrams of carbon per liter (mg C l^{-1}; [*Weishaar et al.*, 2003]).

Using the EEM's data, we calculated two fluorescence indices, biological/autochthonous index (BIX) and the fluorescence index (FI). BIX was calculated by taking the ratio of emission wavelengths at 380nm to that at 430nm, at a fixed excitation wavelength at 310 nm [*Huguet et al.*, 2009] using equation (2.4):

$$BIX = [(em380 \text{ at } ex310) / (em430 \text{ at } ex310)]. \quad (2.4)$$

FI was calculated by taking the ratio of emission wavelengths at 450 nm to that at 500 nm, at a fixed excitation wavelength of 370 nm [*McKnight et al.*, 2001] using equation (2.5):

$$FI = [(em450 \text{ at } ex370) / (em500 \text{ at } ex370)]. \quad (2.5)$$

2.3.5 Parallel Factor Analysis (PARAFAC) Modeling

This study used the "DOMFluorToolbox" in MATLAB according to *Stedmon and Bro* [2008] and outlier identification and model validation was performed according to *Walker et al.,* [2009]. The PARAFAC analysis was carried out on the diluted samples to ensure an even weighting between samples during the modeling process. Post modeling, the dilution factors were reapplied to the fluorescence signal of each sample to provide the actual fluorescence intensities. The PARAFAC analysis was conducted on 74 samples and no outliers were identified using the leverage plots. A five component model was derived and validated using split-half validation and the model fit was assessed by residual analysis.

2.3.6 CDOM Relationships to Lignin Biomarkers

In order to interpret the optical properties determined in this study we relate them to previously determined biomarker signatures of lignin phenols and p-hydroxybenzenes [*Amon et al.*, 2012]. Alkaline CuO oxidation of DOM and the quantification of lignin oxidation products (LOP) were performed according to *Louchouarn et al.* [2000, 2010] and *Kuo et al.* [2008]. Using this approach, the determined LOP's include vanillin (Vl), vanillic acid (Vd), acetovanillone (Vn), syringealdeyde (Sl), syringic acid (Sd), acetosyringone (Sn), p-coumaric acid (Cd), ferulic acid (Fd), p-hydroxybenzaldehyde (Pl), p-hydroxyacetophenone (Pn), p-hydroxybenzoic acid (Pd), and 3,5 dihydroxybenzoic acid (3,5Bd). Relationships between the different LOP's are often used to infer sources and the degradation state of terrestrially derived DOM in aquatic

environments. In an attempt to characterize CDOM sources we related various optical parameters to lignin phenol concentrations, including Σ8 (defined by the sum of the cinnamyl, syringyl, and vanillyl phenols) and Λ8 (the carbon normalized yields of Σ8 (mg lignin (100 mg $OC^{)-1}$)), P-yield, Pn/P, and (Ad/Al)v.

Lignin phenols are an important component of vascular plants and an unambiguous terrestrial biomarker when found in aquatic systems. In large Arctic rivers lignin is strongly related to the ^{14}C-age of DOC, with higher concentration of lignin typically associated with younger and fresher river DOM [*Raymond et al.,* 2007]. In conjunction with lignin composition signatures, these results indicate that young, boreal forest-derived leachates predominate during spring flood, whereas older, soil, peat, and wetland-derived DOC is a major component in rivers during groundwater dominated low-flow conditions, particularly in the Ob and Yukon [*Amon et al.*, 2012]. Here we thus use increased lignin phenol concentrations as an indicator for fresh vascular plant inputs.

p-hydroxybenzenes (Pn, Pl, and Pd) can have several sources, but different Sphagnum species and some peat soils have been shown to be enriched in Pn [*Williams et al.*, 1998]. As a result, elevated P-yield (the sum of Pn, Pl, and Pd) values are typically higher in moss and peat soils [*Williams et al.*, 1998] but typically lower for vascular plants [*Hedges et al.*, 1982]. Elevated P-yield values were observed in large Arctic rivers, particular during low flow regimes [*Amon et al.*, 2012], and are used here to indicate increased contributions of mosses and/or peat to the riverine CDOM pool.

The ratio of vanillic acid to vanillin (Ad/Al)v has traditionally been used as a diagenetic indicator to infer the oxidative degradation of OM, where increasing values

indicate an increased degradation state. More recently however, elevated Ad/Al ratios have also been shown to indicate selective leaching and redistribution of acid moieties [*Hernes et al.*, 2007; *Houel et al.*, 2006]. Based on findings by *Amon et al.* [2012], Ad/Al ratios in large Arctic rivers were highest during peak discharge periods when the average ^{14}C-DOC age is young. These results suggest that a significant fraction of river DOM comes from recently produced vascular plant and litter leachates during freshet. As a result, the (Ad/Al)v in the present study serves as an indicator for leachates derived from plants and litter.

2.4 Results

2.4.1 CDOM Indices

To probe the quality of CDOM, we examined a_{350}, $S_{(275\text{-}295)}$, SUVA, BIX, and FI over the annual hydrograph within the different rivers (Fig. 2.2). The absorbance coefficient at 350 nm (a_{350}), a measure of CDOM concentration, generally increased with discharge, with elevated levels occurring during the spring freshet relative to winter base flow conditions and ranged from 2.29 to 36.6 m^{-1}. During all flow regimes, a_{350} was highest in the Lena (peak flow 36.6, base flow 13.13 m^{-1}) and lowest in the Mackenzie (peak flow 5.90, base flow 2.29 m^{-1}), where the Lena and Yenisei display the largest seasonal shift. $S_{(275\text{-}295)}$, a qualitative measure of CDOM, generally decreased with increased discharge, with elevated levels observed during winter base flow relative to peak flow conditions, and ranged from 13.26 – 22.33 μm^{-1}. In general, $S_{(275\text{-}295)}$ values

were higher in the Mackenzie relative to the other rivers. Similar to a_{350}, average SUVA values, a measure of CDOM aromaticity, were generally elevated during peak flow relative to winter base flow conditions and ranged from 1.81 – 3.32 L mg^{-1} m^{-1}. Overall, highest SUVA values were observed in the Lena (peak flow 3.32 L mg^{-1} m^{-1}, base flow 2.74 L mg^{-1} m^{-1}), whereas lowest values were observed in the Mackenzie (peak flow 2.26 L mg^{-1} m^{-1}, base flow 1.81 L mg^{-1} m^{-1}).

Average BIX values, a measure of autochthonous CDOM contributions, display a slight increase from peak flow relative to base flow conditions and ranged from 0.45 – 0.68. FI values, a measure of CDOM source, were somewhat constant over the annual hydrograph in all rivers, with the exception of the Mackenzie, and ranged from 1.12 – 1.24. The Mackenzie is the only river that displayed a distinct seasonal trend, where average FI were higher during base flow relative to peak flow conditions. In comparing the rivers, FI and BIX were elevated in the Mackenzie relative to the other rivers during all three discharge periods.

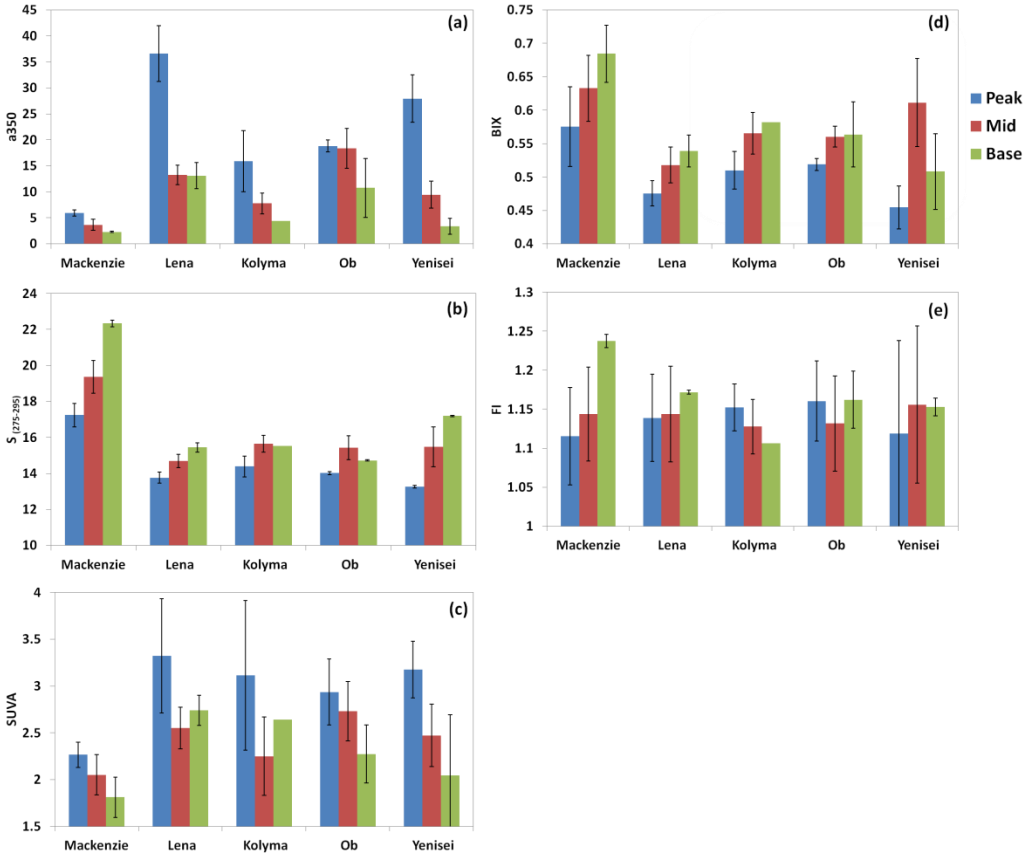

Figure 2.2. Average CDOM indices during freshet, mid flow, and base flow in the five rivers.

2.4.2 Fluorescence Characterization by PARAFAC

Five unique fluorescent components were identified by the PARAFAC model and are referred to as PAR-components (PARC1 – PARC5; Fig. 2.3). The spectral characteristics of individual PAR-components are compared with those from earlier studies in Table 1. PARC1 has excitation peaks < 250 nm and at 310 nm and a broad emission peak from 350 to 550 nm (emission peak max at 432 nm). PARC2 has a primary excitation peak at 370 nm and secondary peak at 270 nm with a broad emission

peak from 386 to > 550 nm (emission peak max at 462 nm). PARC3 has an excitation peak < 250 nm and at 275 nm with a broad emission peak from 416 to > 550 nm (emission peak max at 546 nm). PARC4 has a primary excitation maximum at 260 nm with a secondary peak at 370 nm and a broad emission peak from 350 to > 550 nm (emission peak at 452 nm). PARC5 has an excitation peak < 250 nm and at 275 nm with an emission peak at 344 nm.

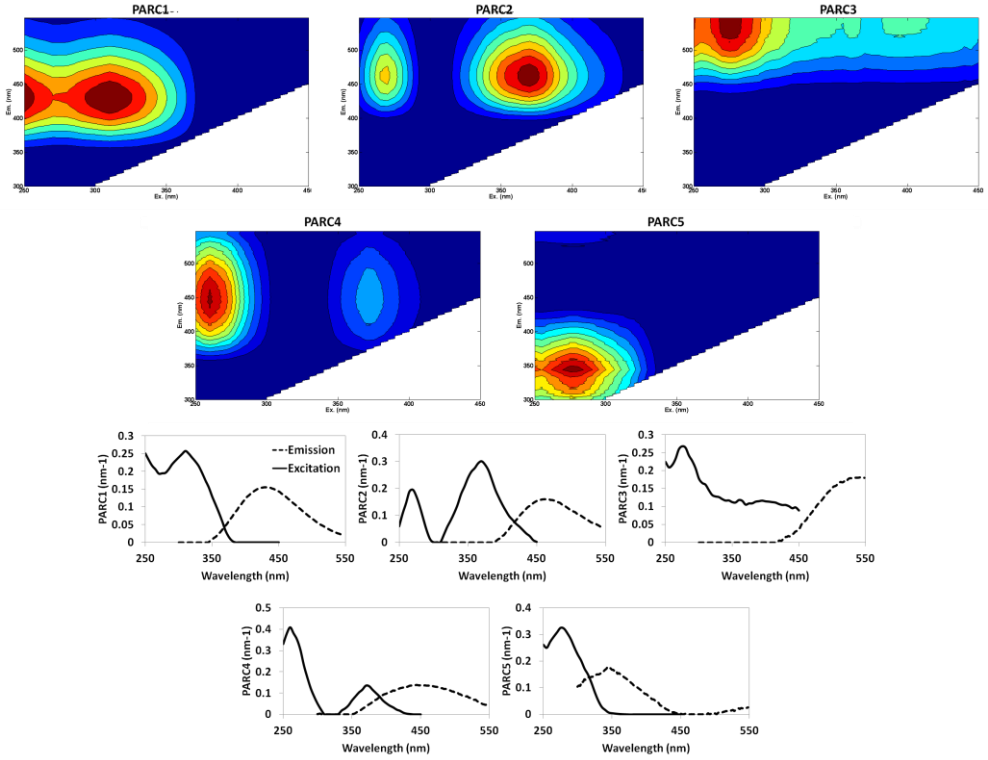

Figure 2.3. Three dimensional fluorescence landscapes and the excitation and emission spectra for the five different PAR-components identified by the PARAFAC model. Intensity is shown in Raman units (nm^{-1}).

Table 2.1. Spectral characteristics of the five components identified by PARAFAC compared to previously identified components.

Component	Excitation maximum (nm)	Emission maximum (nm)	Coble 1996	Cory and McKnight 2005	Walker et al.. 2009	X. Yao et al., 2011	Balcarczyk et al., 2009	Ohno and Bro 2006	Muller et al., 2012
PARC1	<250, 310	432	A+C	C10	BERC1	C2*	C1, C8	C3	C2
PARC2	270, 370	462	A+C	SQ1/SQ2/SQ3	BERC3	C3*	C6*	C1	C1
PARC3	<250, 275	546		HQ/SQ1/C6			C4	C2	
PARC4	260, 370	452	A+C		BERC2	C3*		C4	
PARC5	<250, 275	344	T		BERC4	C1	C10		C4

*indicates similar components but not an exact match.

2.4.3 PARAFAC Components - Seasonal Trends and Source Identification

For all rivers, excluding the Ob, PAR-components increased with discharge, with elevated levels observed during spring freshet and lowest levels during winter base flow conditions (Fig. 2.4 a-c). In the Ob PAR-components displayed the opposite trend, with elevated levels observed during winter base flow conditions relative to peak flow months (Fig. 2.4 a-c). In terms of how the individual PAR-components varied with the changing hydrograph, only PARC2 in the Mackenzie and PARC1 and PARC2 in the Yenisei were significantly correlated to discharge ($P < 0.0001$; Table 2.2). In comparing the rivers, PAR-components were overall higher in the Lena during peak discharge months, whereas during summer mid and winter base flow conditions PAR-components were overall higher in the Ob relative to other rivers (Fig. 2.4 a-c). PARC1 (excitation 310 nm at emission 432 nm) is by far the most predominant CDOM component identified over the annual hydrograph in all rivers (Fig. 2.4 d-f) and explains on average ~ 39 % (range 33 – 45 %) of the total CDOM signal. In comparison, PARC2 (range 11 – 23 %), PARC3 (range 14 – 19 %), PARC4 (range 7 – 23 %), and PARC5 (range 7 – 16 %) only explain on average 18 %, 17 %, 15%, and 12 % of the total CDOM signal, respectively (Fig. 2.4 d-f).

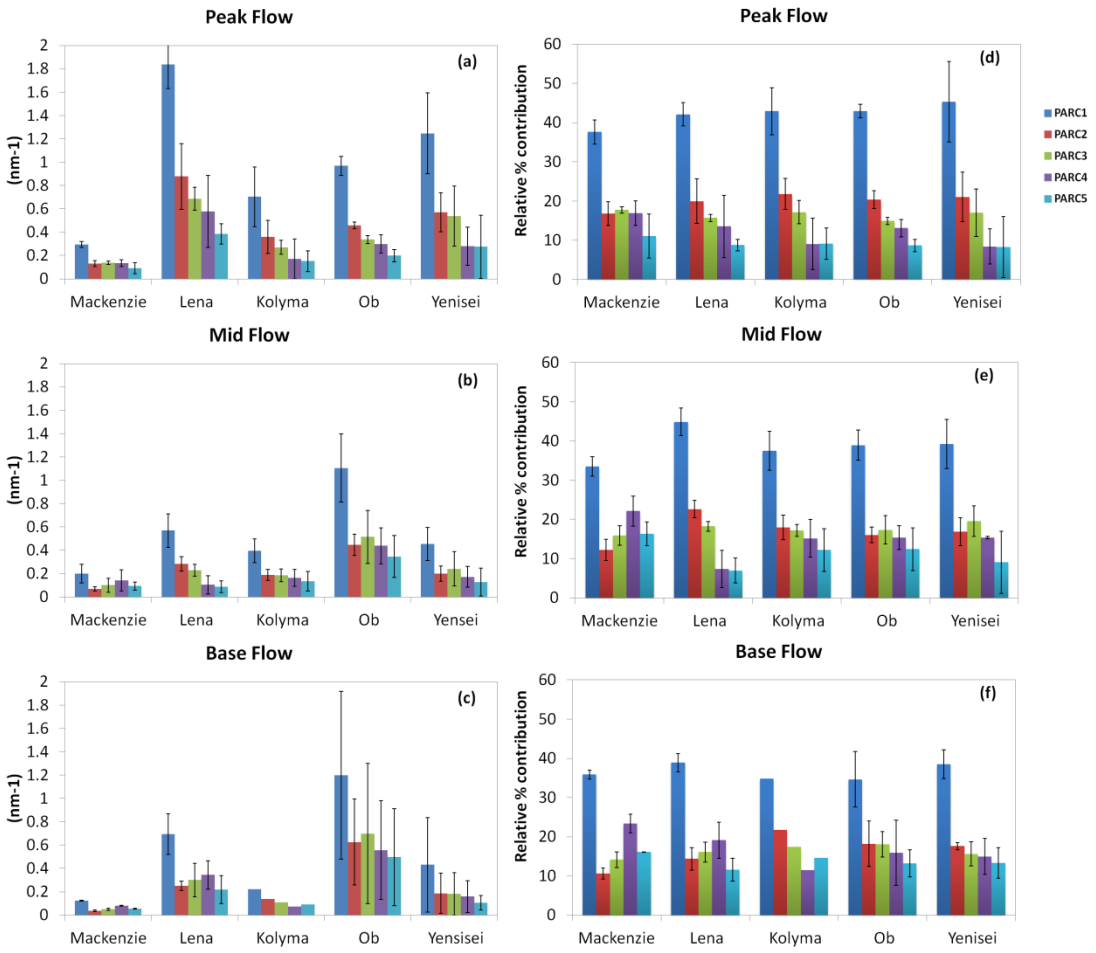

Figure 2.4. Average PAR-component loadings (a–c) and their relative percent contributions (d–f) during freshet, mid flow, and base flow in the five rivers.

To probe the qualitative aspects of PAR-components, we investigated their potential relation to a_{350}, DOC concentrations, lignin phenol and p-hydroxybenzene compositions, and to the ^{14}C-DOC age. Table 2.2 illustrates the R^2 values of these relationships, where ** indicates $P < 0.01$ and * indicates $0.01 < P > 0.05$. Below is a description of how the individual components relate to these various biomarkers, where

only significant correlations at the 99% level ($P<0.01$) and R^2 above 0.7 are discussed. In the Mackenzie, Lena, and Yenisei PARC1 and PARC2 were significantly correlated to a_{350}, DOC, lignin phenol concentrations ($\Sigma 8$ and $\Lambda 8$), and the P-yield, but were not significantly correlated to these parameters within the other watersheds, except in the Kolyma where both were significantly correlated only to a_{350}. PARC1 was significantly correlated to (Ad/Al)v, in the Lena and Yenisei, and to the ^{14}C-DOC age in the Lena. Similar to PARC1, PARC2 was correlated to (Ad/Al)v, but only in the Yenisei, and to the ^{14}C-DOC age, but only in the Lena. In the Lena and Yenisei, PARC3 was significantly correlated to a_{350}, DOC, lignin phenol concentrations, and the P-yield, but is unrelated to these parameters within the other rivers. In the Lena PARC3 was significantly correlated to (Ad/Al)v and the ^{14}C-DOC, but exhibits no significant relations to these parameters within the other rivers. No significant relationships were observed between PARC4 and the biomarkers used for this analysis. Similar to PARC4, we saw no significant relationships between PARC5 and the biomarkers used in this analysis, except in the Lena where this component was significantly correlated to a_{350}, DOC concentrations, and to the ^{14}C-DOC age.

Table 2.2. The R^2 values of the relationships between the individual components to biomarkers measured in the five rivers.

	Discharge	DOC	a_{350}	Sig8	lambda	Pyield	(Ad/Al)v	14C-DOC
Mackenzie								
PARC1	0.652*	0.828**	0.897**	0.864**	0.738**	0.858**	0.592*	n.s.
PARC2	0.817**	0.709**	0.916**	0.911**	0.798**	0.828**	0.369*	n.s.
PARC3	0.444*	0.667*	0.694*	0.666*	0.566*	0.717*	0.672*	n.s.
PARC4	n.s.	0.264*	0.223*	0.229*	n.s.	n.s.	0.519*	n.s.
PARC5	n.s.	0.328*	0.221*	n.s.	n.s.	0.275*	0.253*	n.s.
Lena								
PARC1	0.573*	0.906**	0.979**	0.939**	0.859**	0.937**	0.758**	0.88**
PARC2	0.487*	0.717**	0.898**	0.952**	0.94**	0.953**	0.651*	0.791**
PARC3	0.51*	0.839**	0.934**	0.85**	0.787**	0.849**	0.69**	0.857**
PARC4	0.392*	0.512*	0.432*	0.286*	0.215*	0.286*	0.383*	0.338*
PARC5	0.344*	0.685**	0.707**	0.58*	0.492*	0.567*	0.639*	0.685**
Kolyma								
PARC1	0.559*	0.505*	0.915**	0.661*	0.676*	0.617*	0.424*	n.a.
PARC2	0.421*	0.399*	0.908**	0.619*	0.659*	0.613*	0.344*	n.a.
PARC3	0.492*	0.424*	0.638*	0.465*	0.508*	0.396*	0.328*	n.a.
PARC4	n.s.	n.s.	n.s.	0.23*	0.253*	0.763*	0.417*	n.a.
PARC5	0.233*	n.s.	n.s.	n.s.	n.s.	n.s.	n.s.	n.a.
Ob								
PARC1	n.s.	0.42*	0.697*	0.224*	n.s.	0.511*	n.s.	0.302*
PARC2	n.s.	n.s.	0.436*	0.393*	0.356*	0.547*	n.s.	0.442*
PARC3	n.s.	0.252*	0.419*	n.s.	n.s.	0.211*	0.282*	n.s.
PARC4	n.s.	n.s.	n.s.	n.s.	n.s.	n.s.	n.s.	n.s.
PARC5	n.s.	n.s.	n.s.	n.s.	n.s.	n.s.	n.s.	n.s.
Yenisei								
PARC1	0.889**	0.841**	0.911**	0.901**	0.872**	0.847**	0.875**	0.76*
PARC2	0.847**	0.826**	0.89**	0.862**	0.825**	0.817**	0.866**	0.72*
PARC3	0.705*	0.582*	0.654*	0.74*	0.785**	0.734**	0.594*	0.467*
PARC4	0.576*	0.426*	0.503*	0.577*	0.6*	0.71*	0.712*	0.336*
PARC5	0.275*	n.s.	n.s.	0.304*	0.34*	0.306*	n.s.	n.s.

** P <000.1; * 0.0001 < P > 0.05; n.s P > 0.05; n.a. not available

2.5. Discussion

2.5.1 Optical Indices: Implications of CDOM Sources Under Different Flow Regimes

By relating the various optical parameters to DOC and biomarker concentrations we were able to investigate CDOM sources during the different flow regimes within these five rivers. Here we discuss the different optical indices and describe how CDOM in large Arctic rivers change on a seasonal basis. The absorption coefficient at 350 nm (a_{350}) is used as a quantitative measure for CDOM concentrations in natural environments. Because aromatic compounds derived from lignaceous materials (hydrophobic compounds) absorb light in the UV region to a greater degree than aliphatic groups (hydrophilic compounds), increased a_{350} values suggest inputs from plant/soil DOM sources [*Mladenov et al.*, 2008; *Weishaar et al.*, 2003]. We chose to use the wavelength at 350 nm based on its ability to best estimate DOC concentrations and inputs of terrestrial DOM in Arctic rivers [*Spencer et al.*, 2009] and values reported here are similar to those previously reported for large Arctic Rivers [*Spencer et al.*, 2009].

During this study, a_{350} was strongly related to DOC and lignin phenol concentrations during all flow regimes (Fig. 2.5). These results suggest a_{350} is well suited to trace quantitative changes regarding vascular plant inputs over the annual hydrograph within these five rivers. Based on these results, vascular plant inputs are more dominant during freshet, particularly in the Lena and Yenisei (Fig. 2.5). In contrast, base flow CDOM is slightly less influenced by fresh vascular plant sources. These results are consistent with extremely high lignin phenol concentrations, confirming previous

observations that most of the annual lignin discharged to the Arctic (> 75 %) occurs during spring freshet [*Amon et al.,* 2012].

$S_{(275-295)}$ provides insights to the characteristics (chemistry, sources, diagenesis) of CDOM, and is largely independent of DOC concentrations [*Helms et al.*, 2008; *Stedmon et al.*, 2011]. The UV-visible absorption spectrum for CDOM increases exponentially with decreasing wavelength [*Twardowski et al.*, 2004], where steeper slopes (or higher S values) indicate a more rapid decrease in absorption with increasing wavelength. Because low molecular weight CDOM absorbs at shorter wavelength radiation, the shape of the absorption spectrum should shift to a greater relative absorption at shorter wavelengths (i.e. from 275 – 295 nm). Higher $S_{(275-295)}$ values therefore reflect a lower molecular weight CDOM pool whereas lower $S_{(275-295)}$ values indicate a higher molecular weight CDOM pool [*Helms et al.,* 2008]. The narrow range of wavelengths between 275-295 nm is used in this study because it can be measured with high precision and appears to be particularly sensitive to shifts in molecular weight and/or DOM sources, whereas the more commonly used broader wavelength ranges (300-700 nm) is not sensitive enough to identify such shifts [*Helms et al.,* 2008].

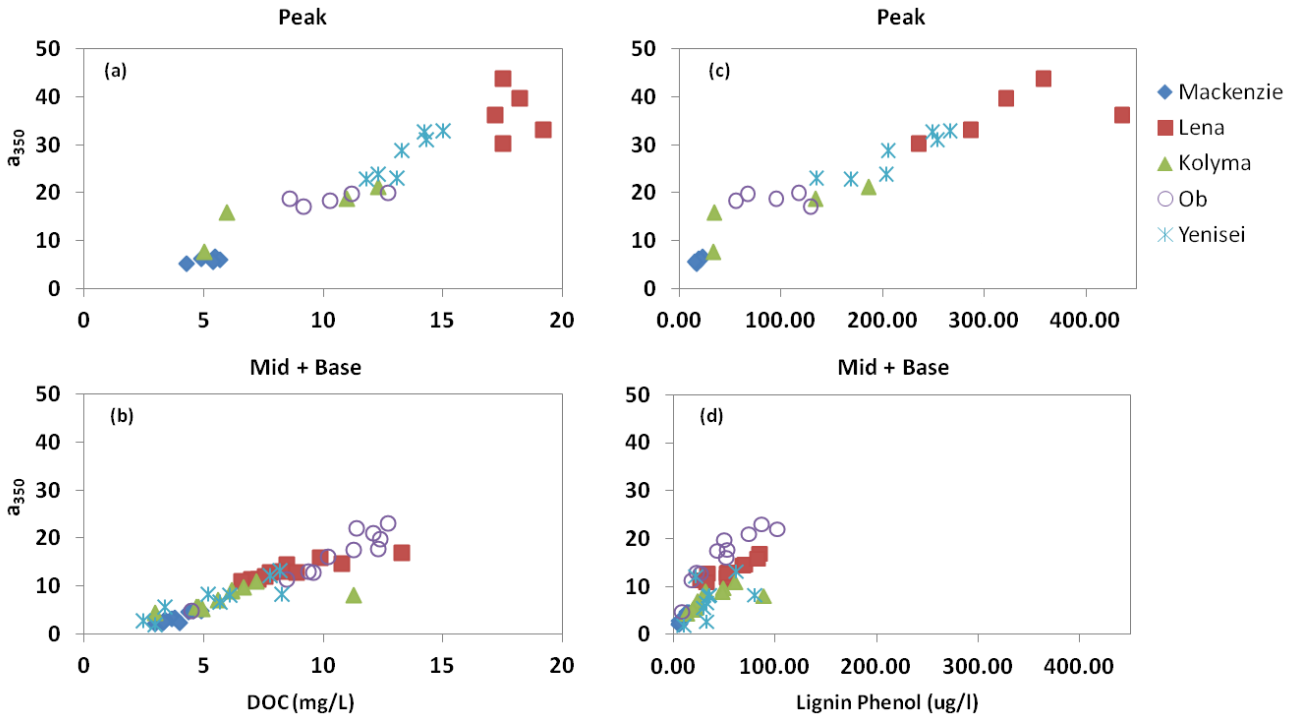

Figure 2.5. The relationship of dissolved organic carbon and lignin phenol concentrations to a_{350} in the five rivers during high (peak) and low (mid + base) discharge periods.

Based on the relationships between a_{350}, $S_{(275\text{-}295)}$, and lignin phenol concentrations (Fig. 2.5, 2.6) inputs from high molecular weight, DOC dominated by vascular plant DOM sources are more substantial during peak flow relative to winter base flow conditions for all rivers, excluding the Mackenzie. During freshet, lignin monomer and ^{14}C-DOC signatures provide strong evidence for leaching of relatively young terrestrial plant litter [*Amon et al.*, 2012; *Neff et al.*, 2006; *Raymond et al.*, 2007]. Based on the lignin composition and ^{14}C-DOC age, surface run-off is the predominant path for watershed drainage during high runoff conditions and mainly affects vegetation

cover, surface litter and top soils. Therefore, the lower $S_{(275-295)}$ at higher a_{350} and lignin phenol concentrations during peak flow likely reflects a higher surface runoff and leaching of surface litter and top soil layers [*Amon et al.*, 2012; *Holmes et al.*, 2008; *Spencer et al.*, 2008a]. During mid-flow conditions, water percolates through deeper soil horizons, which introduces DOM that is older, more humified, with less aromatic and lignin phenol components [*Neff et al.,* 2006, *Amon et al.,* 2012; *Raymond et al.,* 2007]. Therefore, during lower discharge periods the increase in $S_{(275-295)}$ at lower a_{350} and lignin concentrations (Fig. 2.6) likely reflects increased inputs from ground water that has been in contact with the mineral horizons of soils.

To estimate the degree of aromaticity in bulk CDOM we investigated the specific UV absorbance at 254 nm (SUVA; [*Weishaar et al.,* 2003, *Mladenov et al.,* 2007]). Terrestrially derived DOM has a higher aromatic carbon content than microbially derived DOM, reflecting the presence of tannin-like and humic-like substances that originate from plant and soil organic matter [*Battin*, 1998]. Because aromatic compounds absorb more light in the UV-visible region of the spectrum, higher SUVA values indicate increased aromaticity from allochthonous inputs and lower SUVA values indicate a decrease in aromaticity and a more autochthonous or modified terrestrial source. SUVA values reported here are similar to those previously reported in large Arctic rivers [*Neff et al.,* 2006, *Spencer et al.,* 2008, 2009, *Stedmon et al.* 2011]. Elevated SUVA values during peak flow, when DOC age is relatively young [*Amon et al.,* 2012; *Raymond et al.,* 2007], suggest a more aromatic CDOM pool relative to base flow CDOM. Similarly to $S_{(275-295)}$, these results are consistent with increased inputs

from surface litter and top soil layers. Relatively lower average SUVA values observed during base flow (Fig. 2.2) are consistent with inputs of CDOM originating from deeper soil layers where selective removal of aromatic compounds occurs, such as lignin-derived polyphenols [*O'Donnell et al.*, 2010], and/or a shift to a more autochthonous CDOM pool.

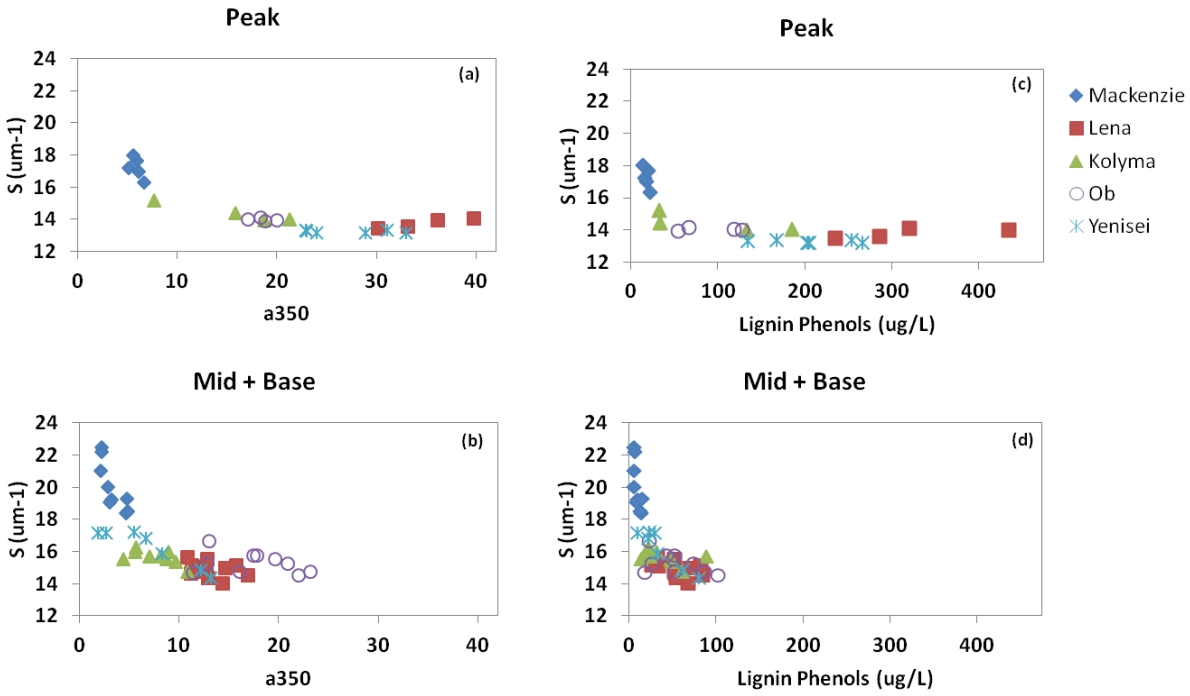

Figure 2.6. The relationship of a_{350} and lignin phenol concentrations to $S_{(275\text{-}295)}$ in the five rivers during high (peak) and low (mid + base) discharge periods.

To directly assess the relative contribution of microbially altered DOM, we investigated the biological/autochthonous index (BIX) and the fluorescence index (FI). In general, BIX and FI are influenced by the presence of two commonly identified terrestrial (peak C) and microbial-like peaks (peak M or a more diagenetically altered form of the peak M fluorophores) within the fluorescence spectra [*Burdige et al.*, 2004; *Coble*, 1996; *McKnight et al.*, 2001]. BIX values between 0.8 and 1.0 correspond to freshly produced DOM of microbial origin, whereas values below 0.6 are considered to contain little autochthonous DOM [*Birdwell and Engel*, 2010]. A low FI (< 1.4) is consistent with DOM derived from predominantly terrestrial sources whereas a high FI (> 1.9) suggest increased inputs from autochthonous and/or microbially derived DOM [*Balcarczyk et al.*, 2009; *McKnight et al.*, 2001]. Based on these previous investigations we would expect a positive correlation between BIX and FI, which is not apparent in this data set (data not shown).

In large Arctic rivers BIX never exceeds 0.6 (Fig. 2.6), excluding the Mackenzie, and the FI never exceeds 1.4, which suggests that CDOM is predominantly derived from higher plant/terrestrial DOM sources in all rivers and during all flow regimes. With that said, there is a slight shift to higher BIX values during mid and base discharge periods in all rivers. This seasonal trend was not apparent in the FI, with the exception of the Mackenzie where higher FI values were observed during lower flow regimes. The shift to higher BIX values during base flow, as is most apparent in the Mackenzie River, indicates a greater proportion of microbially processed material, relative to fresh tDOM sources, and suggest a more recalcitrant CDOM pool. Based on previous experimental

results during lower flow regimes, bacterial consumption of Yenisei River DOM was limited by its refractory nature, rather than by nutrient limitation [*Kohler et al.*, 2003]. These results, combined with other investigations conducted during lower flow regimes, lead researchers to assume that Arctic riverine DOC was largely refractory in nature and could potentially make its way to the Arctic Ocean and North Atlantic deep water formation sites [*Amon and Benner*, 2003; *Amon et al.*, 2003; *Benner et al.*, 2005; *Dittmar and Kattner*, 2003; *Lobbes et al.*, 2000]. More recently, samples collected during peak discharge months, when the majority of tDOC is discharged to the Arctic Ocean [*Amon et al.,* 2012], revealed that Arctic peak flow DOM is more bioavailable relative to base flow DOM [*Hansell et al.*, 2004; *Holmes et al.*, 2008; *Manizza et al.*, 2009]. Therefore, lower BIX values during peak discharge indicate a relatively fresh, undegraded CDOM pool whereas the higher BIX during lower flow regimes reflect more extensive microbial degradation of the terrestrially derived CDOM, which is most pronounced in the Mackenzie.

2.5.2 PARAFAC Component Source Identification: Limitations and Applications

In the present study, five fluorescent PARAFAC components were identified Their spectral characteristics are similar to previously identified components in other aquatic environments (Fig. 2.3, Table 2.1; [*Coble*, 1996; *Cory and McKnight*, 2005; *Mueller et al.*, 2012; *Ohno and Bro*, 2006; *Walker et al.*, 2009; *Yao et al.*, 2011]. PARC1 – PARC4 display dual excitation maxima with a single emission maximum. The two peaks within the fluorescence landscape of PARC1 – PARC3 are in the traditional peak

A and C region of the EEM defined by *Coble* [1996], which are considered terrestrial in nature. Components similar to these have been isolated from soil and aquatic humic substances and were classified as humic-like and fulvic-like molecules (Table 2.1; [*Sierra et al.*, 2005]). Further, PARC1, PARC2, and PARC4 are similar to three components identified in Canadian Archipelago and Mackenzie River plume surface waters and were strongly correlated to lignin phenol concentrations [*Walker et al.,* 2009]. PARC1 and PARC3 are considered to be ubiquitous in aquatic environments and PARC3 has been shown to be high in humic acids and very sensitive to microbial and photochemical degradation [*Stedmon et al.*, 2007]. While a similar component to PARC4 was associated with lignin phenols in the Canadian Archipelago [*Walker et al.,* 2009], a component with similar spectral characteristics was also identified as being introduced via microbial processing of algae-derived DOM [*Ohno and Bro,* 2006; *Yao et al.,* 2011]. PARC5 has spectral loadings similar to the traditional T peak assigned by *Coble* [1996] and is similar to the spectral characteristics of tryptophan. This component has been frequently isolated in DOM solutions that have proteins containing this amino acid [*Stedmon and Markager*, 2005a] and is associated with autochthonous DOM sources.

In spite of the description above, at present little is actually known regarding PARAFAC component sources, even though PARAFAC is becoming a widely used tool to classify CDOM quantity and quality all over the world [*Stedmon et al.,* 2003; *Walker et al.,* 2009; ref. within]. To date, PARAFAC components have mainly been associated with generic classes of molecules (i.e. humic and fulvic acids and DOC concentrations;

[*Cory and McKnight,* 2005]) and only recently with more specific biomarkers present in environmental matrices (i.e. lignin phenol concentrations; [*Walker et al.,* 2009]). Here, we attempt to relate PARAFAC components to a_{350}, DOC concentrations, lignin phenol and p-hydroxybenzene concentration and composition [*Amon et al.,* 2012], and to the ^{14}C-DOC age (Table 2.2; [*Raymond et al.,* 2007]). This unique opportunity allowed us to: (a) investigate if there is a potential to use PARAFAC components to determine source contributions from fresh vascular plants (Σ8 and Λ8), mosses and peat (Pyield), leachates from vascular plants and litter ((Ad/Al)v), and microbially altered DOM (^{14}C-DOC, optical indicators) and (b) to identify the appropriate terrestrial-derived endmember components useful for tracing CDOM within the Arctic Ocean.

Based on the relationships between PAR-components, a_{350}, and DOC concentrations (Table 2.2), PARC1, PARC2, and PARC3 are best suited to describe trends observed within the total DOC pool in large Arctic rivers and can be traced using a_{350}. The strong relationship between these three components and lignin phenol concentrations suggest that they originate from vascular plant sources while their strong relation P-yield values suggest that they are also derived from moss sources (Table 2.2). In addition, their strong relation to (Ad/Al)v and to the ^{14}C-DOC age in the Lena and Yenisei (Table 2.2) suggest that they are also introduced as a result of leaching of surface litter during high runoff periods when the DOC is predominately young. Based on these results, it is not possible to isolate specific terrestrial-like PARAFAC components to the level of source identification attempted in this study; in general, components appear to be derived from a variety of sources, which are difficult to

discriminate. We suggest that while PARAFAC components can be linked to a general class of CDOM sources (i.e. terrestrial versus autochthonous/microbial), PARAFAC is not useful to differentiate more specific terrestrial sources such as vascular plant, moss and/or peat, or litter leachates.

One of the overarching goals of this investigation was to determine the usefulness of PARAFAC to trace terrestrial CDOM during transport and mixing. While we were not able to isolate a component based on specific sources, we were able to confirm the terrestrial origin of components PARC1, PARC2, and PARC3. Because PARC1 is ubiquitous in aquatic environments, describing ~ 39 % of the total CDOM signal during all flow regimes (Fig. 2.4 d,e,f), is strongly related to DOC and lignin phenol concentrations (Table 2.2), and has been identified in coastal waters within the Mackenzie River plume [*Walker et al.,* 2009], we suggest that this component is best suited to trace tCDOM inputs to the Arctic Ocean and its surrounding watersheds. In addition, based on the overall relationships between PARC2, PARC3 and the terrestrial biomarkers, we suggest that these components can also be used to trace tCDOM inputs. To confirm the ability of these components to trace terrestrially derived CDOM, we related the sum of their relative concentrations (PARC1 + PARC2 + PARC3) to lignin phenol concentrations (Fig. 2.7). These results confirm the terrestrial origin of these components in Arctic rivers. The overall lack of a relationship between PARC4 and PARC5 to a_{350}, DOC and the terrestrial biomarkers suggests the potential for these components to indicate microbially altered tDOM within these rivers.

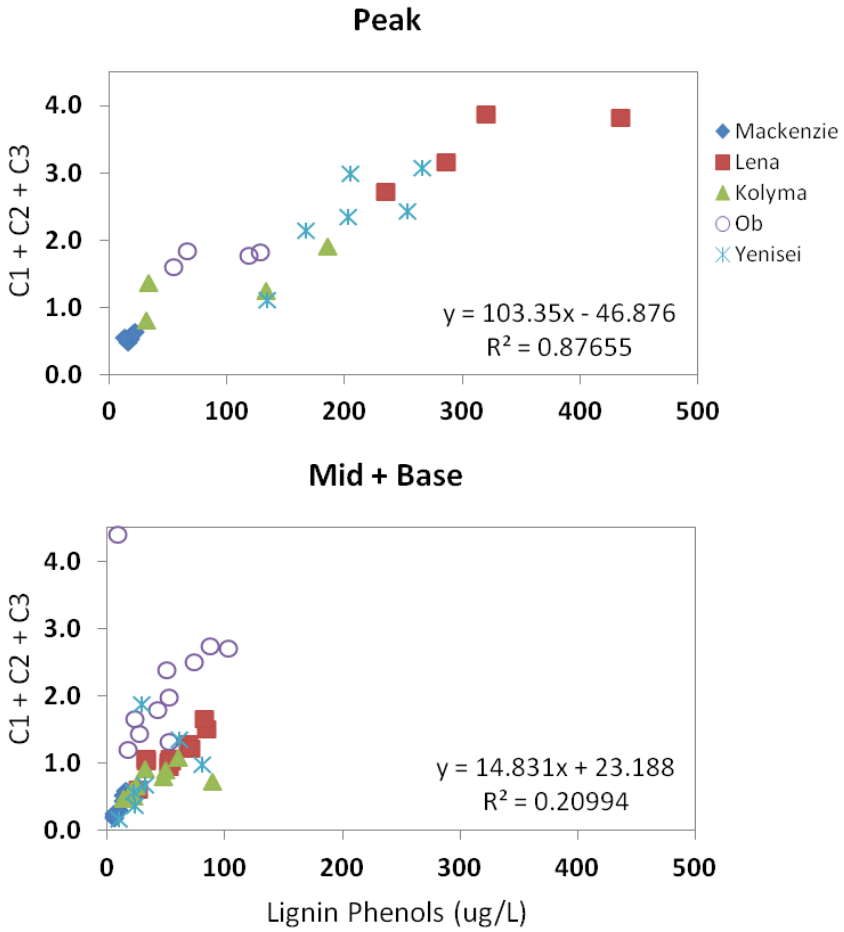

Figure 2.7. The relationship of lignin phenol concentrations to the terrestrial fluorescence PARAFAC signal (PARC1 + PARC2 + PARC3) in the five rivers during high (peak) and low (mid + base) discharge periods.

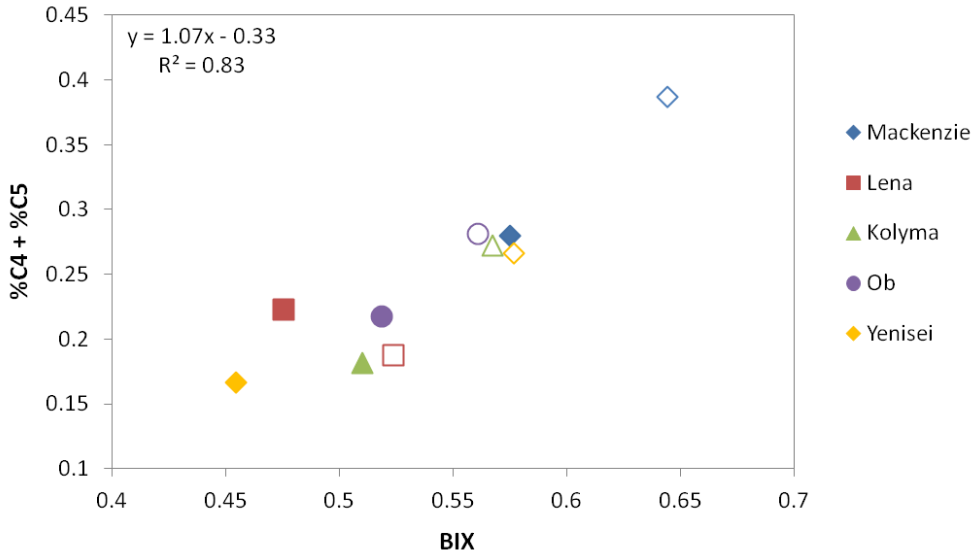

Figure 2.8. A property plot of the BIX values and the autochthonous/microbial-like PARAFAC components (%PARC 4 + %PARC 5) in the five rivers during high (peak: filled symbols) and low (mid + base: open symbols) discharge periods.

While PARAFAC may not be able to decipher specific plant CDOM end-members, the relative concentration of PAR-components, as well as their relation to BIX values are potentially useful to distinguish between freshly leached and microbially altered tDOM sources. A property plot of the autochthonous/microbial-like PARAFAC components (PARC 4 and PARC 5) and the BIX values (Fig. 2.8) clearly separates CDOM sampled during peak flow from base flow CDOM, with base flow tDOM indicating more microbial alteration. More interestingly, the property plot also separates the Mackenzie River DOM from the rest of the rivers and indicates that microbial

degradation is more extensive in tDOM from the Mackenzie River during all flow regimes.

2.5.3 Linking Watershed Characteristics to CDOM Quality: A Comparison of CDOM in Large Arctic Rivers

In large Arctic Rivers, variations in CDOM quality can be explained by individual watershed characteristic as well as physical and biological processes. Here we discuss how the different physical and biological processes influence the optical signature of CDOM and then interpret variations in CDOM based on the individual watershed characteristics. In addition to sources, there are several additional processes that likely influence the optical signature of DOM in freshwaters systems, including climate, permafrost extent, photooxidation, sorption of DOM to suspended sediments, and microbial degradation. Because permafrost soil layers tend to act as a seal and do not allow for the exchange between surface waters and ground water, rivers with a higher extent of permafrost likely receive higher contributions from surface litter, reflected by higher (Ad/Al)v values. During photobleaching, the high molecular weight fraction of the CDOM pool is destroyed [*Helms et al.,* 2008]. This results in a significant portion of the CDOM shifting from a high molecular weight, more aromatic CDOM pool, to a lower molecular weight, less aromatic CDOM pool (e.g. due to bond cleavage and/or disaggregation; [*Helms et al.,* 2008]). Therefore, upon irradiation a_{350} and SUVA generally decrease while $S_{(275\text{-}295)}$ increases [*Helm et al.,* 2008]. In addition to photooxidation, sorption of DOM in rivers with high suspended sediment loads likely

leads to a loss of the more hydrophobic DOM pool. This would also lead to an overall lower molecular weight, lower aromatic DOC pool reflected by lower a_{350} and SUVA values and higher $S_{(275-295)}$ values. In contrast to photooxidation and sorption processes, *Helms et al.,* [2008] suggest that microbial activity shifts $S_{(275-295)}$ in the opposite direction than photochemical degradation, but to a lesser extent. This would indicate that bacteria tend to preferentially utilize the lower molecular weight fraction of the DOM pool. These results contradict previous findings, which indicate that microbes preferentially utilize high molecular weight DOC [*Amon and Benner*, 1996] , suggesting that in general, microbial activity should result in increased $S_{(275-295)}$ values. With that said, upon irradiation recalcitrant, high molecular weight DOM species are converted into lower molecular weight components available for microbial consumption [*Miller and Moran*, 1997], which would lead to a loss of lower molecular weight DOC reflected by a decrease in $S_{(275-295)}$. This likely explain the observed decrease in $S_{(275-295)}$ from microbial degradation presented by *Helms et al.* [2008]. Here we interpret lower a_{350} and SUVA values and higher $S_{(275-295)}$ values to be indicative of microbial processing of tDOM sources.

In the Lena and Yenisei, overall higher discharge rates [*Amon et al.,* 2012], increased average a_{350} values (Fig. 2.5), and increased contributions from terrestrial-like PAR-components (Fig. 2.7) observed during spring freshet, when the majority of terrestrial DOC is exported to the Ocean [*Amon et al.,* 2012], underline the quantitative significance of these two rivers in terms of CDOM discharge to the Arctic Ocean. These results are consistent with the extremely high lignin phenol concentration during spring

freshet suggesting that the Lena, Yenisei, and Ob contribute ~ 90 % of the combined lignin discharged by large Arctic rivers [*Amon et al.,* 2012]. In conjunction, higher average SUVA values (> 3.0 mgC^{-1}) were observed in the Lena, Kolyma, and Yenisei during peak flow conditions. These three rivers are unique in that their watersheds comprise a greater extent of continuous permafrost relative to the other rivers (Lena 77%, Yenisei 31%, and Kolyma 99%). *Balcarczyk et al.* [2009] suggest that watersheds with a greater extent of permafrost tend to have higher SUVA values (3.0 mgC^{-1}) than watersheds with a lower extent of permafrost (2.4 mgC^{-1}). The higher SUVA values are attributed to a great extent of coniferous vegetation that has a higher aromatic carbon content (hydrophobic compounds) relative to litter produced from deciduous vegetation, which has a lower aromatic carbon content and decomposes faster than coniferous forest litter [*Balcarczyk et al.,* 2009]. Therefore, the higher SUVA values in these three rivers during peak flow conditions likely reflect the large proportion of coniferous vegetation and the higher extent of permafrost within their watersheds, which limits the exchange with soils layers. This higher percentage of permafrost in these watersheds is also reflected by the strong relationship observed between the terrestrially derived PAR-components to (Ad/Al)v ratios and the ^{14}C-DOC age within the Lena and Yenisei (Table 2.2), supporting the notion that leaching is one of the dominant sources of CDOM within these rivers.

In the Kolyma, Ob, and Mackenzie overall lower a_{350}, DOC, and lignin phenol concentrations suggest that vascular plant inputs during freshet were relatively lower within these rivers (Fig. 2.5). Further, the overall lack of a relationship between PAR-

components and the terrestrial biomarkers in the Kolyma and Ob suggest either that DOC sources not represented by the PARAFAC model are important or that individual watershed characteristics control the overall quality of CDOM within these rivers. The Ob further stands out in that it is the only river where the quality of CDOM changes only slightly over the annual hydrograph (Fig. 2.2). The Ob watershed is unique in that it experiences the mildest climate, has the least amount of permafrost (4 – 10 %) within its catchment, contains the largest peat bog system, and is more populated and influenced by industrial activities and agricultural development [*Yang et al.*, 2004]. In addition, most of the lower reaches of the catchment are relatively flat with slopes between 0 – 2 % [*Stolbovi et al.*, 1998], which results in enormous flood plains. The overall lower slope of this watershed results in increased hydrological connectivity during peak flow conditions, which can affect solute transport [*Jensco et al.*, 2009] and result in a longer water residence time. It is possible that increased hydrological connectivity and a longer residence time leads to the removal of the more labile fractions of the CDOM pool during peak discharge. This is likely why we do not see a significant change in a_{350} within the Ob over the different flow regimes. Similarly, this is also likely why we see very little changes in $S_{(275\text{-}295)}$ in the Ob, indicating that the overall molecular weight of the CDOM pool changes very little throughout the year in this river.

In the Mackenzie River, CDOM quality is very different from the other rivers. Overall higher $S_{(275\text{-}295)}$ at lower a_{350} and SUVA values highlights the uniqueness of this river and suggest that the CDOM pool is of a lower molecular weight and less aromatic in nature relative to the other rivers. The Mackenzie is unique with respect to its higher

load of suspended sediments (SPM = 124 10^6t/y; [*Holmes et al.,* 2002]), which could lead to a higher degree of DOM loss, particularly in the hydrophobic/aromatic fraction, via sorption processes. Additionally, the Mackenzie contains a higher abundance of large lakes in its watershed (i.e. open water makes up 10.3% of the Mackenzie catchment based on GCL data; [*Amon et al.,* 2012]). Open water bodies have a longer water residence time than the river itself and tend to act as a buffer for hydrological events [*Gibson and Prowse*, 2002], allowing for more extensive photodegradation, and/or increased microbial degradation of the CDOM pool. Combined, all the above could lead to a preferential removal of the high molecular weight fresh vascular plant derived DOM during freshet, reflected by the overall higher $S_{(275\text{-}295)}$ and lower a_{350} and SUVA values observed in this river. On the other hand, a significant relationship was observed between PARC4 and PARC5 and DOC concentrations during lower flow regimes (data not shown). This combined with elevated BIX (Fig. 2.2, 2.8) and FI (Fig. 2.2) signatures and an elevated microbial fluorescence signal (Fig. 2.4) indicates microbial sources are more important in this river relative to the others, especially during lower flow periods. The observed shift in optical properties thus point to microbial processing, rather than photooxidation and/or sorption processes, as a major transformation pathway of DOM in the Mackenzie.

2.6 Conclusion

The optical properties of DOM indicate an apparent seasonal change in CDOM quality and quantity within large Arctic Rivers. In general, the CDOM pool has a higher molecular weight, is more aromatic, and largely derived from fresh vascular plant DOM sources during peak flow relative to mid and base flow conditions. In addition the Lena and Yenisei clearly dominate in terms of tCDOM discharge to the Arctic Ocean. During low flow periods, the CDOM pool shifts to a lower molecular weight, is less aromatic, and has a greater microbial imprint, especially in the Mackenzie. The overall CDOM character from the different watersheds can be distinguished from each other reflecting variations in climate, vegetation, permafrost extent, topography, and hydrological connectivity. The greater extent of continuous permafrost within the Lena and Yenisei watersheds results in a higher molecular weight, higher aromatic CDOM pool which is largely derived from litter leachates during peak discharge months. In the Ob, increased hydrological connectivity, particularly during spring freshet, and a longer residence time leads to the removal of the more labile fractions of the CDOM pool during peak discharge, which is likely why CDOM quality changes very little throughout the year in this river. The Mackenzie was the most unique river in terms of CDOM quality. Based on the higher abundance of lakes within this watershed, combined with the observed pattern of optical properties, we suggest that microbial processing may be more important for the observed shift in optical properties, rather than photooxidation and/or sorption processes. Based on the results determined during this study, residence times

play a significant role controlling CDOM quality in large Arctic Rivers. This is important in a warming climate, where increased precipitation and hydrological connectivity will likely increase the supply of DOM exported to the Arctic Ocean [*Amon et al.,* 2012]. If this is the case, as atmospheric temperatures continue to increase, it is possible that a significant fraction of the DOC released from permafrost erosion will be remineralized before reaching the Arctic Ocean.

CHAPTER III

THE USE OF PARAFAC MODELING TO TRACE TERRESTRIAL DISSOLVED ORGANIC MATTER AND FINGER-PRINT WATER MASSES IN COASTAL CANADIAN ARCTIC SURFACE WATERS*

3.1 Overview

The optical properties of chromophoric dissolved organic matter (CDOM) were investigated in the Canadian Archipelago and coastal Beaufort Sea surface waters using fluorescence spectroscopy coupled with parallel factor analysis (PARAFAC). Environmental dynamics of individual components were evaluated and compared to salinity, in situ fluorescence, absorption at 312 nm (a_{312}), dissolved organic carbon (DOC) and lignin phenol concentrations. A positive linear relationship between four fluorescent components and lignin phenols suggests a terrestrial origin, whereas two components were unrelated to a river source, suggesting an autochthonous source. Elevated concentrations of terrestrial components were observed in the Mackenzie River plume near the coast of Alaska and decreased as water was transported to the Canadian Archipelago. The two non terrestrial components exhibited only background levels in concentrations along the transect, suggesting minimal productivity within plume and

---

*Reprinted with permission from "Journal of Geophysical Research" by Authors' Walker, S. A., R. M. W. Amon, C. Stedmon, S. Duan, and P. Louchouarn (2009), The use of PARAFAC modeling to trace terrestrial dissolved organic matter and fingerprint water masses in coastal Canadian Arctic surface waters, J. Geophys. Res., 114, G00F06, Copyright [2009] by JGR.

archipelago surface waters. The relative abundance of terrestrial components in relation to non terrestrial components allowed us to distinguish water masses including Atlantic, Archipelago and Mackenzie River plume, respectively. This study illustrates the usefulness of PARAFAC to finger-print water masses based on the optical characteristics of CDOM and shows promise to improve our understanding of upper Arctic Ocean ventilation.

3.2 Introduction

Dissolved organic matter (DOM) is a heterogeneous mixture of compounds which remains largely uncharacterized, yet it plays an active role in the biogeochemistry of the carbon cycle on a global scale [*Hansell and Carlson*, 2002]. It results from a range of processes including algal exudation, viral lysis, grazing and fluvial inputs and its composition varies depending on proximity to source and exposure to degradation processes [*Hansell and Carlson*, 2002]. Colored DOM (CDOM) represents the light absorbing constituent of the DOM pool in natural waters and absorbs light in the ultraviolet and visible wavelength range [*Hansell and Carlson*, 2002]. The optical properties of CDOM have been previously used to predict dissolved organic carbon (DOC) concentrations, distinguish compositional characteristics and discriminate between terrestrial and marine DOM sources [*Ferrari and Dowell*, 1998; *Spencer et al.*, 2008b; *Stedmon and Markager*, 2005a-a]. More recently, the combination of spectroscopic fluorescence Excitation and Emission Matrices (EEMs) with Parallel

Factor Analysis (PARAFAC) has enabled researchers to decompose the combined CDOM fluorescence signal into components corresponding to a chemical analyte, or group of strongly co-varying analytes [*Murphy et al.*, 2007; *Stedmon and Bro*, 2008; *Stedmon et al.*, 2003]. The ability to differentiate and trace sources of CDOM and to determine the underlying factors controlling speciation during its transport and mixing represents a major progress in the field of CDOM biogeochemistry and opens new possibilities for the use of CDOM as a more specific tracer in oceanography.

In this study, we apply parallel factor analyses of EEMs from a set of samples to characterize CDOM throughout the Canadian Archipelago and coastal Beaufort Sea surface waters and to determine its usefulness to trace river water in the Arctic. The Arctic Ocean is an ideal region to study the fate of terrestrial DOM because it receives ~ 11% of the global river runoff, yet it constitutes ~ 1% of the global ocean volume [*Opsahl et al.*, 1999]. Additionally, the concentration of organic carbon in Arctic rivers is relatively high [*Lobbes et al.*, 2000]. Therefore, the flux of terrestrial DOM to the Arctic is much greater than corresponding fluxes to other oceans in the world, but its fate is not entirely clear. Determining the fate of terrestrial DOM in the Arctic is of global importance because a large fraction of terrestrial organic carbon is stored in soils, mostly in the vast permafrost regions around the Arctic, which are susceptible to climate change. As the climate warms, freshwater discharge by large Arctic rivers is predicted to increase, with a ~7% increase already observed [*Peterson et al.*, 2002]. Therefore, increased freshwater discharge combined with permafrost erosion and extended ice-free

periods have the potential to increase the supply of soil organic carbon to the Arctic Ocean.

The dominant source of terrestrial DOM to the coastal Western Arctic is the Mackenzie River in Northern Canada. The Mackenzie is the fourth largest river in the Arctic in terms of discharge [*Gordeev,* 2006] and supplies the coastal Beaufort Sea with approximately 1.4 x 10^9 kgs of DOC per year [*Raymond et al.*, 2007]. A major portion of its fresh water is thought to be exported through the Fram Strait and the Canadian Archipelago [*Cuny et al.*, 2005].

Terrestrial DOM in the Arctic Ocean has been previously traced by determining the concentration of lignin phenols, an important component of vascular plants [*Opsahl et al.*, 1999]. Unfortunately, using lignin phenol analysis to characterize terrestrial DOM is an expensive and arduous process involving large sample volumes and many time consuming steps of sample preparation and analyses. As the chemical nature of CDOM defines its optical properties, the absorbance and fluorescence properties of DOM have become a much more convenient proxy of DOM in the Arctic [*Amon et al.*, 2003; *Spencer et al.*, 2009]. The goal of this study is to determine how the behavior of PARAFAC components compares to lignin phenol trends as a circulation tracer in the Arctic Ocean and to analyze what additional chemical information can be deduced from their spectral character. To investigate various sources contributing to the fluorescence signal, PARAFAC components were related to salinity, absorbance at 312 nm (a_{312}), DOC, and lignin phenol concentrations. This study illustrates how fluorescence paired

with PARAFAC can be used to describe the nature of DOM and demonstrates its potential to characterize surface waters in the Arctic Ocean.

3.3. Methods

3.3.1 *Sample Collection*

Samples were collected during July 8-28, 2005 aboard the Swedish Icebreaker *Oden*. The transect began at 61°05.159'N, 013°32.750'W in the North Atlantic and ended at 70°58.75'N, 145°13.31'W near Barrow Alaska, via the Canadian Archipelago (Fig. 3.1). In situ fluorescence was recorded and discrete surface samples were collected through a stainless steel intake approximately 12 m below the surface. In addition, we collected one surface ice melt sample (0 m) at station 26 (73°25.54'N, -96°16.15'W). Water samples were analyzed for salinity, DOM absorption and fluorescence, DOC and lignin phenol concentrations.

In situ fluorescence was measured using a backscatter fluorescence probe (Dr. Haardt, Optic & Mikroelektonic, Germany) from the seawater intake line. The fluorometer emits light over a broad range of wavelengths and uses a band pass filter to obtain a fixed excitation ranging from 350-460 nm and collects emission at a fixed wavelength of 550 nm +/- 20 nm. These wavelengths were chosen based on empirical calibrations with terrigenous humic substances in order to obtain an optimal signal-to-noise ratio [Amon *et al.*, 2003].

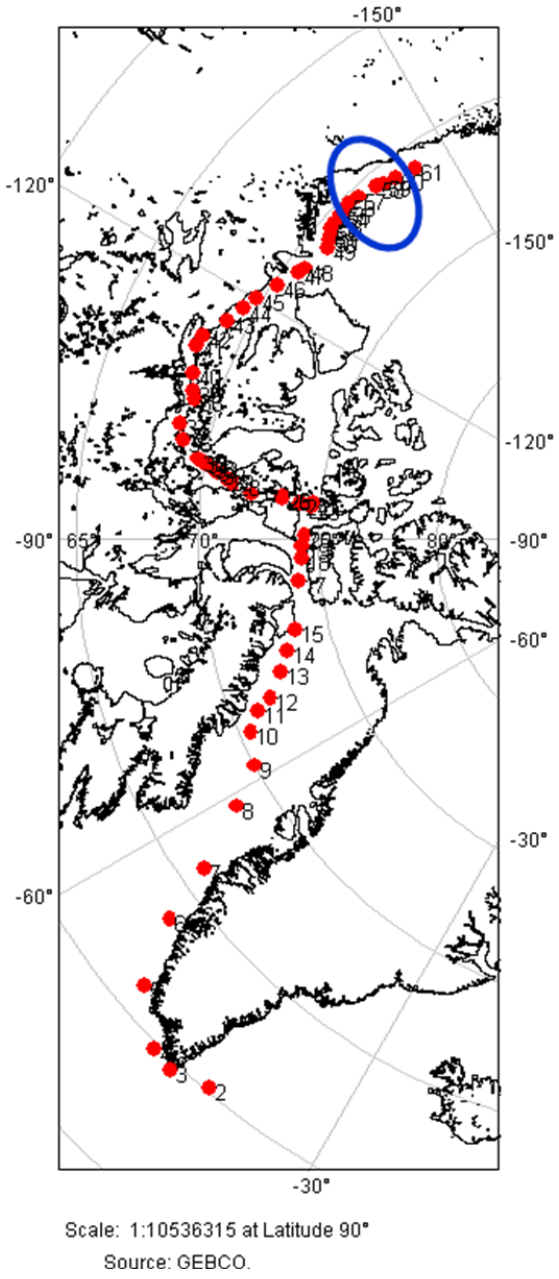

Fig. 3.1. Sample locations during July 8 – 28, 2005. Samples were collected at 12m depth through the ship intake and one surface ice melt collected at station 26. The circled region indicates samples collected within the Mackenzie River plume.

Samples collected for optical properties and DOC were immediately filtered through precombusted 0.7 μm GF/F filters (Whatman) and stored in sealed precombusted glass ampoules at -20°C until analysis in the lab. For lignin samples, 10-15 L of seawater was filtered using a 0.2 μm pore size NuclePore™ filter cartridge, acidified to pH 2.5 using concentrated HCl (reagent grade), followed by solid phase extraction (SPE) using 60 CC/10 gram C18 columns (Varian; [*Louchouarn et al*., 2000]). Cartridges were stored at -20°C until analysis in the lab. Samples for optics, DOC and lignin phenols were analyzed within one year of sample collection.

Spencer et al. [2007a] investigated the effects of freeze/thaw on spectroscopic parameters for fresh water DOM samples with relatively high organic carbon concentrations. They suggest frozen storage of samples for optical properties and DOC concentrations may result in the fading of fluorescence and loss of DOC due to flocculation [*Spencer et al.,* 2007a]. Freshwater DOM samples dominated by somewhat highly colored organic rich samples are typically more prone to flocculation loss during freezing than oceanic samples and therefore, freezing is a common storage method for oceanographic DOM studies [*Amon et al.*, 2003]. Currently, we do not know the long term effects of freezing on fluorescence fading during this study as the recovery sensitivities were not determined but, the loss of DOC during longer time storage at -20°C does not seem to be problematic in the Arctic based on our experience with sample comparisons and mass balances during ultrafiltration.

3.3.2 DOC and Lignin Phenol Analysis

DOC concentrations were determined using a modified MQ-1001 TOC Analyzer [*Peterson et al.*, 2003a; *Qian and Mopper*, 1996a]. Potassium hydrogen phthalate was used as a standard to create a daily calibration curve and deep sea standards supplied by D. Hansell (University of Miami) were un daily to assure quality control. DOC concentrations were calculated using a calibration curve bracketing sample concentrations, followed by subtraction of a Milli-Q blank. The typical coefficient of variation was 3% for samples below 60 μM DOC and the international deep sea standard averaged 47 ± 1.4 μM DOC.

Lignin-derived CuO oxidation products were determined using the method developed by *Hedges and Ertel* [1982] with modifications by *Louchouarn et al.* [2000] and *Kuo et al.* [2008]. Briefly, SPE columns were eluted with 35 ml HPLC grade methanol in to a 250 ml flask, and then dried in a Savant SpeedVac (SC210A). The dried SPE extracts (2-5 mg OC; [*Louchouarn et al.*, 2000]) were mixed with CuO (≈ 300 mg) and $Fe(NH_4)_2(SO_4)_2{\cdot}6H_2O$ (≈ 50 mg) in a stainless steel mini-reaction vessel, to which 8 wt% nitrogen-sparged NaOH solution was added (3 mL). *Trans*-cinnamic acid (3-phenyl-2-propenoic acid) and ethyl vanillin (3-ethoxy-4-hydroxy-benzaldehyde) were used as surrogate standards and were added directly (~3 μg) to each mini-vessel after cooling. The aqueous solution was then acidified with 6N HCl and extracted (x 3) with ethyl acetate. Extracts were dried with Na_2SO_4 and evaporated to dryness using a LabConco™ solvent concentrator. The CuO reaction products were re-dissolved in a small volume of pyridine (300 μL), and a sub-sample was derivatized with *N,O*-

bis(trimethylsilyl)trifluoroacetamide (BSTFA) containing 1% trimethylchlorosilane (TMCS) at 75°C in a heating block (1 h). Separation and quantification of trimethylsilyl (TMS) derivatives of CuO oxidation by-products were performed using gas chromatography-mass spectrometry (GC/MS) with a Varian Ion Trap 3800/4000 system fitted with a fused silica column (VF 5MS, 30 m x 0.25 mm i.d. or 60 m x 0.25 mm i.d.; Varian Inc.). Each sample was injected, under splitless mode, into a deactivated glass liner inserted into the GC injection port and using He as the carrier gas (~ 1.0 mL min^{-1}). The GC oven was programmed from 65°C (with a 2 min initial delay) to 300°C (held 10 min) using a 4°C min^{-1} temperature ramp. The GC injector and GC/MS interface were maintained at 280°C and 270°C, respectively. The mass spectrometer was operated in the electron ionization mode (EI, 70 eV) using multiple reaction monitoring (MRM). Compound identification was performed using GC retention times and by comparing precursor/product spectra with those of commercially available standards. The analytical precision of the major CuO oxidation products and related parameters was derived from replicate analyses of standard estuarine sediments (i.e. NIST SRM 1944; [*Kuo et al.*, 2008]), as well as standard fulvic acid extracts (IHSS 1S101F), and averaged 10% or lower.

Lignin parameters characterized in this study are found in Table 1 and include Sigma6 (Σ6; defined by the sum of six major CuO oxidation products of lignin: vanillin, acetovanillone, vanillic acid, syringaldehyde, acetosyringone, and syringic acid) and Lambda6 (Λ_6, carbon normalized yields of lignin (mg (100mg OC)$^{-1}$)). Λ_6 was used to calculate the percent of terrestrial DOM within a water mass using the formula %tDOM

= (($\Lambda_{6\ Ocean}$/ $\Lambda_{6\ River}$) *100%) according to *Opsahl et al.* [1999].

3.2.3 Optical Measurements

Samples were warmed to room temperature prior to optical analysis. Absorbance measurements were recorded on a Shimadzu UV-2401PC/2501PC using a 5cm quartz cuvette. Absorbance spectra were measured from 200-800nm at 0.5nm increments and were blank corrected using Milli-Q water as a reference. Absorption coefficients (*a*, m-1) were calculated by the formula (2.303*A)/L, where A is absorbance at a specific excitation wavelength and L is the cuvette path length in meters.

Fluorescence measurements were made on a Photon Technologies International Fluorometer (Quanta Master-4 SE) using a 1 cm quartz cuvette with excitation and emission slit widths set to 5 nm. Excitation emission matrix scans (EEMs) for each sample were obtained by collecting a series of emission wavelengths ranging from 230 to 600 nm (2 nm increments) at excitation wavelengths ranging from 220 to 450 nm (5 nm increments). Emission and excitation correction files generated by the manufacturer were applied to each sample EEM to correct for instrument specific biases; the signal was normalized to that from a reference detector during measurement to account for fluctuations in light source characteristics. Due to deteriorating signal to noise ratios, excitation wavelengths below 240 nm and emission wavelengths below 300 nm were removed from the data [*Stedmon et al.*, 2003].

Table 3.1. DOC, lignin phenol, and optical signatures of different water masses in the study area.

	Atlantic	Archipelago	Eastern plume edge	MR Plume	Western plume edge	High salinity in Archipelago	Low salinity in Archipelago	Ice melt (0m)	Mackenzie River*
Salinity	33.5	28.1	25.4	17.1	26.4	29.9	23.0	nm	0
In situ Fmax (V)	62	74	143	255	89	91	67	nm	n.a.
DOC (μM)	59	80	125	243	116	90	70	36	n.a.
a_{312} (m^{-1})	0.47	0.70	2.23	4.85	1.20	0.58	0.75	0.14	n.a.
Σ_6 (μg/L)	0.16	0.28	n.m.	1.84	1.28	0.12	n.m.	n.m.	8.1
Λ_6 (mg (100mg OC)$^{-1}$)	0.030	0.028	n.m.	0.060	0.092	0.011	n.m.	n.m.	0.16
BERC1 (nm-1)	0.012	0.022	0.074	0.17	0.032	0.021	0.023	0.0032	0.56
BERC2 (nm-1)	0.011	0.020	0.058	0.094	0.028	0.019	0.024	0.0034	n.d.
BERC3 (nm-1)	0.0065	0.011	0.036	0.076	0.015	0.010	0.011	0.0012	n.d.
BERC4 (nm-1)	0.0079	0.014	0.026	0.057	0.013	0.019	0.013	0	n.d.
BERC5 (nm-1)	0.031	0.028	0.021	0.056	0.025	0.051	0.021	0.014	n.d.
BERC6 (nm-1)	0.012	0.0097	0.014	0.023	0.0068	0.014	0.0062	0.010	0.02
Group I (nm-1) †	0.0093	0.017	0.048	0.10	0.022	0.019	0.018	0.0020	n.a.
Group II (nm-1) †	0.021	0.017	0.018	0.039	0.016	0.041	0.013	0.012	n.a.

n.m. = not measured; n.a. = not available; n.d. not detected; †average of terrestrial (Group I) and non terrestrial (Group II) fluorescent components; * Fluorescence and lignin data used to represent the Mackenzie River end-member were obtained from the PARTNERS project (Chapter 2). Stations used to represent other end-members are as follows: Atlantic 1 – 8; archipelago 10 – 49; eastern plume edge 50 – 52; MR plume 54 – 59; western plume edge 60 – 61; high salinity archipelago stations 18, 19, 30 and 34; low salinity archipelago stations 37 – 39, 43 and 44; Ice melt (0m) 26.

For many samples, absorption coefficients were high enough to influence the excitation and emission light in the cuvette and therefore an inner filter effect correction was applied [*Lakowicz,* 2006]. An inner filter factor (*I*) was calculated by $I = 10^{-((a\_ex)(0.005)) + ((a\_em)(0.005)))}$, where *a* is the absorption coefficient. *I* was then divided into each excitation emission pair within each EEM. Next, the fluorescence spectra were Raman calibrated by normalizing the data to the area under the Raman scatter peak at excitation wavelength 350 nm of a Milli-Q water sample ran daily [*Lawaetz and Stedmon,* 2009]. To remove the Raman signal, the Raman normalized Milli-Q EEM was then subtracted from each sample EEM, resulting in Raman units (R.U., nm^{-1}). Rayleigh scatter effects were removed by deleting emission measurements at wavelengths less than or equal to excitation wavelengths + 20 nm.

3.3.3 PARAFAC Modeling

This study used the "DOMFluorToolbox" in MATLAB according to the recommendations for data pretreatment and validation given by Stedmon and Bro (2008). A total of 62 samples were used to generate the model. To organize the data for the modeling process, regions of no fluorescence or scatter were removed. This resulted in EEMs that ranged from 240 to 400 nm along the excitation axis and 320 to 580 nm along the emission axis. Next, a region of zeros were inserted in areas of no fluorescence (where excitation >>emission). To aid in correcting second order scatter, emission wavelengths of 550 nm and greater were excluded. Cutting off these higher emission wavelengths greatly reduced the size of the region of missing values, aiding in the

PARAFAC modeling process. Once the data were organized, outlier identification was performed and a six component PARAFAC model was validated using split-half validation and residual analysis.

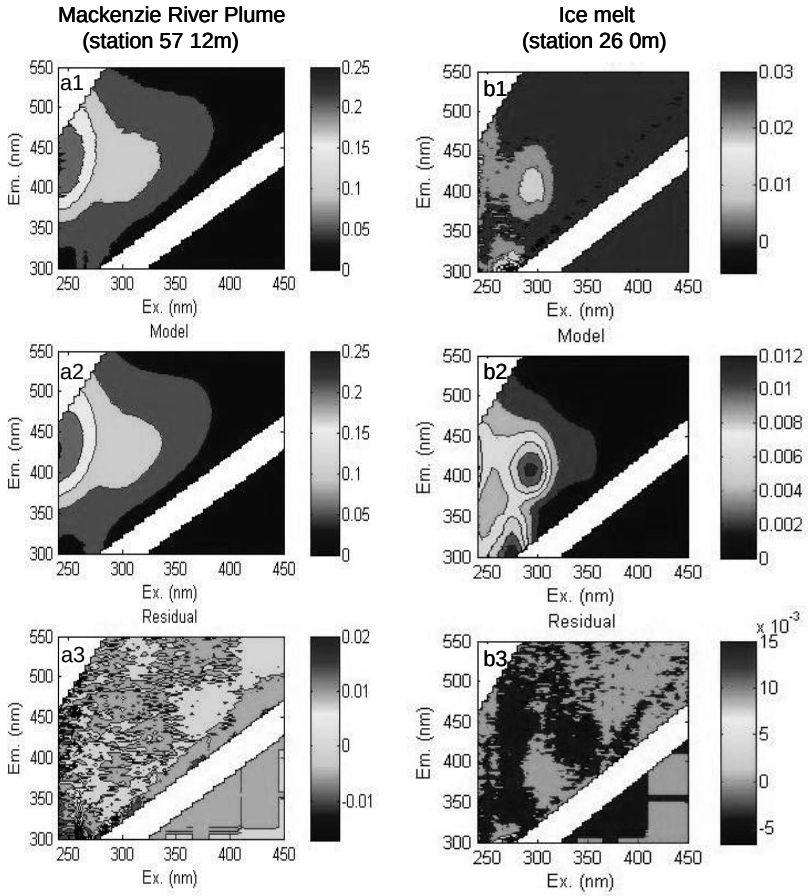

Fig. 3.2. Example of residual analysis. Results for a sample in the Mackenzie River plume (left panel) and an ice melt water sample (right panel): (a1, b1) measured, (a2, b2) modeled and (a3, b3) residual EEMs. Fluorescence is shown in Raman units (R.U., nm-1).

To identify potential outliers, the initially model was run with non-negativity constraints with simple two to four- component models and sample weights for each model were compared. No outlier EEMs were identified during the analysis. A series of PARAFAC models were then run with 2 to 9 components fitted to the data, narrowing down that five to seven components may be adequate to describe the fluorescent variation within the data. Next, split-half validation was used to divide the data into two random halves of equal size and the model was run independently on the two halves. A strong overlapping of component loadings from the two halves provided evidence that a six component model best suited this data set because it did not reflect random noise, rather it reflected the intrinsic variation of the two independent data sets. Further, a seven component model could not be split-half validated. Next, residual analysis was used to help assess how much fluorescence was not being explained by the PARAFAC model. Examples of measured, modeled and residual EEMs for the six component model can be seen in Figure 3.2. Subtraction of the modeled from the measured spectra yielded a residual fluorescence an order of magnitude lower than the measured EEMs. Also, the six component model was capable of characterizing the fluorescence of DOM from two contrasting environments, plume waters versus ice melt, further confirming a six component model is adequate. Because both split-half validation and residual analysis of the EEMs validated a six component model and because the components identified by the model have unimodal emission maxima [*Stedmon and Bro,* 2008], we assume the six component model successfully grouped the fluorophores present in the study area.

3.4 Results

3.4.1 Fluorescence Characterization by PARAFAC

The six components identified by the PARAFAC model are referred to as BERC1 – BERC6 (Fig. 3.3) and their spectral characteristics are compared with those from earlier studies in Table 3.2. Results from previous studies have identified BERC1-BERC3 as being terrestrially derived material. *Stedmon and Markager* [2005a] found a similar component to BERC1 and showed this component to be humic and ubiquitous to a wide range of environments. In a study on surface ocean DOM, *Murphy et al.* [2006] identified a comparable component to BERC2 and defined it as being humic-like and associated it with terrestrially derived DOM. Additionally, *Stedmon et al*. [2007a] found a similar component to BERC2 that was produced after exposing Baltic Sea water to UVA light and suggests it is a common product of terrestrially derived DOM, removed by either microbial or physical processes. Most noteworthy is the wide range of studies that have identified a fluorescent component identical to BER3, suggesting it is ubiquitous to a wide range of environments [*Murphy et al.*, 2006; *Stedmon and Markager*, 2005a; *Stedmon et al.*, 2003; *Stedmon et al.*, 2007a]. In earlier studies, BERC3 has been shown to represent terrestrial humic-like DOM and its production is dependent on the presence and quantity of other humic-like components [*Stedmon and Markager*, 2005a; *Stedmon et al.*, 2007a]. BERC4 has not been reported in previous studies and is grouped with the terrestrial humic-like components based on its positive relation to terrestrial biomarkers used in this study.

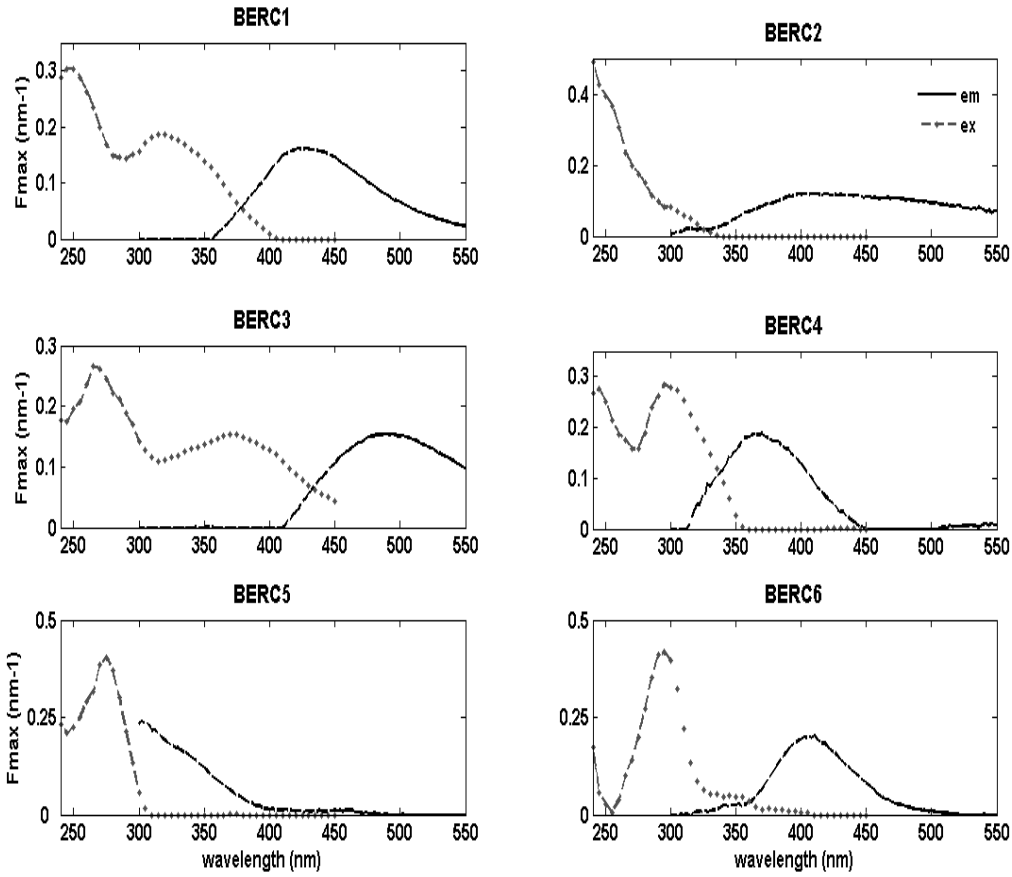

Fig. 3.3. Excitation and emission spectra for the six different fluorescent components identified by the PARAFAC model for Beringia 2005. Intensity is shown as Fmax in Raman units (nm-1).

Table 3.2. Spectral characteristics of the six components identified by PARAFAC compared to previously identified components

Components	Excitation maximum (nm)	Emission maximum (nm)	Stedmon et al., 2003	Cory & McKnight 2005	Stedmon & Markager 2005a	Stedmon & Markager 2005b	Murphy et al., 2006	Stedmon et al., 2007a	Stedmon et al., 2007b	PARTNERS+ Project	Coble (1996)
BERC1	320(250)	428			C4*				C1	PARC1	
BERC2	<240	404			C1*		C9	C6			
BERC3	370(265)	488	C3	SQ2*	C2		C3	C3	C2		
BERC4	295(245)	302									
BERC5	275	302		C8 + C13		C4	C6*	C5			B
BERC6	295(<240)	410								PARC5	M

* Components not exact match

The fluorescence spectrum of BERC5 is similar to the excitation and emission wavelength range of free or protein bound amino acids and therefore may be a mixture of tryptophan and tyrosine. Previous studies have associated this component with microbial activity, indicating autochthonous derived DOM [*Coble,* 1996; *Murphy et al.*, 2006; *Stedmon and Markager*, 2005a]. BERC6 is similar to that of the classic M peak defined by *Coble* [1996] and is defined as a marine humic-like component.

3.4.2 Spatial Variation of Salinity, DOC, DOM Absorption, Fluorescence, and Lignin Phenols

Figure 3.4 (and Table 3.1) illustrates the distribution of salinity, *in situ* fluorescence, the absorbance coefficient a_{312}, DOC, and lignin phenols along the cruise transect at 12 m water depth. All parameters clearly indicate the Mackenzie River plume between station 54 and 59 at around 140°W. Salinity values ranged from 12.2 to 35.2 and averaged 27.9. Higher salinity values were observed in the North Atlantic (salinity of 35.2; station 1), at the southern edge of Greenland within the tip of the East Greenland Current (EGC; average salinity of 34.9; stations 2) and the southeastern side of the Davis Straight in the West Greenland Current (WGC; average salinity of 32.8; stations 3 – 8). Rudels (2001) suggests Atlantic return water flows south within the EGC, which has been shown to mix with Polar surface waters enriched in terrigenous DOM [*Opsahl et al*., 1999; *Amon et al.*, 2003]. Additionally, *Cuny et al.* [2005] reported waters remnant of the Gulf Stream flows north within the WGC which can explain the higher salinities observed at these stations. Within the archipelago, salinity slightly decreased as we

approached the Mackenzie River plume (average salinity of 28.1; stations 10 to 49). Average salinities within the Archipelago are lower than that defined by Rudels (2001) for the outflow through the upper Canadian Archipelago (salinity 32.5 – 33), which likely results from the influence of ice melt at 12m water depth. Salinity values began to decrease slightly between stations 50 – 52 (average salinity 25.4), defining the eastern edge of the plume located near the entrance of the archipelago. A dramatic decrease in salinity occurred between stations 54 to 59, defining the plume region (average salinity 17.1). Between stations 60 – 61 salinity values began to increase slightly, indicating the western edge of the plume located in the coastal Beaufort Sea (average salinity 26.4) and a region more likely influenced by the inflow of Pacific water through the Bering Strait [*Rudels*, 2001; *Yamamoto-Kawai et al.*, 2005].

The optical properties, DOC and lignin phenol concentrations all exhibit an inverse relationship to salinity along the transect, experiencing higher values inside the Mackenzie River plume and lower values within the Archipelago and regions influenced by the Atlantic (Fig 3.4a,b; Table 3.1). All parameters showed minor variations between stations 1 to 49 with an obvious increase between stations 54 to 59. A slight decease occurred at station 60 to 61 for in situ fluorescence, a_{312}, DOC and lignin phenols, once again indicating the western edge of the plume.

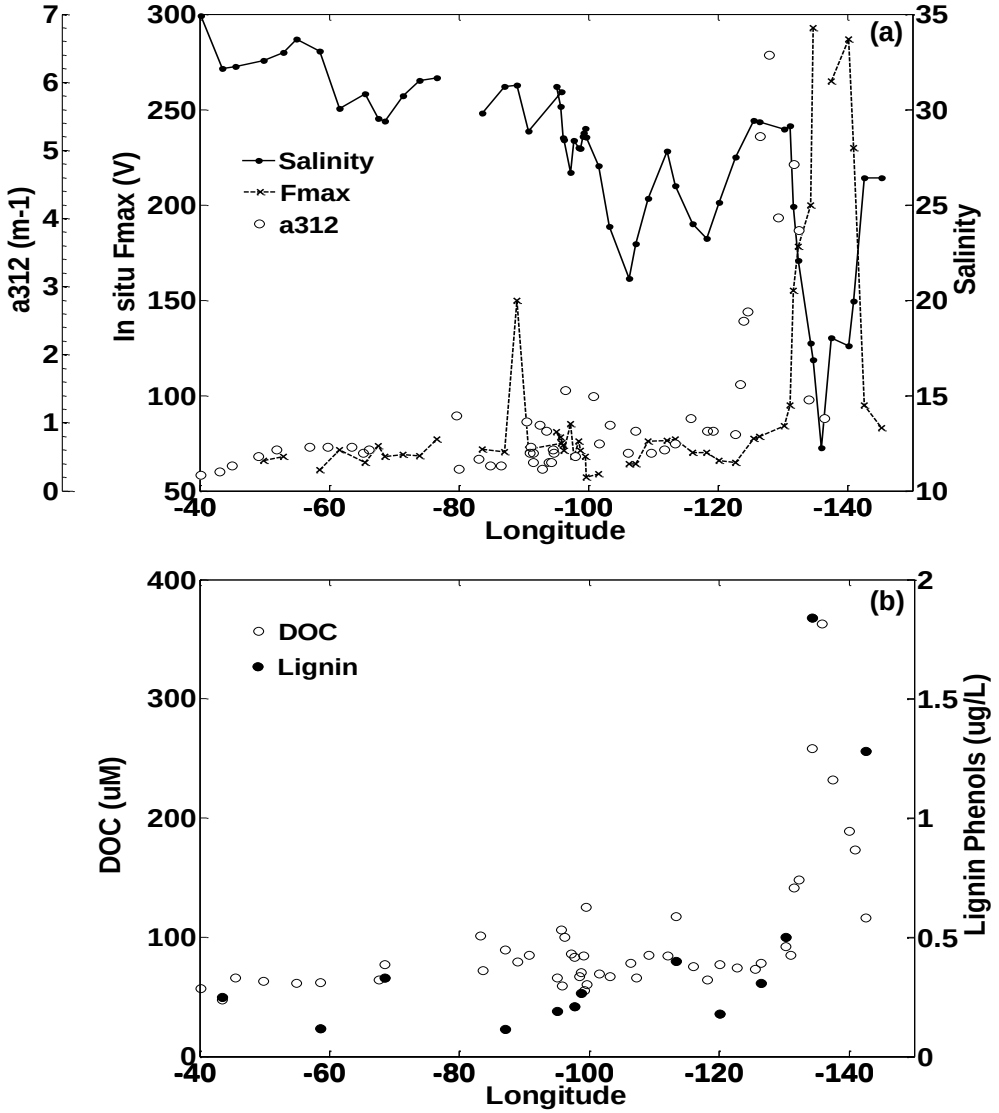

Fig. 3.4. Distribution of (a) salinity, *in situ* fluorescence (Fmax), a_{312} and (b) DOC and lignin phenol concentrations measured at 12 m depth. Clear distinction of Mackenzie plume between stations 54 – 59 (around 140°W).

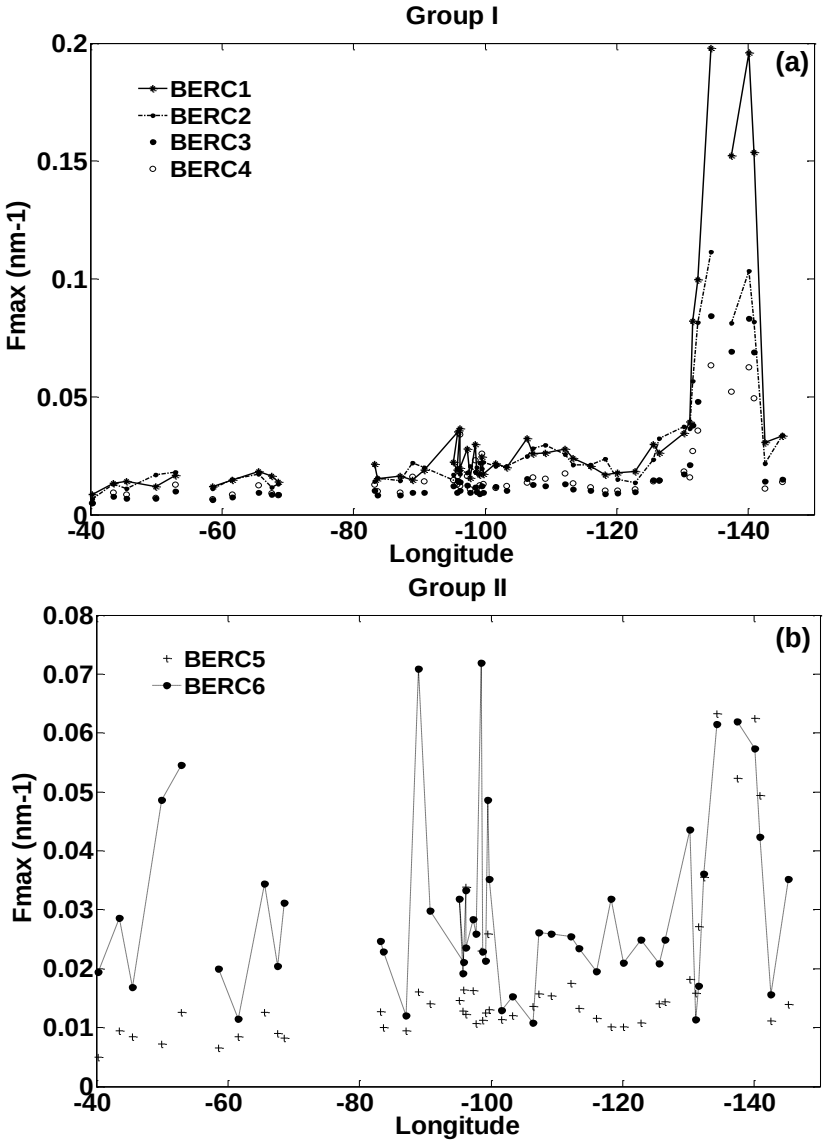

Fig. 3.5. Distribution of PARAFAC fluorescence components, Group I (a) and Group II (b) along the cruise transect at 12m depth. Group I components follow similar trend to terrestrial biomarkers and indicate the Mackenzie River plume between stations 54 – 59 (around 140°W).

The fluorescent components identified can be grouped into two patterns (Fig. 3.5a,b) based on their relation to other parameters in this study. Group I components (BERC1-4) follow the same trend as *in situ* fluorescence, a_{312}, lignin phenol and DOC concentrations, showing higher concentrations in the Mackenzie River plume region and lower concentrations in the archipelago and regions influenced by the Atlantic (Fig. 3.5a). Group II components (BERC5-6) were highly variable along the transect and were less prominent in plume waters relative to Group I components (Fig 3.5b).

3.4.3 Salinity Relationships

The relationship between DOM parameters and salinity was used to identify different end-members present in this study (Fig. 3.6; Table 3.1). It is clear there are two low salinity water masses, including the Mackenzie River Plume (low salinity 17.1, high DOM) and Archipelago surface waters heavily influenced by ice melt (low salinity 28.1, low DOM). Lower salinity samples were identified within the Archipelago region to represent locations mainly influenced by ice melt (salinity 23.0) and higher salinity samples were also identified (salinity 29.9). The one high salinity marine end-member includes waters derived from the Atlantic within the North Atlantic and within the EGC and WGC (high salinity 33.5, low DOM), which are at least partially mixed with Polar Surface Water (PSW). Two areas have been classified as mixing regions due to their moderately higher salinities and lower DOM concentrations relative to plume waters and represent the eastern (entrance to Archipelago; salinity 25.4) and western edge of the plume (coastal Beaufort Sea; salinity 26.4), respectively. The higher salinities observed

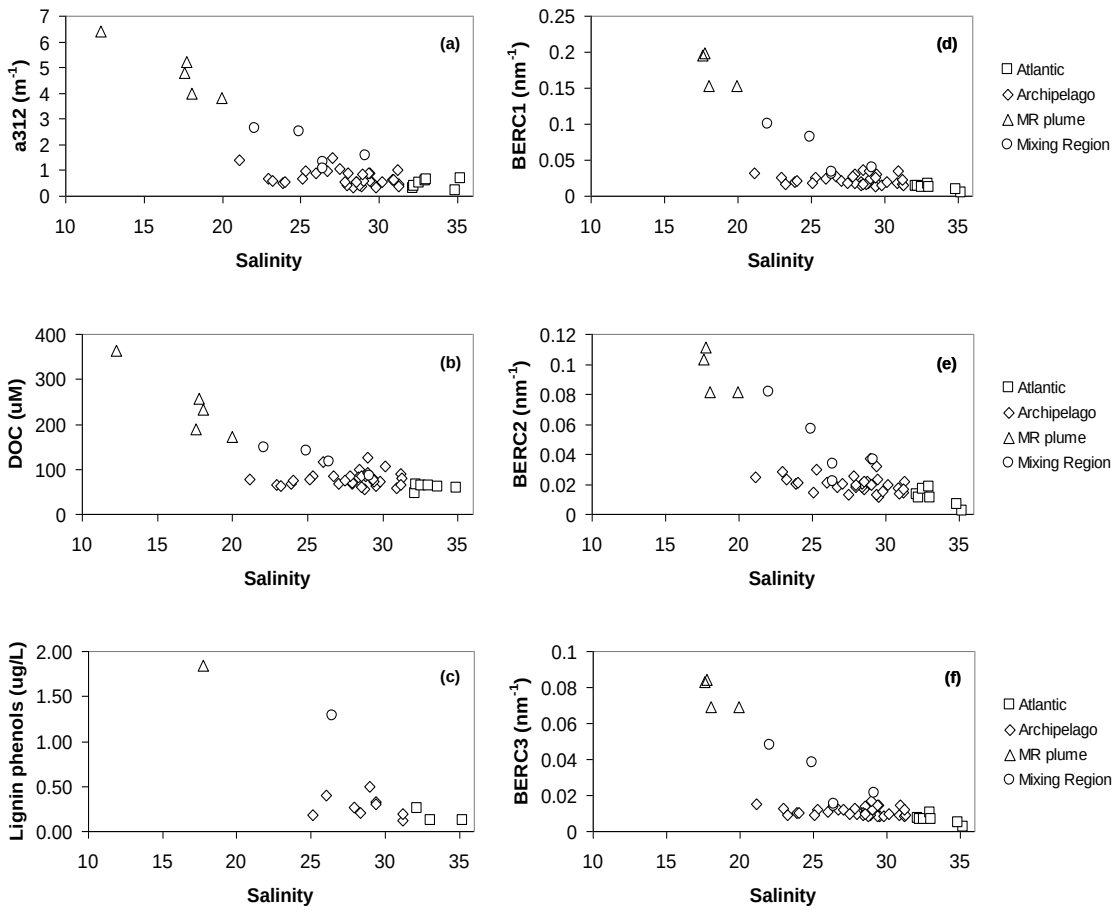

Fig. 3.6. Salinity correlations at 12m water depth. (a) a_{312} verses salinity, (b) DOC verses salinity, (c) Lignin phenols verses salinity, (d) BERC1 verses salinity, (e) BERC2 verses salinity and (f) BERC3 verses salinity. End-members identified include Atlantic (station 1 – 8), Archipelago (stations 10 – 49), Mackenzie River plume (stations 54 – 59) and mixing regions (stations 50 – 52 and 60 – 61).

in Beaufort Sea coastal waters at the western edge of the plume likely results from the influence of Pacific inflow waters which enter through the Bering Strait [*Rudels,* 2001; *Yamamoto-Kawai et al.*, 2005]. The slight decrease in salinity observed in the Beaufort

Sea relative to the Atlantic end-member is reasonable as Pacific water has a lower salinity (32.5) than Atlantic waters (35) [*Rudels*, 2001] and because it is likely Beaufort Sea coastal waters are influenced by plume waters. The samples from the Mackenzie plume were easily distinguishable from the rest of the data and fell along its own mixing line (Fig. 3.6).

Linear regressions were tested for their significance on the Mackenzie plume data and the remaining data (Table 3.3). The Mackenzie plume data had a significant ($P<0.001$) relation to salinity for DOC, a_{312}, and BERC1-4. The regressions for the remaining data (excluding the western plume edge in the costal Beaufort Sea) were not significant ($P>0.01$) for most parameters.

3.4.4 PARAFAC – Terrestrial Biomarker

Optical parameters used to detect terrestrial DOM in this study show a significant relation to salinity and to the concentration of lignin phenols (Fig. 3.6 and Fig. 3.7) in the river plume region. The absorbance coefficient a_{312} (Fig. 3.7a) and fluorescence component BERC1 (Fig. 3.7b) are significantly correlated to the terrestrial biomarker within the plume region, with a_{312}, BERC1 and BERC3 (data not shown) showing the strongest relationship. Lignin phenols, a_{312} and terrestrial component BERC1 show a significant relation to the DOC concentration in the plume region (Fig. 3.7c,d) and explain much of the variability in the DOC data set, with lignin explaining 79% (data not shown), a_{312} 88% (Fig. 3.7c) and BERC1 78% (Fig. 3.7d) of the variability, respectively. The relationship of the optical parameters to DOC is much weaker outside the plume

(Fig. 3.7c,d), indicating the presence of other DOM sources or the preferential removal due to photobleaching of chromophoric DOM during coastal mixing [*Osburn et al.*, 2009].

Table 3.3. Results of the regression analysis carried out between the parameters and salinity. The data were split into two groups; Mackenzie River (MR) plume region (Station 49-59 inclusive) and the remainder (Archipelago; Station 1-48) of the data excluding the Beaufort Sea. Only regressions which were significant ($P<0.01$) are shown.

Parameter	**Data**	**Slope**	**Intercept**	**R^2**
DOC	MR	-14.6	495	0.88
	Archipelago	n.s.	n.s.	
a_{312}	MR	-0.39	12.9	0.95
	Archipelago	n.s.	n.s.	
BERC1	MR	-0.014	0.43	0.96
	Archipelago	n.s.	n.s.	
BERC2	MR	-0.0056	0.20	0.94
	Archipelago	-0.0012	0.052	0.47
BERC3	MR	-0.0056	0.18	0.97
	Archipelago	-0.0003	0.019	0.18
BERC4	MR	-0.0039	0.13	0.94
	Archipelago	n.s.	n.s.	n.s.

n.s. = not significant

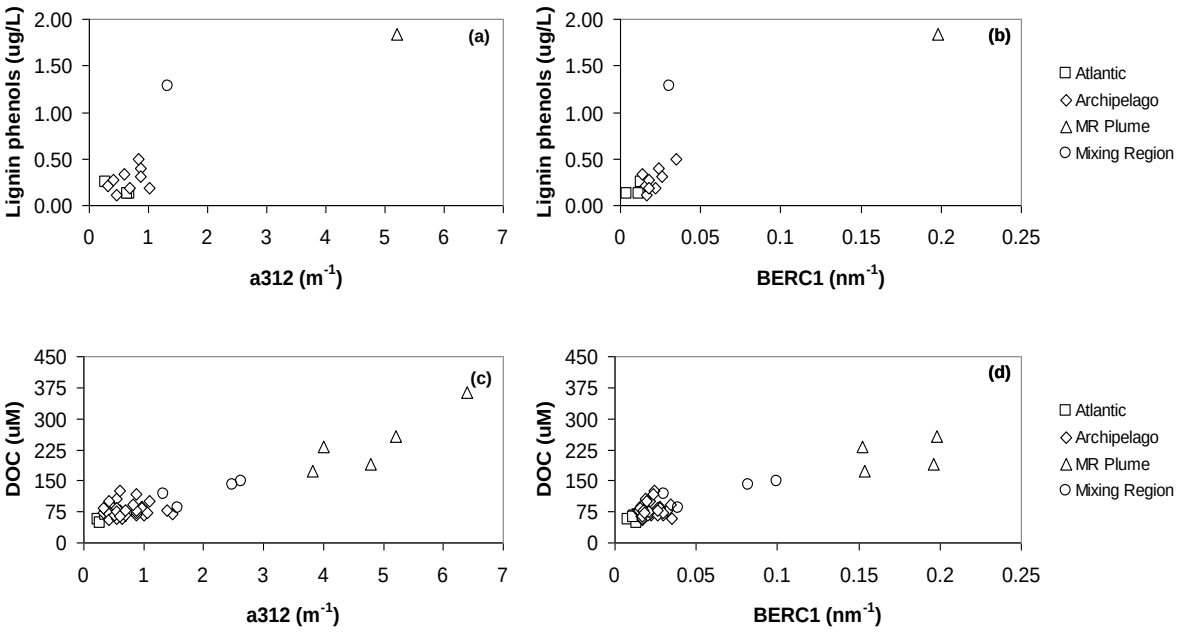

Fig. 3.7. Relationship of optical properties to DOC and lignin phenols. (a) Lignin phenols verses $a_{312,}$ (b) Lignin phenols verses BERC1, (c) DOC verses a_{312} and (d) DOC verses BERC1. Clear distinction of elevated terrestrially derived DOM in plume waters relative to other end-members.

3.5 Discussion

3.5.1 Role of OM Sources for PARAFAC Model Components

Terrestrially derived DOM is mainly responsible for total DOC concentrations within plume surface waters and is less abundant in surface waters found in the archipelago (heavily influenced by ice melt) and surface waters influenced by the Atlantic (Fig. 3.7). Group I components clearly follow the trend of salinity and terrestrial

biomarkers (Fig. 3.4, 3.5) and exhibit a significant positive relation to lignin phenols (Fig. 3.7 b), indicating their link to riverine DOM. Although more data points are required to fully validate the relationship of different PARAFAC model components to lignin phenols, initial results suggest that Group I components have the potential to trace terrestrial organic matter in the Arctic Ocean.

BERC3 showed the strongest relationship to the *in situ* fluorescence signal (data not shown; R^2 0.8) whereas BERC1 was best explained by lignin phenol concentrations (Fig. 3.7 d) and was found to be more relevant in all waters in comparison to the other terrestrial components (Fig. 3.5 a). In addition, a component very similar to BERC1 was identified by a PARAFAC model using data from the 6 largest Arctic rivers, which includes seasonal data and represents peak flow conditions during 2004 and 2005 (Table 3.1, 3.2) (PARTNERS project, chapter 2). Collectively, these results suggest that while all components could be used as a potential proxy of river water in Arctic surface waters, BERC1 may be best suited to track river water being exported from the Mackenzie.

Group II components showed little to no relation to salinity or lignin phenols and were highly variable along the transect (Fig. 3.5b). Both BERC5 and BERC6 are indicative of autochthonous production of DOM [*Stedmon and Markager*, 2005a; *Stedmon et al.*, 2007b] and are not associated with terrestrial biomarkers. Because both components exhibited low fluorescence along the transect, there is likely minimal microbial production within the upper 12m of plume and archipelago surface waters. *Holmes et al.* [2008] describes a substantial seasonal variability in the lability of DOC transported by Alaskan rivers to the Arctic Ocean, with DOC being more labile during

peak discharge in late May to early June when freshet occurs and the majority of DOC is exported, and more refractory during mid to late summer months. While these components are non conservative and cannot be used as a tracer, the low production observed in plume waters likely results from sampling past peak flow conditions.

3.5.2 Relative Contribution of Terrestrially Derived DOM

Carbon normalized yields of lignin oxidation products (Λ_6) have been used in end-member mixing models to estimate the relative contribution of terrestrial DOM (% tDOM) in marine systems, assuming dissolved lignin is removed from seawater at similar rates as riverine DOC [*Opsahl et al.*, 1999]. In our data set, Λ_6 indicates that 37 % of DOM is of terrestrial origin in the plume area, 17 % of DOM in the surface waters of the Archipelago is of terrestrial origin and 19 % is terrestrially derived in waters within the EGC and the WGC. This estimate falls within the range of that reported by *Opsahl et al.* [1999], who estimated 14-24% of the total DOC in polar surface water is terrigenous.

Two avenues have been proposed as possible export routes of polar surface waters with relatively high concentrations of terrigenous DOM, including the EGC and the Canadian Archipelago [*Opsahl et al.*, 1999]. *Amon et al.* [2003] found a fluorescence maximum within the EGC and used the relationship between in situ fluorescence and lignin to show the terrestrial fraction of DOC ranged between 1.5 and 25% in near surface waters in the EGC. Further, *Opsahl et al.* [1999] used lignin oxidation products to show that 9 – 27% of surface waters in the EGC were of terrigenous origin. While our

sampling focused on the upper 12m of Archipelago waters, meaning we likely missed a major portion of the river derived DOM leaving the Arctic Ocean through the Canadian Archipelago, a substantial fraction of DOM in these waters is of terrigenous origin and is comparable to values found in the EGC.

3.5.3 PARAFAC Components as a Finger-Print for Water Masses in the Arctic

In a property/property plot of the two fluorescent component groups different water masses could be clearly distinguished, where Group I is used to represent terrestrially derived DOM and Group II represents marine production in the different water masses (Fig. 3.8). The Atlantic end-member is mainly characterized by low production with minimal fluvial input. The two stations which stand out are 5 – 6 along the coast of Greenland, showing slightly elevated levels of Group II components, indicating a slight increase in production. Results from *Hood and Scott* [2008] suggest that reductions in glacial extent have the potential to deliver increased amounts of labile DOM, which would increase production in near-shore coastal ecosystems and may explain the slight increase in production observed at these stations.

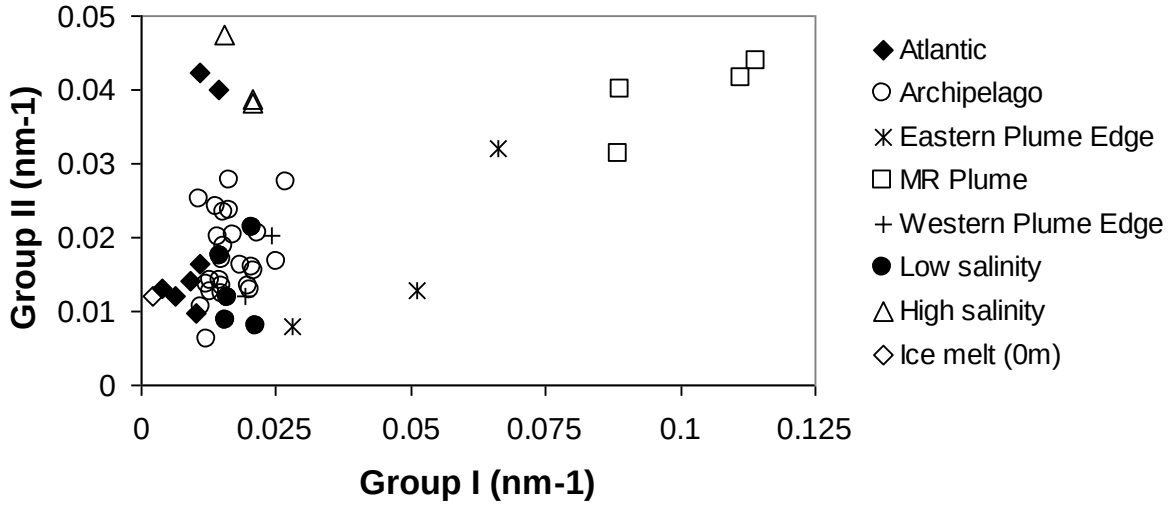

Fig. 3.8. Property/property plot of the two PARAFAC model component groups, Group I and Group II in the different water masses. Group I is an average of terrestrial components BERC1-4 and Group II, associated with autochthonous DOM is an average of BERC5-6 for each sample. Stations used to represent end-members are as follows: Atlantic 1 – 8; archipelago 10 – 49; eastern plume edge 50 – 52; MR plume 54 – 59; western plume edge 60 – 61; high salinity archipelago stations 19, 30 and 34; low salinity archipelago stations 37 – 39, 43 and 44; Ice melt (0m) 26.

Archipelago surface waters are characterized by minimal autochthonous DOM production and low levels of terrestrial DOM which likely results from the influence of ice melt at 12m water depth. Within the Archipelago, ice melt at 0 m has a similar GroupI/GroupII signature as the Atlantic end-member, characterized by little in situ production and minimal fluvial influence and was lower than all other samples within the Archipelago. On the other hand, stations with elevated salinities sporadically identified throughout the archipelago at 12m are characterized by low levels of terrestrial DOM with slightly elevated levels of Group II components relative to plume and

Atlantic waters. We have no information on the microbial community in those samples but, it is possible that primary production and microbial processing of organic matter within sea ice plays a role in the increased levels of Group II components [*Amon et al.*, 2001].

The eastern plume edge mixing region lies between plume and Archipelago end-members, showing a slight increase in both Group I and II components relative to the Archipelago end-member. Plume waters are characterized by a slight increase in production and reflect the abundance of terrestrial DOM being transported from the Mackenzie River to the coastal Arctic Ocean. The western edge plume mixing region, located in the coastal Beaufort Sea, has a similar GroupI/GroupII signature as the Archipelago end-member, which likely reflects the influence of Pacific inflow waters through the Bering Strait. Overall, results indicate a clear distinction of water types based on the relationship between modeled fluorescence components and suggest the usefulness of parallel factor analyses of EEMs to finger-print water masses in the Arctic Ocean where DOM is characterized by a variety of sources and alterations [*Amon and Meon*, 2004].

3.6 Conclusion

This study illustrates the potential of parallel factor analysis of EEMs to deliver model fluorescence components that can be related to biomarkers, in particular to lignin phenols. To date, there are limited studies which relate CDOM and lignin phenols

concentrations [*Hernes and Benner*, 2003; *Spencer et al.*, 2008b; *Spencer et al.*, 2009; *Spencer et al.*, 2007b] and this is the first known attempt to relate PARAFAC components to this unambiguous tracer for terrestrial organic matter. Because the analysis of lignin is expensive, requires large water samples and is extremely labor intensive, the use of EEMs combined with PARAFAC can deliver a valid proxy for lignin phenols and most importantly can greatly increase sample resolution. Results from this study provide evidence that, in conjunction with a suitable calibration to lignin phenol measurements, PARAFAC components are a valuable asset for tracing the distribution of terrestrial organic matter in the Arctic Ocean, even when environmental concentrations are low.

Components derived in this study were grouped into two classes based on sources, allowing for the distinction between terrestrial and marine derived DOM. Lignin parameters agree well with 4 of the derived fluorescent components tracing the influence of the Mackenzie River along the coastal Beaufort Sea into the Canadian Archipelago. Two components seem to be related to autochthonous DOM and suggest minimal production within surface waters at 12m water depth. The relationship between the two groups of fluorescent components allowed us to distinguish different water masses encountered in this study and indicates the potential of this approach to trace water masses on a larger scale in the Arctic Ocean.

CHAPTER IV

RESOLVING CHROMOPHORIC DISSOLVED ORGANIC MATTER (CDOM) COMPONENTS ACROSS THE ARCTIC BASIN: THE USE OF PARAFAC TO TRACE RIVER RUNOFF WITHIN THE INTERIOR ARCTIC OCEAN

4.1 Overview

The Arctic Ocean receives ~ 10% of the global annual river discharge, which is increasing with global warming [*Peterson et al.,* 2002]. As the climate warms a major shift in the Arctic's hydrological cycle could significantly impact sea ice processes within the Arctic and deep water formation in the North Atlantic. A good constraint on the nature and distributions of freshwater (FW) is therefore paramount to understand the role climate change may play for the Arctic's hydrological cycle. To better understand the distribution and nature of river runoff across the Arctic Ocean, we attempt to use the spatial distributions of terrestrially derived chromophoric dissolved organic matter (CDOM). The optical properties of CDOM were evaluated using Excitation/Emission Matrix (EEM) spectroscopy coupled to Parallel Factor Analysis (PARAFAC) and the quality and fate of CDOM was investigated. Environmental dynamics of individual PARAFAC components were evaluated and compared to *in situ* fluorescence, dissolved organic carbon (DOC), and lignin phenol concentrations. Three components were derived from terrestrial CDOM sources and associated with runoff waters and three were associated with autochthonous/microbial CDOM sources. In the polar surface water

(PSW) layer of the Eurasian Basin (EB), an elevated terrestrial CDOM signal points to the presence of Eurasian river CDOM entrained within river runoff. In the Canadian Basin (CB), autochthonous/microbial CDOM sources become more important and the terrestrial CDOM signal is much lower relative to the EB.

4.2 Introduction

The Arctic Ocean receives 3300 km^3 yr^{-1} of river discharge [*Aagaard and Carmack*, 1989] equivalent to ~ 10% of the global river discharged annually [*Opsahl et al.*, 1999a]. At the same time, atmospheric temperatures have increased at a faster rate in the Arctic region than the global mean [*Polyakov et al.*, 2004], resulting in an increase in freshwater (FW) discharge to the Arctic by up to ~7% [*Peterson et al.*, 2002]. Increased FW discharge to the Arctic could have a significant impact on the ventilation of the upper Arctic Ocean and the Nordic Seas. This is important because the Arctic Ocean and Nordic Seas play an important role in the global FW cycle [*Woodgate and Aagaard*, 2005] and Atlantic meridionial overturning circulation (AMOC) [*Aagaard and Carmack*, 1994], and can influence sea ice dynamics and climate patterns on a global scale.

FW sources to the Arctic Ocean include salinity deficient-Pacific water (relative to the inflow of salty Atlantic water), sea ice melt, and runoff waters, predominantly from Eurasian Rivers [*Guay et al.*, 2009]. Much of this FW enters the interior Arctic via lateral processes at the periphery of the basin, such as wind-driven offshore Ekman

transport [*Pickart and Stossmeister*, 2009; *Yang*, 2006] and mesoscale eddies [*Spall et al.*, 2008; *Watanabe*, 2011]. River runoff is one of the dominant FW components in the upper Arctic Ocean [*Jones et al.*, 2008a; *Yamamoto-Kawai et al.*, 2008] as well as the East Greenland Current (EGC) [*Amon et al.*, 2003; *Jones et al.*, 2008b].

In the Eurasian Basin (EB), Eurasian river water enters along the extensive shelf and is advected eastward and subsequently transferred into the Transpolar Drift [*Yamamoto-Kawai et al.*, 2005]. After flowing along the Lomonosov Ridge a significant fraction is ultimately delivered to the North Atlantic via the East Greenland Current (EGC) [*Jones et al.,* 2008b]. As a result, Eurasian runoff is the dominant source of FW in the upper ~ 100 m of the water column in the EB. More recent data from within the Transpolar Drift suggest that surface waters formerly believed to be of Pacific origin, based on alkalinity and nutrients, are more likely to have originated from nutrient rich shelf waters advected into the Arctic interior from the Laptev Sea [*Bauch et al.*, 2011]. These findings suggest that the export of shelf waters containing Eurasian runoff may be more significant for central Arctic Ocean surface waters than previously thought.

A significant fraction of Eurasian runoff waters are also shown to persist within the upper water column in the Canadian Basin (CB) [*Morison et al.*, 2012]. It is proposed that the fraction of Eurasian runoff that does not become entrained within the Transpolar Drift continues to flow eastward along the coast, passing over the Chukchi shelf and subsequently entering the CB [*Morison et al.,* 2012; *Amon et al.,* in prep]. However, the precise mechanisms by which this injection occurs, as well as the geographical area where it happens, are not presently well understood. At the same time,

North American Rivers (most notably the Mackenzie and Yukon) are thought to have little influence on the FW budget of the interior CB. It is believed that they are instead exported toward the Canadian Archipelago via the Alaskan Coastal Current and Beaufort shelf-break jet [*Guay et al.*, 2009; *von Appen and Pickart*, 2012]. However, easterly winds drive offshore Ekman transport into the CB [*Pickart et al.*, 2011], which can flux waters northwestward from the Mackenzie Delta into the Beaufort Gyre [*Guay et al.,* 2009]. This might partially explain the large surface freshening observed during 2006 and 2007 in the southern CB [*Yamamoto-Kawai et al.*, 2009], in concert with the recent dominance of the Beaufort High and the enhanced Ekman transport [*Watanabe*, 2011].

Due to the large river discharge combined with limited light availability, ~ 5 – 22 % of the total terrestrial DOC discharged into the Arctic Ocean persists within surface waters over the central basin and 9 – 27 % within EGC surface waters [*Opsahl et al.*, 1999b]. As a result, ~ 25-33 % of the terrigenous DOC discharged annually to the Arctic has been shown to be exported to the North Atlantic [*Benner et al.*, 2005]. Further, the export of terrestrial DOC from the Arctic to the North Atlantic is thought to be the main mechanism for its removal, rather than photochemical reduction [*Benner et al.*, 2005]. Although, as sea ice cover decreases due to global warming, photoremineralization of terrestrial DOM in the Arctic is predicted to accelerate [*Bélanger et al.*, 2006]. The elevated levels of terrestrial DOM observed within Arctic surface waters combined with its refractory nature, highlight its potential as a tracer for runoff waters in the Arctic and Nordic Seas [*Amon et al.,* 2003].

To better understand DOM quality and its fate within the Arctic Ocean as well as river runoff distributions, the optical properties of chromophoric dissolved organic carbon (CDOM) were evaluated during the Arctic Ocean Section (AOS) 2005 transect. To our knowledge this is the first time CDOM has been characterized on a basin scale for this region. Here we present results using Excitation/Emission Matrix Spectroscopy (EEM's) coupled to a recent technique, Parallel Factor Analysis (PARAFAC). PARAFAC is a multivariate technique capable of decomposing the combined CDOM fluorescence signal into specific components that can be traced to a source [*Stedmon and Bro*, 2008; *Stedmon et al.*, 2003].

The objectives of this study were to: 1) Determine PARAFAC component sources and distributions across the upper Arctic Ocean, 2) Investigate the underlying factors controlling PARAFAC component speciation during transport and mixing, 3) Determine if PARAFAC components can be used to trace river runoff across the upper Arctic Ocean, and 4) Compare and contrast PARAFAC runoff distribution estimates to estimates based on traditional tracer techniques.

4.3 Methods

4.3.1 Sampling Collection

Samples were collected from the 21st of August to the 23rd of September 2005 aboard the Swedish Icebreaker Oden. The transect began at 71.384N, -152.293W in Barrow Alaska and ended at 81.853N, 33.536W in Svalbard (Figure 4.1). Discrete

optical samples, collected using a CTD rosette, were immediately filtered through precombusted 0.7 mm GF/F filters (Whatman), and were stored in sealed precombusted glass ampoules at -20°C until analysis in the lab. Water samples were analyzed for dissolved organic carbon (DOC; [*Amon et al,.* in prep]), DOM absorption and fluorescence, lignin phenols [*Amon et al*., in prep], and salinity.

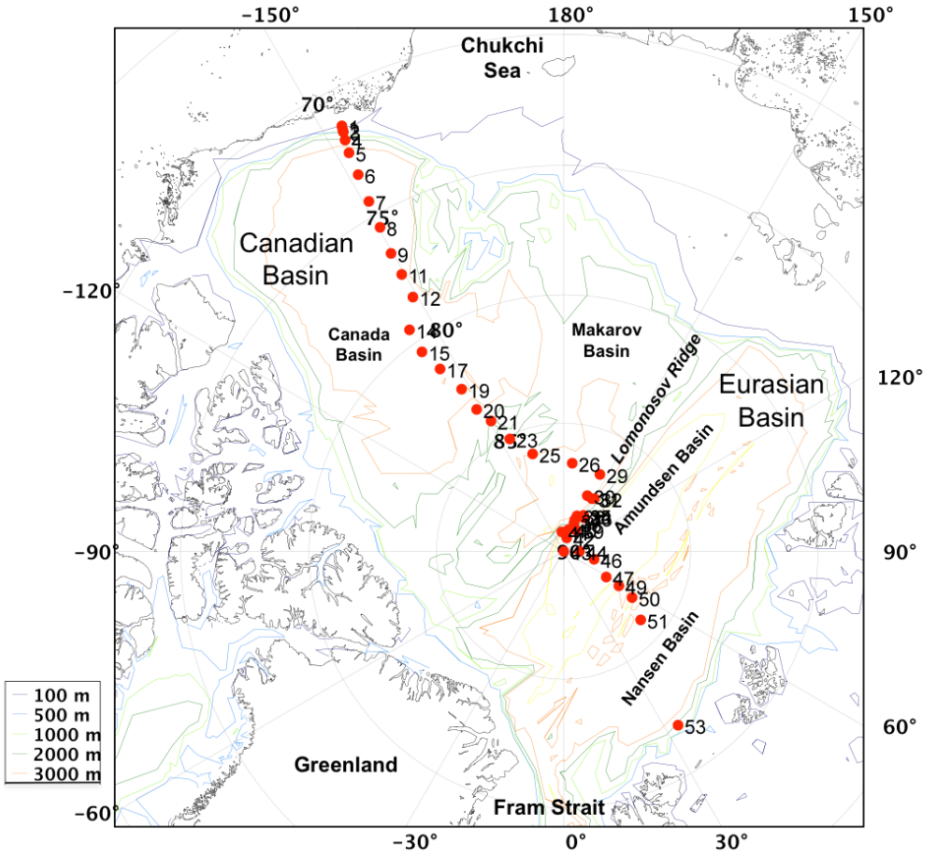

Figure 4.1. Map of stations locations during AOS 2005.

4.3.2 Dissolved Organic Carbon (DOC)

DOC concentrations were determined using a modified MQ-1001 TOC Analyzer [*Peterson et al.*, 2003b; *Qian and Mopper*, 1996b]. Potassium hydrogen phthalate was used as a standard to create a daily calibration curve and deep sea standards supplied by D. Hansell (University of Miami) were run daily to monitor instrument performance. DOC concentrations were calculated using a calibration curve bracketing sample concentrations, followed by subtraction of a Milli-Q blank. The typical coefficient of variation was 3% for samples below 60 mM DOC and the international deep sea standard averaged 47 ± 1.4 mM DOC.

4.3.3 In situ *Fluorescence*

In situ fluorescence was measured using a backscatter fluorescence probe, which emits light over a broad range of wavelengths. A band pass filter is used to obtain a fixed excitation ranging from 350-460 nm and a fixed emission at a wavelength of 550 nm +/- 20 nm. These wavelengths were chosen based on empirical calibrations with terrigenous humic substances [*Amon et al.*, 2003].

4.3.4 Optical Measurements

Absorbance measurements were determined using a Shimadzu UV-2401PC/2501PC with a 5 cm quartz cuvette. Absorbance wavelengths were obtained from 200 to 800 nm at 0.5 nm increments and were blank corrected using Mill-Q

containing < 1 ppb of carbon as the reference. Absorption coefficients *(a)* were calculated by using equation (4.1):

$$a = (2.303*A)/L, \quad (4.1)$$

where A is absorbance at any particular wavelength and L is the cuvette path length in meters. Excitations/Emission Matrix spectroscopic measurements were generated using a Photon Technologies International Fluorometer (Quanta Master-4 SE) using a 1 cm quartz cuvette with excitation and emission slit widths set to 5 nm. Excitation emission matrix scans (EEMs) for each sample were obtained by collecting a series of emission wavelengths ranging from 230 to 600 nm (2 nm increments) at excitation wavelengths ranging from 220 to 450 nm (5 nm increments). Emission and excitation correction files generated by the manufacturer were applied to each sample EEM to correct for fluctuations in light source intensity. Post acquisition, raw EEM's were exported to Matlab, Raman calibrated, corrected for inner filter effects, Rayleigh and Raman scatter, and organized for the modeling process according to *Walker et al.* [2009] (Chapter III). An example of corrected EEM's from two distinct types of samples collected during AOS 2005, a terrestrial DOM verses a marine DOM dominated signal, is shown in Fig. 4.2.

4.3.5 Parallel Factor Analysis (PARAFAC) Modeling

This study used the "DOMFluorToolbox" in MATLAB according to *Stedmon and Bro* [2008] and outlier identification and model validation was performed according to *Walker et al.,* [2009]. The PARAFAC analysis was conducted on 327 samples and no

outliers were identified using the leverage plots. A six component model was derived and validated using split-half validation and the model fit was assessed by residual analysis, where the model was capable of characterizing the fluorescence behavior of CDOM from two contrasting environments, including a terrestrial and a marine dominated environment (Fig. 4.2). A strong overlapping of component loadings during split-half validation provides evidence of the model best suited for the data set. Using residual analysis subtraction of the modeled from the measured spectra yielded a residual fluorescence an order of magnitude lower than the measured EEMs (Fig. 4.3). Based on these results, we assume the model successfully grouped the fluorophores present in the study area.

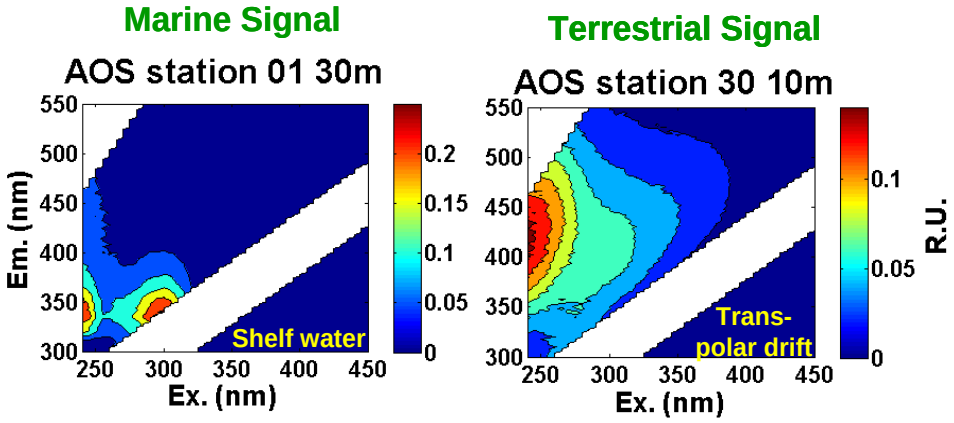

Figure 4.2. Example of a terrestrial verses a marine dominated EEM signal collected during the AOS 2005 trans-Arctic transect. Intensity is shown in R.U. (nm $^{-1}$).

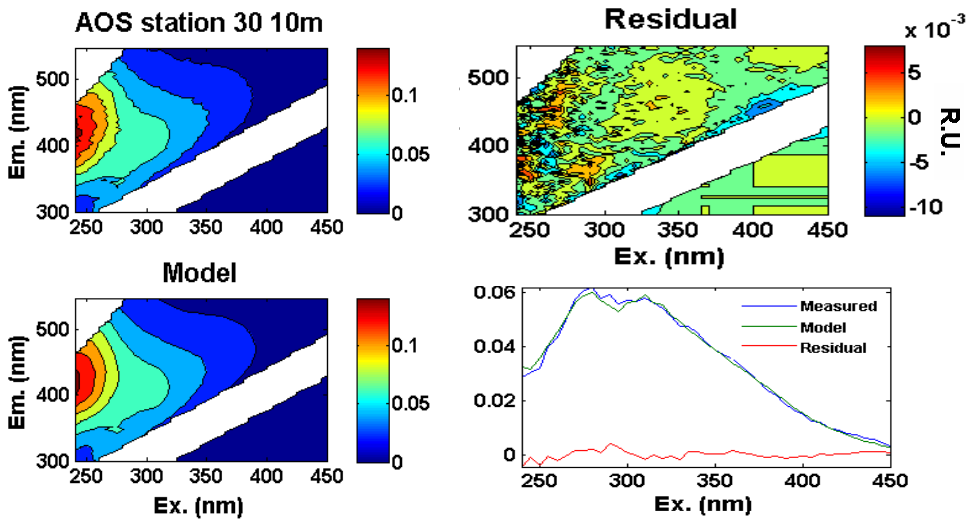

Figure 4.3. Example of a measured, modeled, and residual EEM after the validation of a six component model for the AOS 2005 trans-Arctic transects. AOS station 30 at 10 m was collected in the Trans-Polar Drift and intensity is in Raman Units (nm^{-1}).

4.3.6 PARAFAC Components Relationships to Lignin Biomarkers

In an attempt to characterize CDOM sources we related the PARAFAC components to lignin phenol concentrations (Σ8: defined by the sum of the cinnamyl, syringyl, and vanillyl phenols; [*Amon et al.,* in prep]). Lignin phenols are an important component of vascular plants and an unambiguous terrestrial biomarker. Alkaline CuO oxidation of DOM and the quantification of lignin oxidation products (LOP) were performed according to *Louchouarn et al.* [2000, 2010] and *Kuo et al.* [2008]. Using this approach, the determined six major LOP's include vanillin (Vl), vanillic acid (Vd), acetovanillone (Vn), syringealdeyde (Sl), syringic acid (Sd), acetosyringone (Sn).

4.3.7 Water Mass Identification

Water mass identification was based on salinity values reported by *Rudels,* [1996 and 2001] and were evaluated in the EB (station 25 – 53) and CB (station 1 – 21). In the EB, water masses include a polar surface water layer (PSW; salinity range 32.10 to 33.00), halocline water layer (HWL; salinity range 31.04 to 34.33), and an Atlantic layer (Atl; salinity range 34.50 to 34.85), whereas the CB water masses include a polar surface water layer (PSW; salinity range 19.09 to 31.90), upper halocline water layer (UHW; salinity range 32.03 to 33.29), lower halocline water layer (LHW; salinity range 33.80 to 34.56), and an Atlantic layer (Atl; salinity range 34.76 to 34.86). Distinctions between the different water masses were apparent in terms of average water mass depth distributions. In the CB, the PSW layer and mainly the halocline layer are much thicker and penetrate to deeper depths relative to the EB. The deeper depth of the halocline layer observed in the upper CB relative to the EB likely results from the large reservoir of freshwater thought to be stored within the Beaufort Gyre [*Yamamoto-Kawai et al.*, 2005].

4.3.8 Statistical Analysis

To investigate the quality of PARAFAC components a linear regression analysis was performed in excel. PARAFAC component loadings were related to the *in situ* fluorescence signal, DOC and lignin phenol concentrations [*Amon et al.,* in prep], total CO_2 concentrations [*Jones et al.*, 2008a], and apparent oxygen utilization (AOU) estimates. To associate PARAFAC components to different water masses present within

the Arctic Ocean a correspondence analysis was performed in R using the Vegan toolbox and was based on Chi-squared distance. For this analysis, we loaded the relative percent contribution of the individual components within in each sample (including samples from 0 to 300 m water depth) as the species variables. Next, environmental parameter vectors were fit onto the ordination space, where the arrow points to the direction of most rapid change of each parameter and the length represents the strength of the gradient. Environmental parameters include salinity and *in situ* fluorescence vectors, where both relationships to components were significant ($P < 0.01$). PARAFAC components grouped at a low salinity and high *in situ* fluorescence signal were associated with runoff waters, components grouped at a high salinity and low *in situ* fluorescence signal were associated with marine waters, and components grouped at a low salinity and low *in situ* fluorescence were associated with ice melt waters.

4.4 Results

4.4.1 Fluorescence Characterization by PARAFAC

Six unique fluorescent components were identified by the PARAFAC model and are referred to as AOS-components (AOSC1 – AOSC6; Fig. 4.4). The spectral characteristics of individual AOS-components are compared with those from earlier studies in Table 1. AOSC1 has an excitation peak at 305 nm and < 295 nm with an emission peak at 344 nm. AOSC2 has a primary excitation peak at < 240 nm and secondary peak at 290 nm with an emission peak at 408 nm. AOSC3 has a primary

excitation peak < 240 nm and a secondary peak at 360 nm with a an emission peak at 472 nm. AOSC4 has an excitation maximum at 275 nm with an emission peak at 300 nm. AOSC5 has a primary excitation peak 330 nm and secondary peak < 240 nm with a peak at 408 nm. AOSC6 has a primary excitation peak 295 nm and secondary peak < 240 nm with a peak at 408 nm. AOSC2, AOSC3, and AOSC5 all exhibit a humic-like terrestrial fluorescence signal [*Coble,* 1996; *Walker et al.,* 2009] whereas AOSC1, AOSC4, and AOSC6 all exhibit a more marine like fluorescence signal [*Coble,* 1996].

4.4.2 PARAFAC Components – Spatial Distributions and Source Identification

To investigate how the individual PARAFAC components were associated with the different FW components in the upper Arctic, their average loading values (Fig. 4.5) and depth distributions were evaluated within different water masses (Fig. 4.6 and 4.7). In the EB, AOSC2 was the dominant component in the PSW (average 0.36 nm^{-1}; Fig. 4.5 a) and HWL (average 0.29 nm^{-1}; Fig. 4.5 a) and explained on average ~ 33 % of the fluorescence signal in these water masses (Fig. 4.5 b). In the Atlantic layer of the EB, AOSC2 becomes less significant and AOSC1 (average 0.24 nm^{-1}; Fig. 4.5 a)) and AOSC4 (average 0.20 nm^{-1}; Fig. 4.5 a) were the dominant components, explaining ~ 44% of the fluorescence signal in this water mass (Fig. 4.5 b). In the CB, AOSC1 was by far the dominant component in all water masses (average 0.55 nm^{-1}; Fig. 4.5 c) and explained on average ~ 45 % of the fluorescence signal in this basin (Fig. 4.5 d). When comparing the components, AOSC1 displayed the largest variability in both basins and within all water masses. When comparing the basins, the terrestrial-like AOS-

components were generally higher in the EB PSW layer and HWL layers relative to all water masses in the CB.

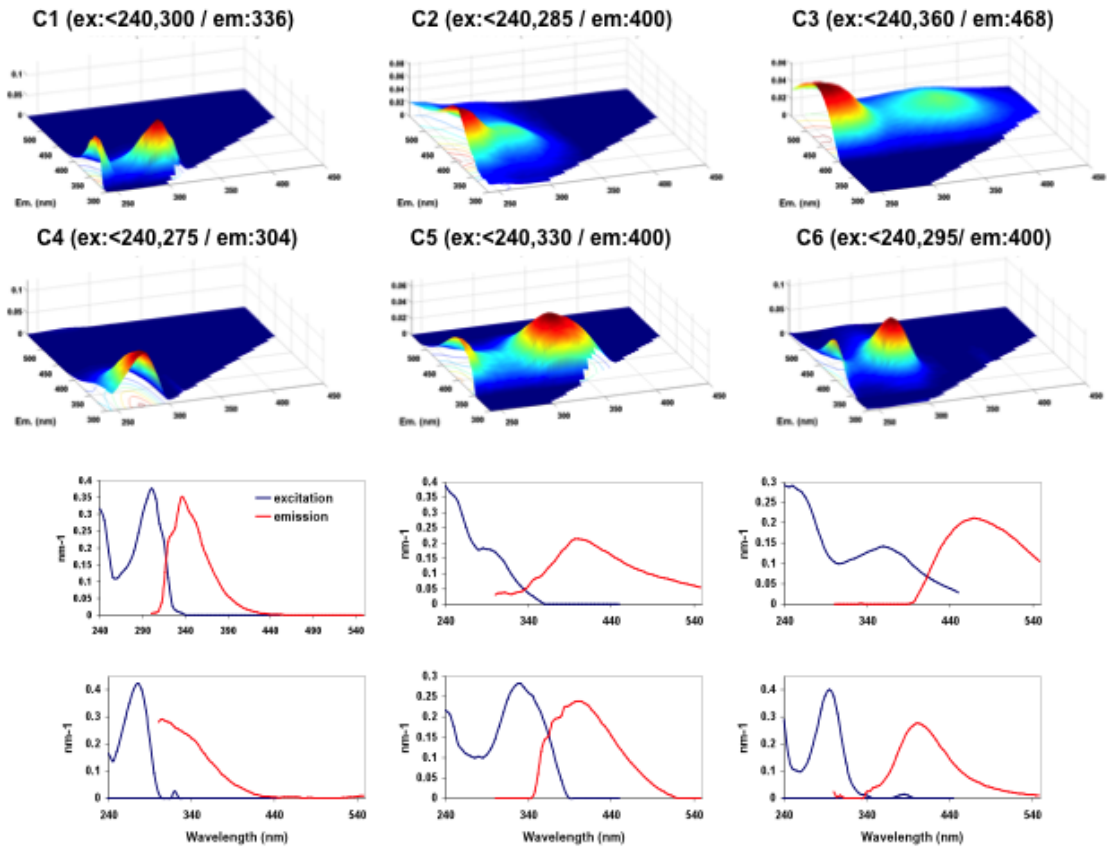

Figure 4.4. EEM's (top panel) and excitation and emission spectra (bottom panel) for the six different fluorescence components identified by the PARAFAC model for AOS 2005. Intensity is shown in Raman Units (nm^{-1}).

Table 4.1. Spectral characteristics of the six components identified by PARAFAC during AOS 2005 and a comparison to previously identified PARAFAC components.

Component	Excitation (nm) maximum (nm)	Emission (nm) maximum (nm)	PARTNERS (chapter1)	Walker et al., 2009	Stedmon et al., 2007a	Stedmon et al., 2007b	Stedmon and Markager 2005a	Coble 1996
AOSC1	305 (<240)	344						B + T
AOSC2	290 (< 240)	408	PARC1*	BERC2	C6		C1*	A
AOSC3	360 (<240)	472	PACR1+PARC3	BERC3	C3	C2	C2	A + C
AOSC4	275	300	PARC5*	BERC5	C5			B
AOSC5	330 (<240)	408	PARC2*	BERC1		C1	C4*	A + C
AOSC6	295 (< 240)	408		BERC6				M

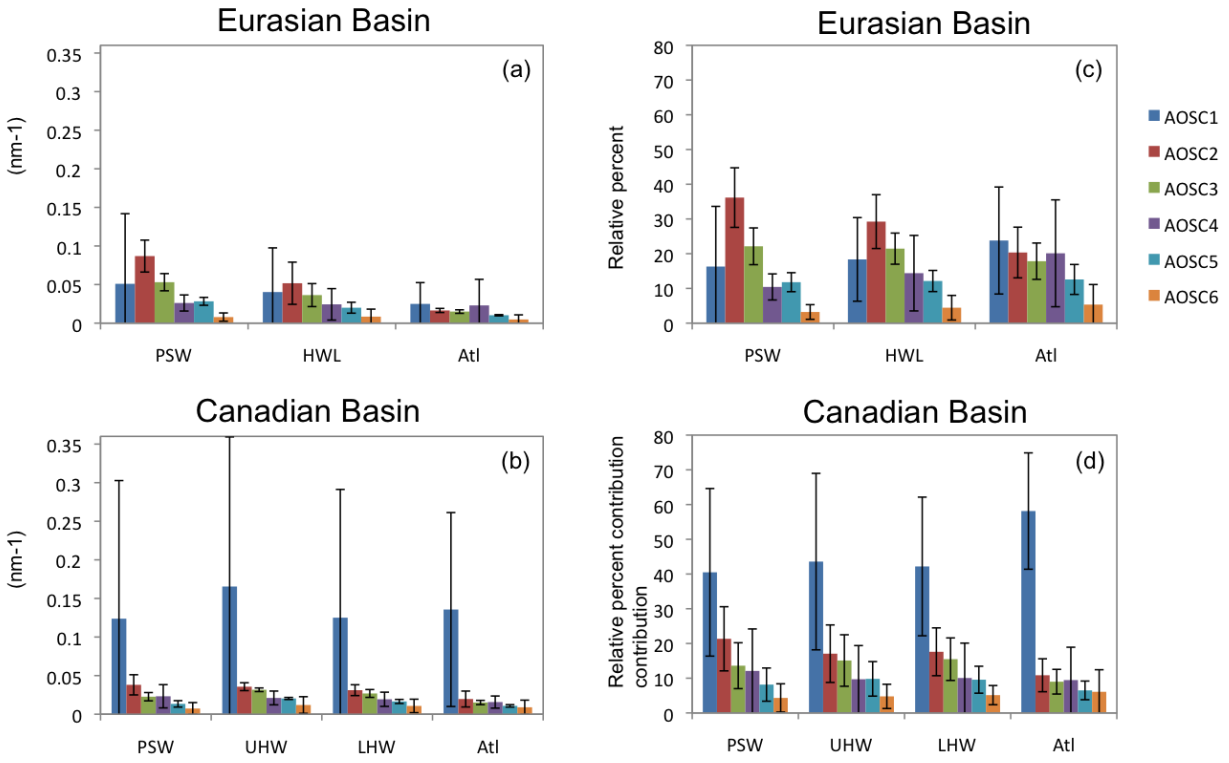

Figure 4.5. Average AOS-component loadings (a,c) and their relative percent contributions (b,d) within the different water mass layers across the upper Arctic Ocean.

For the depth profiles, PARAFAC components were separated into two groups based on source, including a terrestrial-like (AOSC2, AOSC3, AOSC5; Fig. 4.6) and a marine-like group (AOSC1, AOSC4, AOSC6; Fig. 4.7), and plotted to show their depth profiles in the EB and CB. In the EB, the terrestrial-like components were highest in the PSW layer and decreased with depth through the HWL down to the Atlantic layer (Fig. 4.6 a,b,c). In contrast, in the CB the terrestrial-like components (AOSC3 and AOSC5) were lowest in the PSW and Atlantic layers and highest in the UHW and LHW layers

(Fig. 4.6 e,f). AOSC2 differs from AOSC3 and AOSC5 in the CB in that it was slightly higher in the surface and gradually decreased with depth down to the Atlantic layer (Fig. 4.6 d). When comparing the basins, the overall terrestrial-like fluorescence signal in the CB UHW and LHW layers was much lower relative to the EB PSW layer. The depth profiles of the marine-like components differed from the terrestrial-like components in that they did not show a distinct separation between the different water masses. A simple visual comparison of the two basins illustrates that the marine CDOM signal is more predominant throughout the upper CB relative to the EB.

To determine the ability of AOS-components to trace terrestrial CDOM inputs to the Arctic Ocean, we investigated their relation to the *in situ* fluorescence signal, DOC, and lignin phenol concentrations. In the EB, all three AOS terrestrial-like components were related to the *in situ* fluorescence signal (Fig. 4.8 a,b,c), DOC (Fig. 4.9 a,b,c), and lignin phenol concentrations (Fig. 4.10 a,b,c), where AOSC5 exhibited the strongest relation to the in situ fluorescence signal and AOSC2 exhibited the strongest relation to DOC and lignin phenol concentrations. In the CB, AOSC3 and AOSC5 were significantly related to the in situ fluorescence signal (Fig. 4.8 e,f), where AOSC3 exhibited the strongest relation, and AOSC2 was unrelated. Further, no significant relations between the terrestrial AOS-components and DOC (Fig. 4.9 d,e,f) or lignin phenol (Fig. 4.10 d,e,f) concentrations were observed in the CB.

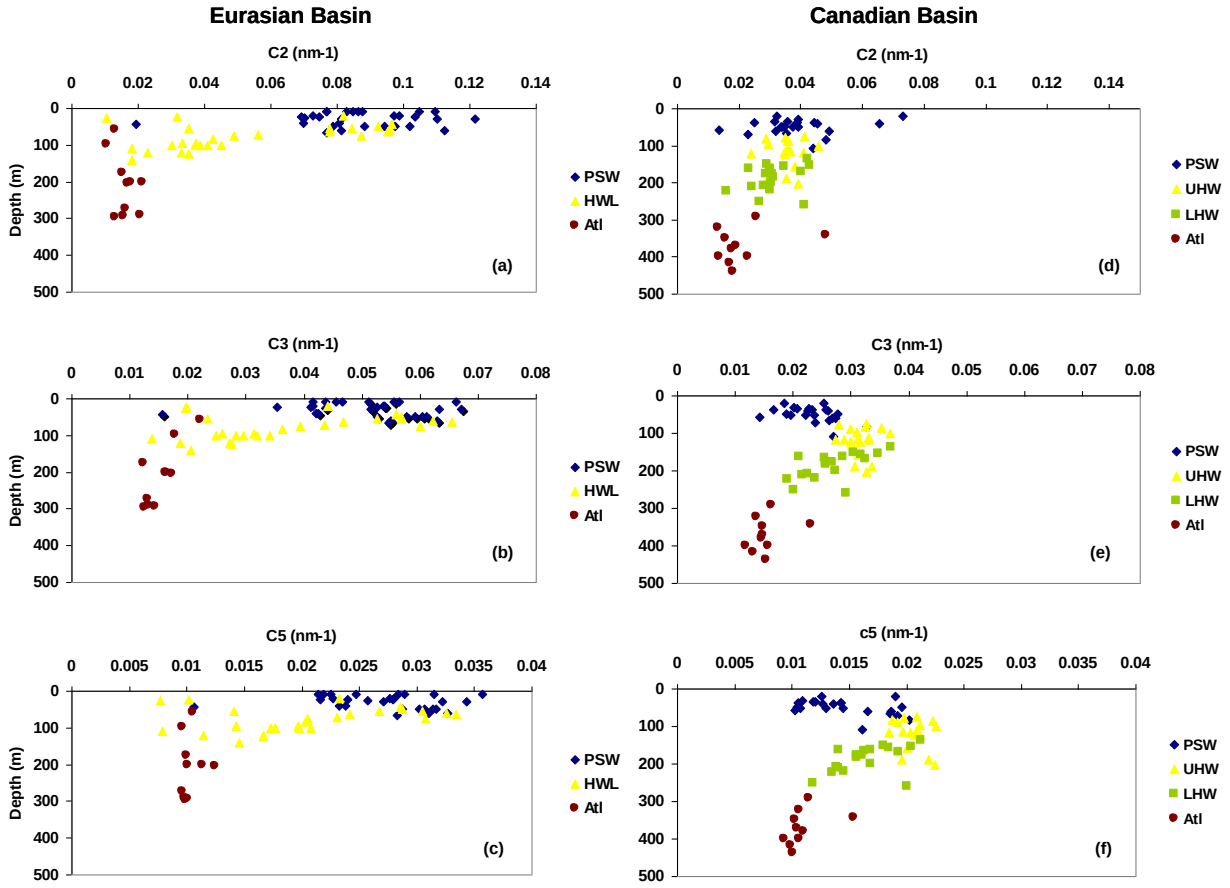

Figure 4.6. Terrestrial AOS-component depth profiles during AOS 2005 in the EB (a,b,c) and the CB (d,e,f). Water masses are separated based on salinity values reported by Rudels 1996 and are illustrated by different colors.

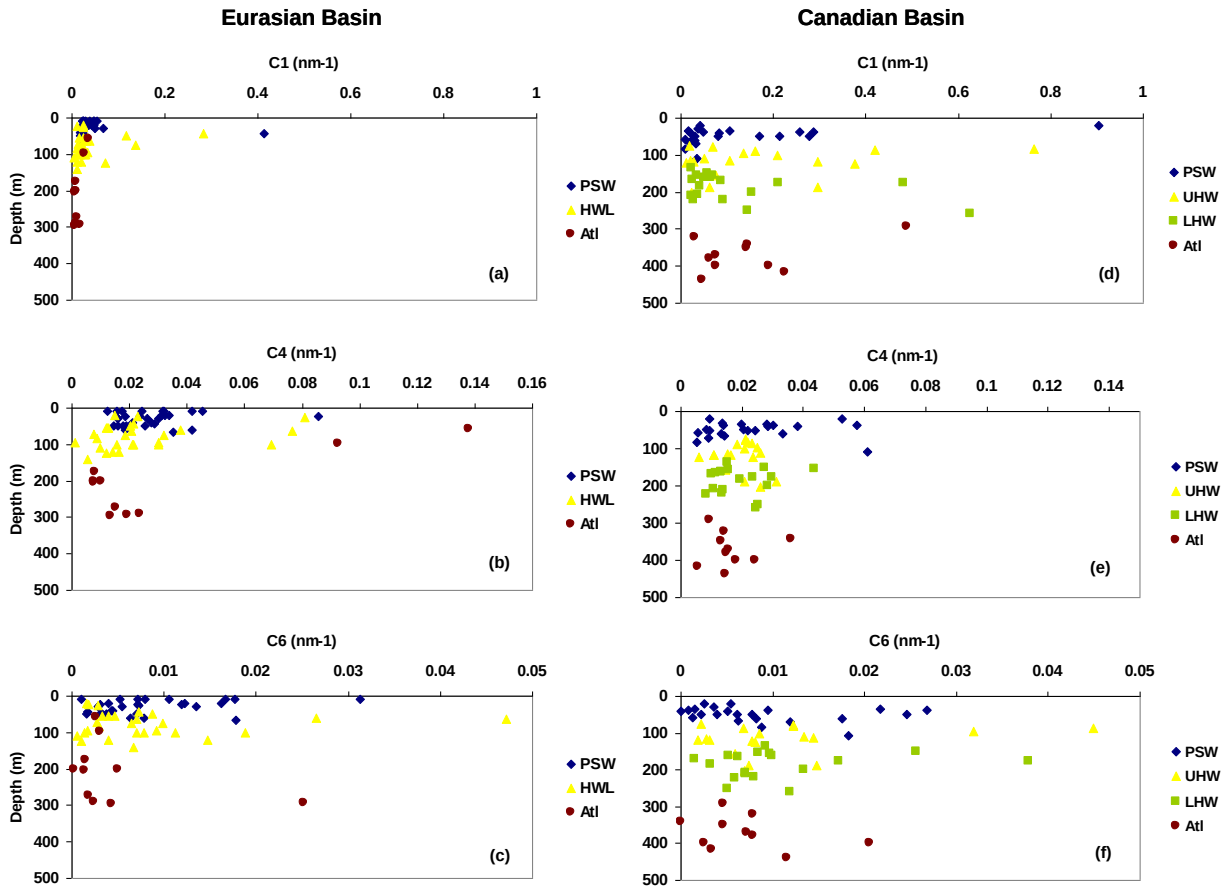

Figure 4.7. Marine AOS-component depth profiles during AOS 2005 in the EB (a,b,c) and the CB (d,e,f). Water masses are separated based on salinity values reported by Rudels 1996 and are illustrated by different colors.

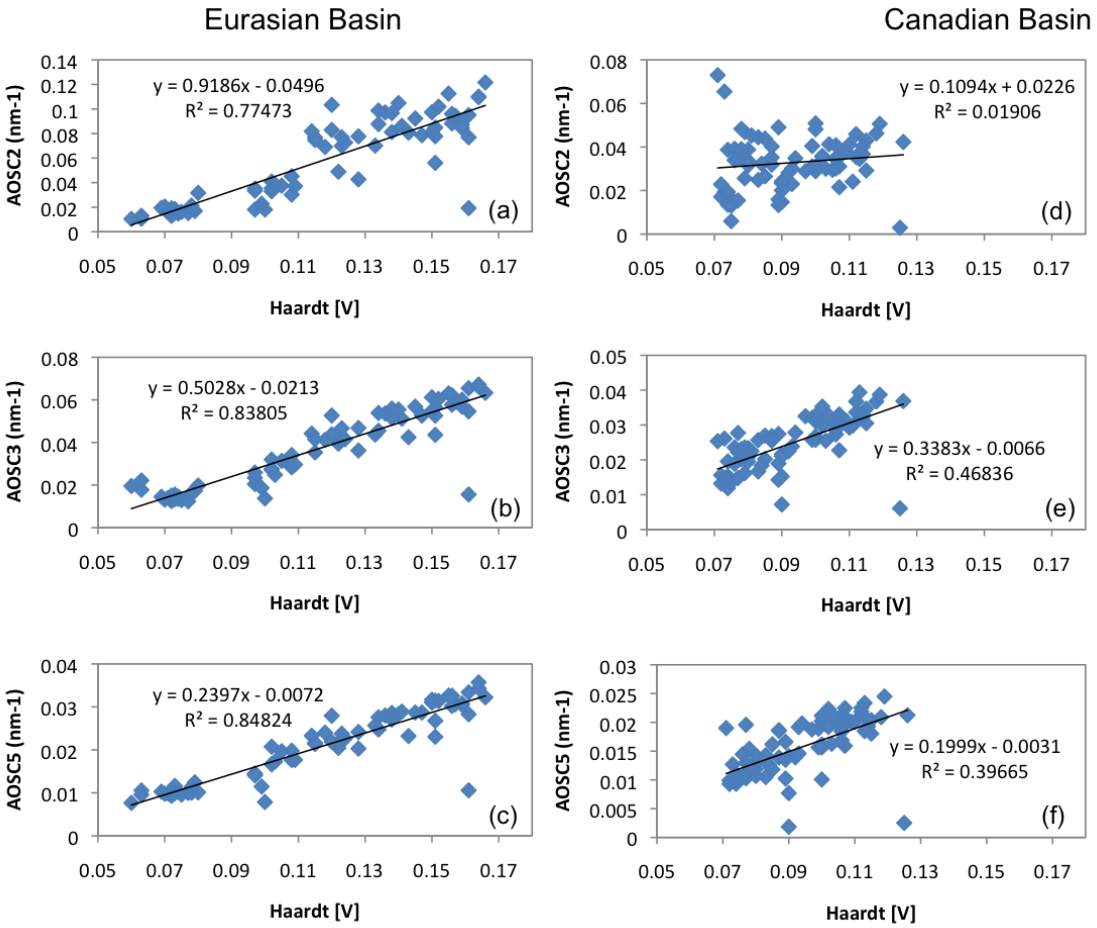

Figure 4.8. AOS 2005 terrestrial-like PARAFAC components relation to in situ fluorescence in the EB (a,b,c) and CB (d,e,f).

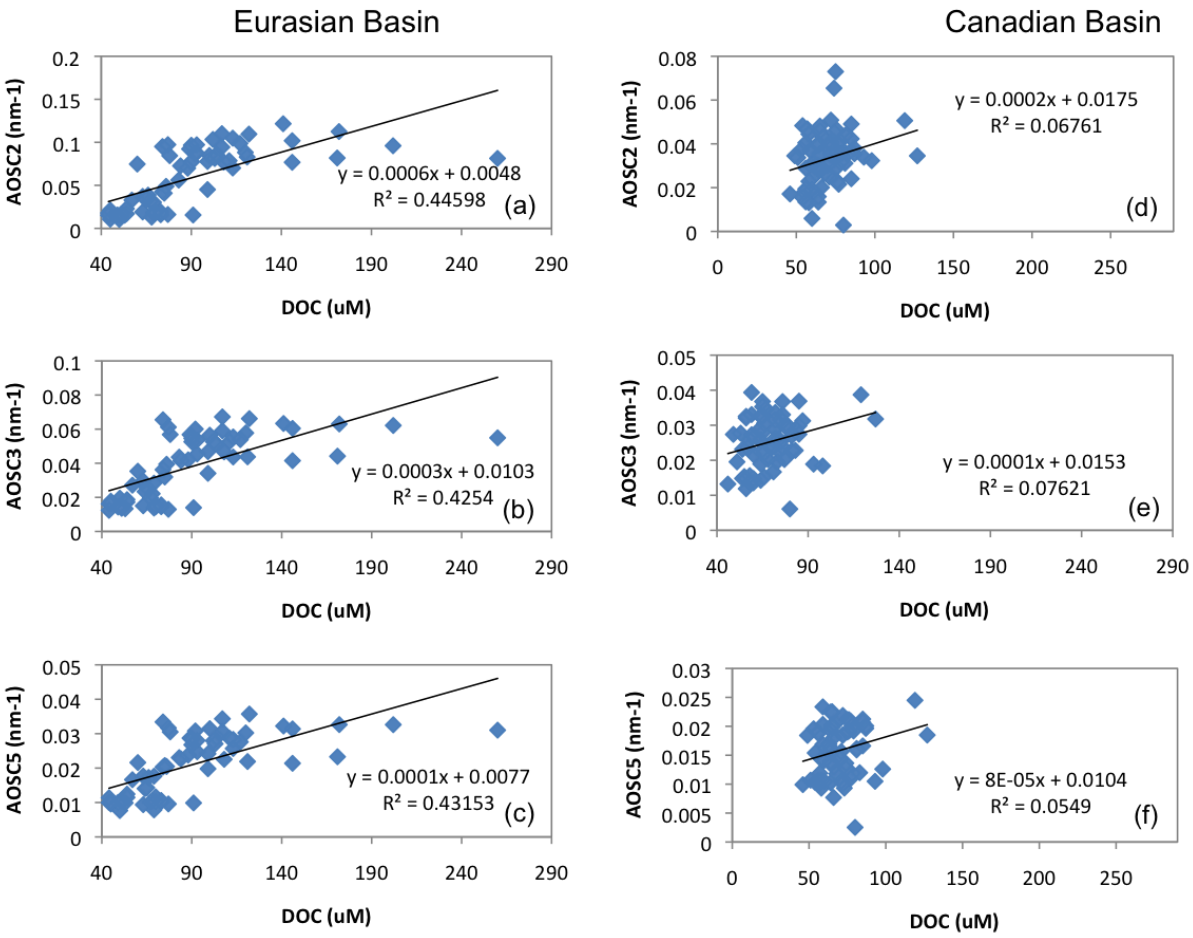

Figure 4.9. AOS 2005 terrestrial-like PARAFAC components relation to dissolved organic carbon concentrations in the EB (a,b,c) and CB (d,e,f).

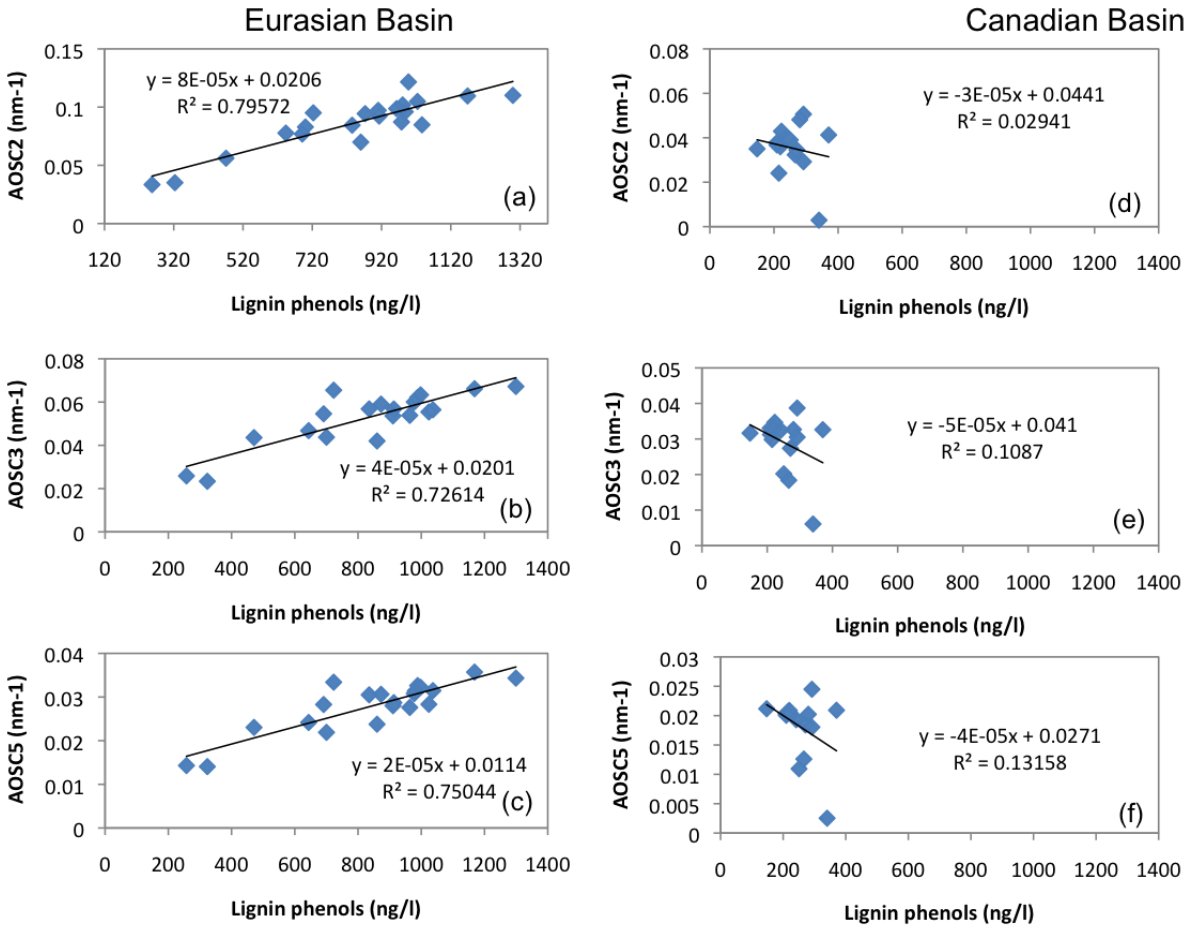

Figure 4.10. AOS 2005 terrestrial-like PARAFAC components relation lignin phenol concentrations in the EB (a,b,c) and CB (d,e,f).

4.4.3 Linking Terrestrial-like PARAFAC Components to Runoff Waters

To determine the ability of the individual PARAFAC components to trace specific water mass types present within the upper Arctic Ocean (0 – 300 m), we explored their relation to each other and to the *in situ* fluorescence signal and salinity using a correspondence analysis. The solution of the correspondence analysis decomposes the total variance into linear components, with CA1 explaining 63.5% and CA2 25.4% (total variance explained 88.9%; Fig. 4.11). AOCS2, AOSC3 and AOC5 grouped together and dominate in waters with low salinity and high fluorescence values. In the Arctic, runoff waters can be differentiated based on their low salinity and elevated fluorescence signal [*Amon et al.*, 2003; *Guay et al.*, 1999]. As a result, we that suggest these three terrestrial components have the potential to indicate the presence of runoff waters within the upper Arctic Ocean. AOSC4 and AOSC6 grouped together in a quadrant dominated by high salinity and a low fluorescence values. Because Atlantic waters are associated with a high salinity and low fluorescence we suggest the marine components are more dominant in waters of oceanic origin. Component AOCS1 stands alone and is shown to dominate in a region of low salinity and low fluorescence values, waters likely influenced by ice melt.

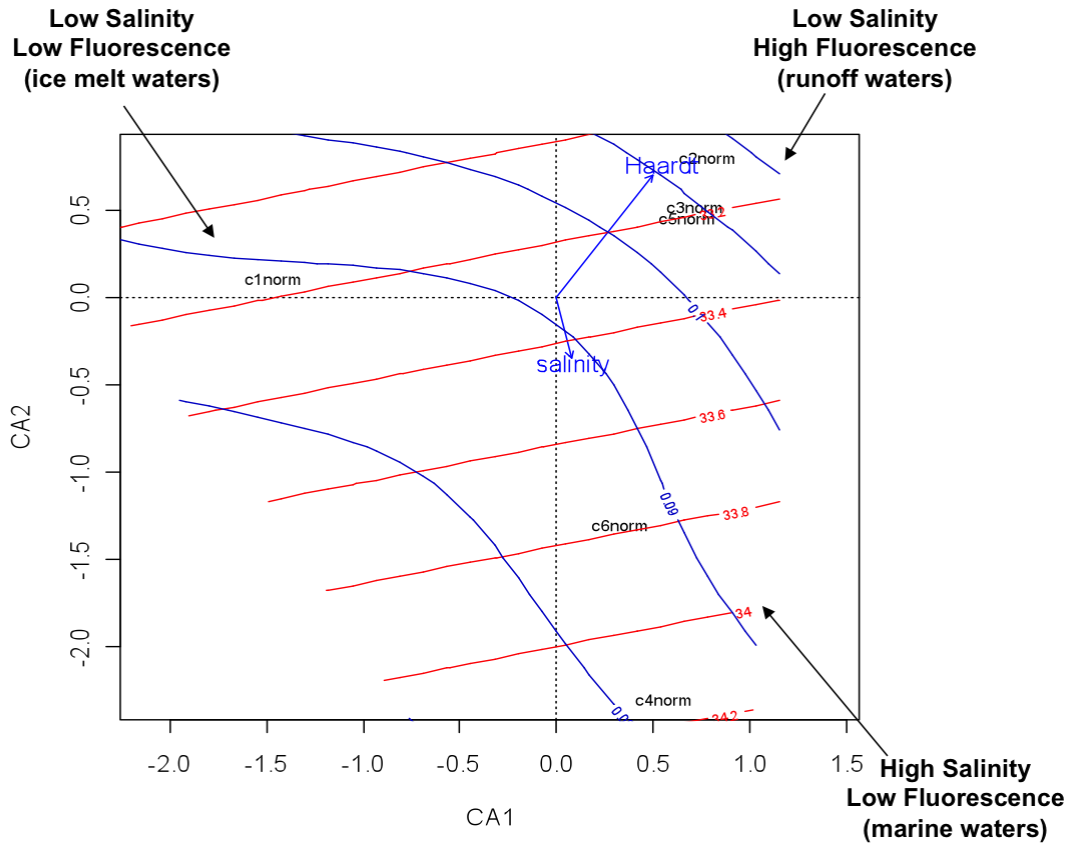

Figure 4.11. Correspondence Analysis of AOS 2005 PARAFAC components with salinity and *in situ* fluorescence vectors overlaid on the ordination space. AOS components are normalized to show relative percent composition within each sample.

4.5 Discussion

4.5.1 PARAFAC Component Source Identification

In the present study, six fluorescent PARAFAC components were identified and their spectral characteristics are similar to previously identified components in other aquatic environments (PARTNERS project chapter 2; [*Walker et al.,* 2009; *Stedmon et al.,* 2007a; *Stedmon et al., 2007b; Stedmon and Markager 2005a; Coble,* 1996]). AOSC2, AOSC3 and AOSC5 all exhibit a broad band along the emission axis and have previously been associated with terrestrially derived DOM sources [*Coble*, 1996; *Cory and McKnight*, 2005; *Stedmon and Markager*, 2005a; *Stedmon and Markager*, 2005b; *Stedmon et al.*, 2007a; *Walker et al.,* 2009]. AOSC1 is similar to the marine peaks B and T [*Coble,* 1996] and to the marine components determined during Beringia 2005 (Chapter III), suggesting a marine origin. AOSC4 is similar to the previously identified spectra of both tryptophan and tyrosine [*Coble,* 1996; *Murphy et al.*, 2006; *Stedmon and Markager*, 2005b] and is associated with a marine source. AOSC6 is similar to the marine humic-like peak (M) identified by *Coble* [1996] and is associated with an autochthonous source. The three terrestrial components (AOSC2, AOSC3, and AOSC5) and the protein-like component (AOSC4) have been identified in a wide range of studies, which suggests they are ubiquitous to many aquatic environments.

When combining the data from the Eurasian and Canadian basins, AOSC2 was significantly related to lignin phenols ($R^2 > 0.87$; data not shown), confirming its terrestrial origin during this study. Further, the significant relation observed between

AOSC3 and AOSC5 and lignin phenol concentrations in the EB (Fig. 4.10 b, c) confirms these components' terrestrial origin. The only other known study to relate PARAFAC components to lignin phenol concentrations in the Arctic Ocean is *Walker et al.,* [2009] (Chapter III), which identified similar terrestrial-like components within Canadian Archipelago surface waters. In conjunction, similar terrestrially-derived components were identified during the PARTNERS project, which includes seasonal data from the six largest Arctic Rivers (Chapter II). The fact that these Arctic studies from contrasting environments identified similar terrestrial-like components and linked them to lignin phenols and DOC concentrations, suggests they are capable of capturing the overall behavior of terrestrially-derived DOC across the Arctic Basin. In contrast, the marine like components (AOSC1, AOSC4, and AOSC6) showed no significant relation to lignin phenol or DOC concentrations (data not shown), suggesting these AOS-components are best used to infer the presence of autochthonous/microbial sources.

4.5.2 Implications of PARAFAC Components Quantity and Quality Across the Arctic Ocean

If we are to use PARAFAC to trace the river runoff we first need to determine their ability to trace different CDOM sources during transport and mixing within the Arctic Ocean. In the EB, the significant relation observed between the terrestrial components (AOSC2, AOSC3, AOSC5) and DOC (Fig. 4.9 a,b,c) and lignin phenol (Fig. 4.10 a,b,c) concentrations confirms their terrestrial origin and suggests they are capable of capturing the overall behavior of terrestrially derived DOC within this basin.

While AOSC3 and AOSC5 best explained the *in situ* fluorescence signal in the EB (Fig 4.8 b,c), we suggest that based on the strong relations between AOSC2 and DOC (Fig. 4.9 a) and lignin phenol concentrations (Fig. 4.10 a), that this component is best suited to trace terrestrial CDOM inputs from large Eurasian rivers. Combined with the elevated signal of AOSC2 and the depleted marine CDOM signal in the PSW layer of the EB (Fig. 4.5 a, 4.6 a), these results suggest terrestrial DOM dominates in Transpolar drift waters, likely from Eurasian runoff [*Guay et al.*, 2009; *Jones et al.*, 2008]. These results support finding by *Stedmon et al.* [2011], who suggest that in the EB, CDOM is mainly associated with riverine material.

The quality and behavior of the AOS-components in the CB are very different from the EB. In the CB, the overall lack of a relationship between the terrestrial AOS-components and DOC and lignin phenol concentrations suggest sources in addition to terrestrial inputs contribute to the overall CDOM pool and are responsible for the fluorescence signal in this basin. Based on the higher concentrations of the marine AOS-components relative to the terrestrial AOS-components (Fig. 4.5 c), where AOSC1 explained the majority of the variability (~ % 46) of the overall the fluorescence signal, we suggest that autochthonous sources are much more significant within the upper CB relative to terrestrial sources. These results support finding by *Stedmon et al.,* [2011], who suggest CDOM in CB surface waters are mainly of an autochthonous origin. With that said, the overall higher concentrations of AOSC3 and AOSC5 in the UHW and LHW waters combined with their significant relation to the *in situ* fluorescence signal, suggest that in the CB, terrestrial like CDOM is restricted to below the PSW and above

the Atlantic Layer. These results were very surprising based on the amount of Eurasian runoff thought to persist in the upper 50 m of the water column in this basin, which one would assume distributes terrestrial CDOM throughout the Arctic Ocean.

To investigate the effects of remineralization and/or secondary production on the overall CDOM pool we related the AOS-components to dissolved inorganic carbon (DIC) concentrations and apparent oxygen utilization (AOU) estimates in the EB and CB. In the EB, AOS-components were unrelated to DIC concentrations and AOU estimates (data not shown) within all water mass layers. This combined with the overall lower concentrations of the marine-like AOS-components in this basin, suggest that microbial process have little influence on the quality of CDOM in the upper EB. These results imply that terrestrial CDOM entrained within the Transpolar drift has undergone little modification during transport and mixing. However, in the CB, when combining the PSW with UHW and the LHW with Atlantic water, AOSC3 exhibited a significant relation to DIC concentrations and AOU estimates. This relation was not observed between the other AOS derived components. These results further confirm that degradation and marine secondary production alters the fluorescence signal within these waters and imply that AOSC3 is a tracer of these processes. On the other hand, this relationship may indicate there is a similar physical process controlling the spatial distribution of these parameters and AOSC3. We suggest that fractionation during sea ice formation may be at least partially responsible for these relationships as well as for the depletion of components AOSC2, AOSC3 (Fig. 4.5 b), and AOSC5 in the PSW and their enrichment in the halocline layers, as also suggested by *Amon et al.* [in prep].

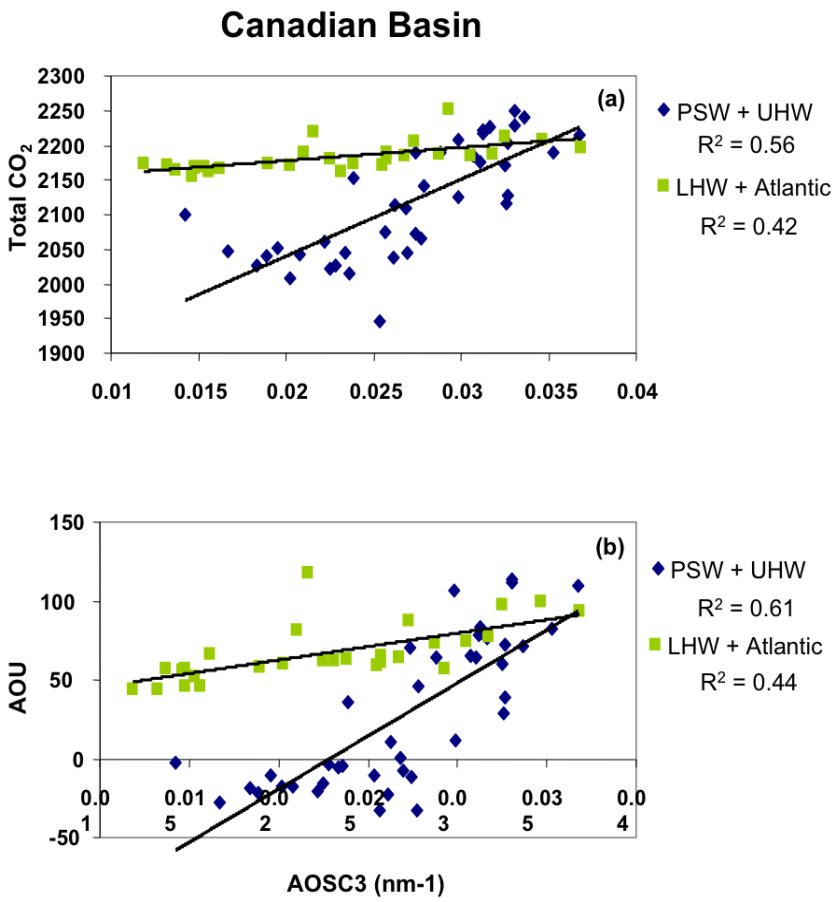

Figure 4.12. AOS 2005 terrestrial-like PARAFAC component AOSC3 relation to dissolved inorganic carbon concentrations (a) and apparent oxygen utilization estimates (b).

4.5.3 River Runoff Distributions in the Eurasian and Canadian Basins

One of the overarching goals of this project was to investigate the ability of PARAFAC components to trace river runoff Across the Arctic Ocean. Based on the overall significant relation of AOSC2 to lignin phenol concentrations (R^2 0.87; data not shown), as well as its association with runoff waters (Fig. 4.11) we suggest that the spatial distribution of the percent contributions of AOSC2 indicates the presence of

Eurasian runoff waters. Based on the significant relation of AOSC3 to DIC concentrations (Fig. 4.12 a) and AOU estimates (Fig. 4.12 b) as well as its association with runoff waters (Fig. 4.11), we suggest this component best describes terrestrial CDOM that has been modified due to degradation and marine secondary production.

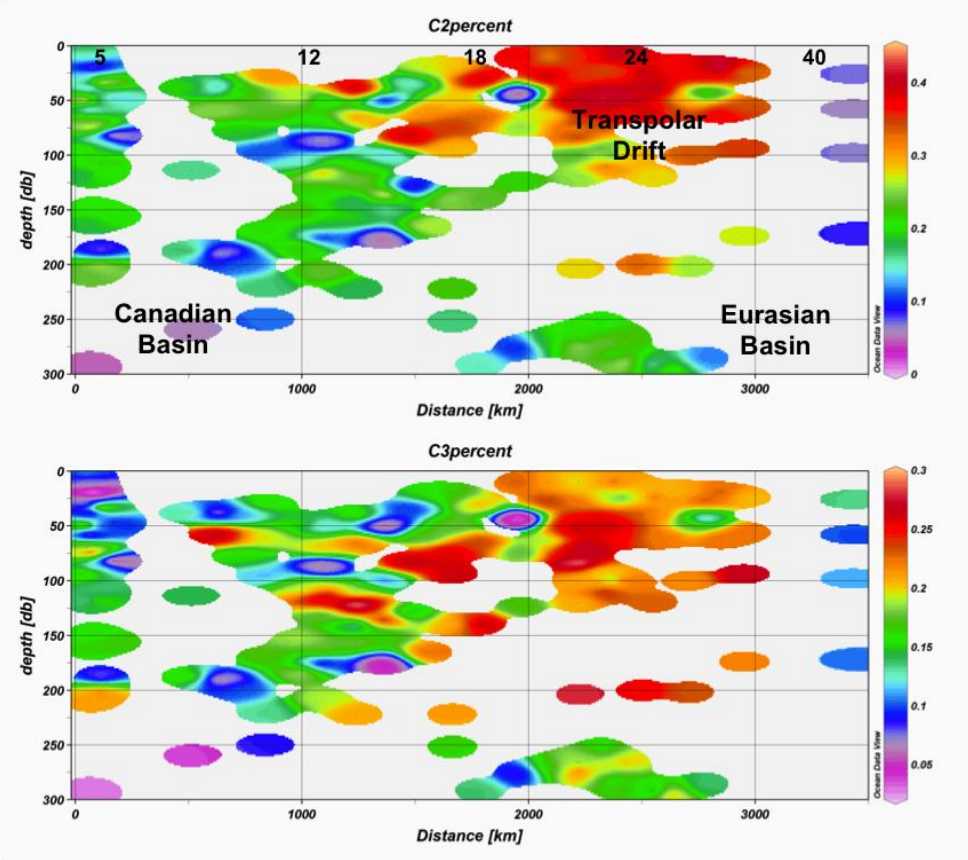

Figure 4.13. Spatial distribution of terrestrial components % AOSC2 and % AOSC3 during AOS 2005.

In the EB, elevated AOSC2 and AOSC3 concentrations in the upper 100 m of the water column clearly indicate the presence of Eurasian runoff within the Transpolar Drift [*Guay et al.*, 2009; *Guay and Falkner*, 1997]. These results imply two things. First, the presence of AOSC2 indicates the presence of runoff waters that have undergone little modifications during transport and mixing whereas the presence of AOSC3 suggest a fraction of the CDOM within this river water has been degraded, which likely results from inputs of CDOM from the sediments where microbial processes are important. Overall, these results are consistent with previous runoff estimates suggesting Eurasian discharge originating from the Siberian Sea shelf [*Bauch et al.,* 2011; *Morrison et al.,* 2012; *Amon et al.,* in prep;] dominates the freshwater component within the Transpolar Drift (Fig. 4.1d, [*Jones et al.,* 2008a, *Yamamoto-Kawai et al.,* 2008; *Guay et al.,* 2009].

In the CB, the lack of a terrestrial fluorescence signal in the upper PSW layer (Fig. 4.6 d,e,f and Fig. 4.13) combined with the fact that AOSC2 and AOSC3 were unrelated to lignin phenols throughout the upper CB (Fig. 4.10 d,e,f) was very surprising based on previous tracer studies who suggest a significant fraction of Eurasian runoff persist within the upper 50 m of the water column [*Jones et al.,* 2008b]. Based on the depleted terrestrial-like fluorescence signal in the PSW layer and the elevated concentrations of AOSC3 in the halocline layers, we suggest that the different PARAFAC components have been partitioned into specific water masses and that runoff may be more influential in maintaining certain halocline layers in the CB than previously thought. This is consistent with *Amon et al.* [in prep] who suggest that sea ice formation and geographically displaced sea ice melt is the main driving force for the vertical

distribution of dissolved solutes in Arctic Ocean surface waters. As a result, we suggest that runoff waters in the upper CB are actually sea ice melt that originally formed from runoff waters.

4.6 Conclusion

The response of the Arctic's hydrological cycle to climate warming is important due to its impact on sea ice formation within the Arctic Ocean and deepwater formation in the North Atlantic. It is therefore critical that we can accurately identify the different FW components contributing to the surface layers of the Arctic Ocean. While much has been learned about FW distributions in the Arctic Ocean, many questions remain regarding the partitioning of the FW components, especially in the CB during this time of climate warming. This study illustrates the ability of PARAFAC to decipher CDOM sources and to trace river runoff throughout the Arctic Ocean. The ability to differentiate and qualitatively trace the different sources of fluorescent components and determine the underlying factors controlling CDOM speciation during transport and mixing opens new possibilities for the use of CDOM as a more specific tracer in oceanography.

The optical properties of DOM indicate a distinct difference between the Eurasian and Canadian basins in terms of CDOM source and quality and river runoff distributions. In the EB, CDOM is mainly associated with riverine material whereas in the CB basin autochthonous CDOM becomes more important. Based on the spatial distribution of the terrestrial PARAFAC components, Eurasian runoff persists within the

Transpolar Drift but is much less significant within the upper CB. Sea ice formation process combined with geographically displaced sea ice is likely responsible for the depleted terrestrial CDOM signal in the upper CB, suggesting that surface waters in this basin are ice melt that originally formed from runoff waters.

CHAPTER V

SUMMARY

In large Arctic Rivers, CDOM during peak discharge is largely derived from fresh vascular plant DOM sources, where the Lena and Yenisei clearly dominate in terms of tCDOM discharge to the Arctic Ocean. During low flow periods, the CDOM pool has a greater microbial imprint, especially in the Mackenzie, and CDOM concentrations are much lower in the Lena and Yenisei. The distinct CDOM character in the Mackenzie combined with the overall lower DOC and lignin phenol concentrations in this river, suggest that microbial processes remove the most labile freshet portion of the tDOM pool on a shorter time scale than the estuarine mixing time. The higher abundance of lakes in this watershed allows for longer water residence times, which increases the chances for microbial and photochemical DOM degradation. Based on the observed pattern of optical properties and the longer residence times in lakes, we suggest that microbial processing may be the driving mechanism governing CDOM quality in this watershed. This is important in a warming climate, where increased temperatures combined with increased precipitation rates will likely accelerate permafrost degradation, and subsequently the supply of DOM exported to the Arctic Ocean. In addition, higher precipitation rates will likely increase hydrological connectivity during winter months, allowing for longer exposure times to microbial processes. These results indicate that it is possible that a significant fraction of the DOC released from permafrost erosion will be remineralized before reaching the Arctic Ocean, thus, leading to an

increase saturation of DIC in these rivers and potentially a positive CO_2 emissions to the atmosphere.

The BER-PARAFAC components could be grouped into two classes based on sources, allowing for the distinction between terrestrial and marine derived DOM. An elevated terrestrial CDOM signal was observed in the Mackenzie River plume surface waters and decreased as water was transported to the Canadian Archipelago. Based on results determined during AOS 2005, CDOM fractionation during ice formation combined with geographically displaced sea ice melt accounts for the depleted CDOM signal in surface layers of the CB. Due to the lack of sampling at depth, it is not possible to estimate the presence of terrestrial CDOM export through Canadian Archipelago during this study. An overall lower marine CDOM signal suggests minimal productivity within plume and archipelago surface waters. The relationship between the sum of the terrestrial-like and marine-like components compared to salinity values allowed us to distinguish different water masses encountered in this study including an Atlantic, Archipelago, and Mackenzie River plume endmember. Results highlight the potential of PARAFAC components to trace river water within the Arctic Ocean.

Within the interior Arctic Ocean, CDOM is fundamentally different in the EB relative to the CB and is caused by varying sources and diagenesis and the influence of sea ice dynamics. In the EB, CDOM is mainly associated with a riverine source whereas in the CB degradation and marine secondary production become more important. During this study we were able to link the terrestrially derived PARAFAC components to low salinity high fluorescence waters, indicative of runoff. This allowed us to investigate

river runoff distributions based on the terrestrial fluorescence signal. Based on this analysis, Eurasian runoff is likely one of the dominant freshwater components within the Transpolar Drift, which agrees with current runoff estimates at this location. This is important because a large fraction (up to 20 – 50%) of the annual river discharge to the Arctic is exported via the Transpolar Drift to the East Greenland Current and ultimately to the North Atlantic [*Amon et al.,* 2003; *Hansell et al.,* 2004] where deep water formation occurs. In contrast, the spatial distribution of the terrestrial PARAFAC components in the CB suggests river runoff is much less significant in the upper water column but may be more influential in sustaining the halocline layer than previously thought. These results are not consistent with current runoff distribution estimates, which suggest that a significant fraction of Eurasian runoff persist within the upper 50 m of the water column in this basin while it is depleted in the halocline layer. We suggest that CDOM fractionation during ice formation and geographically displaced sea ice melt combined with the longer residence times in the Beaufort Gyre, accounts for the depleted CDOM signal in surface layers of the CB. As a result, we suggest that waters currently classified as river runoff in the CB are ice melt waters, which originally formed from runoff waters.

REFERENCES

Aagaard, K., and E. C. Carmack (1994), The Arctic Ocean and Climate: a Perspective, *Geophysical Monograph*, *5*(85).

Aagaard, K., and E. Carmack (1989), The role of sea ice and other fresh water in the Arctic circulation, *J. Geophys. Res., 94*(C10), 14485.

Aagaard, K., L. K. Coachman, and E. C. Carmack (1981), On the halocline of the Arctic Ocean, *Deep Sea Research*, *28*, 529-545.

ACIA (2005), Arctic Climate Impact Assessment. Cambridge University Press, Cambridge, UK, Ch. 5, 151 – 182.

Amon, R. M. W., R. Benner, S. Walker (2012), Dissolved Organic Matter Across the Arctic Ocean, (in prep).

Amon, R. M. W., A. J. Rinehart, S. Duan, P. Louchouarn, A. Prokushkin, G. Guggenberger, D. Bauch, S. Stedmon, P.A. Raymond, J. W. McClelland, B. J. peterson, S. A. Walker (2012), Dissolved Organic Matter Sources in Large Arctic Rivers, *CGA (submitted)*.

Amon, R. M. W., and B. Meon (2004), The biogeochemistry of dissolved organic matter and nutrients in two large Arctic estuaries and potential implications for our understanding of the Arctic Ocean system, *Mar. Chem.,* 92, 311–330, doi:10.1016/j.marchem.2004.06.034.

Amon, R. M. W., and R. Benner (2003), Combined neutral sugars as indicators of the diagenetic state of dissolved organic matter in the Arctic Ocean, *Deep Sea Research I*, *50*(1), 151-169.

Amon, R. M. W., G. Budeus, and B. Meon (2003), Dissolved organic carbon distribution and origin in the Nordic Seas: Exchanges with the Arctic Ocean and the North Atlantic, *J. Geophys. Res.*, *108*(3221), 17.

Amon, R. M. W., H.-P. Fitznar, and R. Benner (2001), Linkages among the bioreactivity, chemical composition, and diagenetic state of marine dissolved organic matter, *Limnol. Oceanogr.,* 46(2), 287–297.

Amon, R. M. W., and R. Benner (1996), Bacterial utilization of different size classes of dissolved organic matter, *Limnol. Oceanogr., 41*, 41-51.

Balcarczyk, K., J. Jones, R. Jaffé, and N. Maie (2009), Stream dissolved organic matter bioavailability and composition in watersheds underlain with discontinuous permafrost, *Biogeochemistry*, *94*(3), 255-270.

Bates, N. R., and J. T. Mathis (2009), The Arctic Ocean marine carbon cycle: evaluation of air-sea CO2 exchanges, ocean acidification impacts and potential feedbacks, edited, Copernicus Publications.

Bates, N. R., J. T. Mathis, and M. A. Jeffries (2010), Air-sea CO2 fluxes on the Bering Sea shelf, *Biogeosciences Discuss.*, *7*, 7271–7314.

Battin, T. J. (1998), Dissolved organic matter and its optical properties in a blackwater tributary of the upper Orinoco river, Venezuela, *Organic Geochemistry*, *28*, 561-569.

Bauch, D., M. Rutgers van der Loeff, N. Anderson, S. Torres-Valdes, K. Bakker, and E. P. Abrahamsen (2011), Origin and freshwater polynya water in the Arctic Ocean halocline in summer 2007, *Progress in Oceanography*, *91*, 482-495.

Bélanger, S., H. Xie, N. Krotkov, P. Larouche, W. F. Vincent, and M. Babin (2006), Photomineralization of terrigenous dissolved organic matter in Arctic coastal waters from 1979 to 2003: Interannual variability and implications of climate change, *Global Biogeochemical Cycles*, *20*(4).

Benner, R., P. Louchouarn, and R. M. W. Amon (2005), Terrigenous dissolved organic matter in the Arctic Ocean and its transport to surface and deep waters of the North Atlantic, *Global Biogeochemical Cycles*, *19*.

Birdwell, J. E., and A. S. Engel (2010), Characterization of dissolved organic matter in cave and spring waters using UV–Vis absorbance and fluorescence spectroscopy, *Organic Geochemistry*, *41*(3), 270-280.

Burdige, D. J., S. W. Kline, and W. Chen (2004), Fluorescent dissolved organic matter in marine sediment pore waters, *Mar. Chem., 89*(1–4), 289-311.

Coble, P. G. (2007), Marine Optical Biogeochemistry: The Chemistry of Ocean Color, *ChemInform*, *38*(20), no-no.

Coble, P. G. (1996), Characterization of marine and terrestrial DOM in seawater using excitation-emission matrix spectroscopy, *Mar. Chem.,* 51, 325–346, doi:10.1016/0304-4203(95)00062-3.

Cory, R. M., and D. McKnight (2005), Fluorescence spectroscopy reveals ubiquitous presence of oxidized and reduced quinones in dissolved organic matter, *Environ. Sci. Technol.,* 39, 8142–8149, doi:10.1021/ es0506962.

Cuny, J., P. B. Rhines, and R. Kwok (2005), Davis Strait volume, fresh- water and heat fluxes, *Deep Sea Res.,* Part I, 52, 519 – 542, doi:10.1016/ j.dsr.2004.10.006.

Dickson, R. R., J. Meincke, S.-A. Malmberg, and A. J. Lee (1988), The ‘‘Great Salinity Anomaly’’ in the northern North Atlantic 1968–1982, *Progress in Oceanography*, *20*, 103-151.

Dittmar, T., and G. Kattner (2003), The biogeochemistry of the river and shelf ecosystem of the Arctic Ocean: a review, *Mar. Chem., 83*(3–4), 103-120.

Euskirchen, E. S., A. D. McGuire, F. S. Chapin, III, S. Yi, and C. Thompson. 2009. Changes in vegetation in northern Alaska under scenarios of climate change 2003–2100: implications for climate feedbacks. *Ecological Applications* 19:1022–1043.

Fabry, V. J., J. B. McClintock, J. T. Mathis, and J. M. Grebmeier (2009), Ocean Acidification at High Latitudes: The Bellwether, *Oceanography 22*(4).

Ferrari, G. M., and M. D. Dowell (1998), CDOM absorption characteristics with relation to fluorescence and salinity in coastal areas of the southern Baltic Sea, *Estuarine Coastal Shelf Sci.,* 47, 91–105, doi:10.1006/ ecss.1997.0309.

Gibson, J. J., and T. D. Prowse (2002), Stable isotopes in river ice: identifying primary over-winter streamflow signals and their hydrological significance, *Hydrological Processes*, *16*(4), 873-890.

Gordeev, V. V. (2006), Fluvial sediment flux to the Arctic Ocean, *Geomorphology*, 80, 94–104, doi:10.1016/j.geomorph.2005.09.008.

Gruber, S., M. Hoelzle, and W. Haeberli (2004), Permafrost thaw and destabilization of Alpine rock walls in the hot summer of 2003, *Geophys. Res. Lett.*, *31*(13), L13504.

Guay, C., F. A. McLaughlin, and M. Yamamoto-Kawai (2009), Differentiating fluvial components of upper Canada Basin waters on the basis of measurements of dissolved barium combined with other physical and chemical tracers, *J. Geophys. Res., 114*.

Guay, C. K., G. K. Klinkhammer, K. K. Falkner, R. Benner, P. G. Coble, T. E. Whitledge, B. Black, F. J. Bussell, and T. A. Wagner (1999), High-resolution measurements of dissolved organic carbon in the Arctic Ocean by in situ fiber-optic spectrometry, *Geophys. Res. Lett.,* 26(8), 1007–1010, doi:10.1029/1999GL900130.

Guay, C. K., and K. K. Falkner (1997), Barium as a tracer of Arctic halocline and river waters, *Deep-Sea Res.*, *44*(8), 1543-1569.

Hansell, D. A., D. Kadko, and N. R. Bates (2004), Degradation of Terrigenous Dissolved Organic Carbon in the Western Arctic Ocean, *Science*, *304*(5672), 858-861.

Hansell, D. A., and C. A. Carlson (2002), Biochemistry of Marine Dissolved Organic Matter, 456 pp., *Academic*, San Diego, Calif.

Hedges, J. I., and J. R. Ertel (1982), Characterization of lignin by capillary gas chromatography of cupric oxide oxidation products, *Anal. Chem.,* 54, 174 – 178.

Hedges, J. I., J. R. Ertel, and E. B. Leopold (1982), Lignin geochemistry of a late quarternary sediment core from Lake Washington, *Geochimica et Cosmochimica Acta*, *46*, 1869-1877.

Helms, J. R., S. Aron, D. R. Jason, E. C. Minor, D. J. Kieber, and K. Mopper (2008), Absorption Spectral Slopes and Slope Ratios as Indicators of Molecular Weight, Source, and Photobleaching of Chromophoric Dissolved Organic Matter, *Limnology and Oceanography*, *53*(3), 955-969.

Hernes, P. J., Robinson A.C., and A. K. Aufdenkampe (2007), Fractionation of lignin during leaching and sorption and implications for organic matter "freshness", *Geophysical Research Letters*, *34*.

Hernes, P. J., and R. Benner (2003), Photochemical and microbial degradation of dissolved lignin phenols: Implications for the fate of terrigenous dissolved organic matter in marine environments, *J. Geophys. Res.,* 108(C9), 3291, doi:10.1029/2002JC001421.

Holmes, R. M., J. W. McClelland, P. A. Raymond, B. B. Frazer, B. J. Peterson, and M. Stieglitz (2008), Lability of DOC transported by Alaskan rivers to the Arctic Ocean, *Geophys. Res. Lett.,* 35, L03402, doi:10.1029/ 2007GL032837.

Hood, E., and D. Scott (2008), Riverine organic matter and nutrients in southeast Alaska affected by glacial coverage, *Nat. Geosci.,* 1, 583 – 587.

Houel, S., P. Louchouarn, M. Lucotte, R. Canuel, and B. Ghaleb (2006), Translocation of Soil Organic Matter Following Reservoir Impoundment in Boreal Systems: Implications for In situ Productivity, *Limnology and Oceanography*, *51*(3), 1497-1513.

Huguet, A., L. Vacher, S. Relexans, S. Saubusse, J. M. Froidefond, and E. Parlanti (2009), Properties of fluorescent dissolved organic matter in the Gironde Estuary, *Organic Geochemistry*, *40*(6), 706-719.

IPCC (2007), Contribution of Working Group I to the Fourth Assessment Report of the IPCC, in *IPCC Climate Change 2007 – The Physical Science Basis.*

Jensco, K. G., B. L. McGlynn, M. N. Gooseff, S. M. WOndzell, K. E. Bencala, and L. A. Marshall (2009), Hydrological Connectivity Between Landscapes and Streams: Transferring Reach and Plot-Scale Understanding to the Catchment Scale, *Water Resour. Res.*, *45*.

Jones, E. P., L. G. Anderson, S. Jutterstrom, and J. H. Swift (2008b), Sources and distribution of fresh water in the East Greenland Curent, *Progress in Oceanography*, *78*, 37-44.

Jones, P. E., L. G. Anderson, S. Jutterstrom, L. Mintrop, and J. H. Swift (2008a), Pacific freshwater, river water and sea ice meltwater across Arctic Ocean basins: Results from the 2005 Beringia Expedition, *J. Geophys. Res., 113*.

Kohler, H., B. Meon, V. V. Gordeev, A. Spitzy, and R. M. W. AMon (2003), Dissolved organic matter (DOM) in teh estuaries of Ob and Yenisei and the adjacent Kara-Sea, Russia, *Proceedings in Marine Sciences*, *6*, 281-309.

Kuo, L. J., P. Louchouarn, and B. E. Herbert (2008), Fate of CuO-derived lignin oxidation products during plant combustion: Application to the evaluation of char inputs to soil organic matter, *Org. Geochem.,* 39, 1522–1536, doi:10.1016/j.orggeochem.2008.07.011.

Lakowicz, J. R. (Ed.) (2006), Principles of Fluorescence Spectroscopy, *Springer*, New York.

Lawaetz, A. J., and C. A. Stedmon (2009), Fluorescence intensity calibration using the Raman scatter peak of water, *Appl. Spectrosc.,* 63(8), 936 – 940.

Lawrence, D., and A. Slater (2008), Incorporating organic soil into a global climate model, *Climate Dynamics*, *30*(2), 145-160.

Lazier, J. R. N. (1980), Oceanographic conditions at Ocean Weather Ship Bravo, *Atmosphere-Ocean, 3*, 227-238.

Lobbes, J. M., H. P. Fitznar, and G. Kattner (2000), Biogeochemical characteristics of dissolved and particulate matter in Russian rivers entering the Arctic Ocean, *Geochim. Cosmochim. Acta, 64*, 2973–2983, doi:10.1016/S0016-7037(00)00409-9.

Louchouarn, P., S. Amon R. M. W., Duan S., Pondell C., Seward S. M., and White N. (2010), Analysis of lignin-derived phenols in standard reference materials and dissolved organic matter by gas chromotography/tandem mass spectrometry, *Mar. Chem.*, 118, 84-97.

Louchouarn, P., S. Opsahl, and R. Benner (2000), Isolation and quantification of dissolved lignin from natural waters using solid-phase extraction (spe) and GC/MS selected ion monitoring (sim), *Anal. Chem.,* 13, 2780 – 2787, doi:10.1021/ac9912552.

Manizza, M., M. J. Follows, S. Dutkiewicz, J. W. McClelland, D. Menemenlis, C. N. Hill, A. Townsend-Small, and B. J. Peterson (2009), Modeling transport and fate of riverine dissolved organic carbon in the Arctic Ocean, *Global Biogeochemical Cycles*, *23*(4), GB4006.

McGuire, A. D., L. G. Anderson, T. Christensen, S. Dallimore, L. Guo, D. J. Hayes, M. Heimann, T. D. Lorenson, R. W. Macdonald, and N. Roulet (2009), Sensitivity of the carbon cycle in the Arctic to climate change, edited, Ecological Monographs Ecological Society of America (ESA).

McKnight, D. M., E. W. Boyer, P. K. Westerhoff, P. T. Doran, T. Kulbe, and D. T. Andersen (2001), Spectrofluorometric characterization of dissolved organic matter for indication of precursor organic material and aromaticity, *Limnology and Oceanography*, *46*(1), 38-48.

Miller, W. L., and M. A. Moran (1997), Interaction of Photochemical and Microbial Processes in the Degradation of Refractory Dissolved Organic Matter from a Coastal Marine Environment, *Limnology and Oceanography*, *42*(6), 1317-1324.

Mladenov, N., P. Huntsman-Mapila, P. Wolski, W. Masamba, and D. McKnight (2008), Dissolved organic matter accumulation, reactivity, and redox state in ground water of a recharge wetland, *Wetlands*, *28*(3), 747-759.

Morison, J., R. Kwok, C. Peralta-Ferriz, M. Alkire, R. Andersen, and M. Steele (2012), Changing Arctic Ocean Freshwater Pathways, *Nature*, *481*, 66-70.

Mueller, K. K., C. Fortin, and P. G. C. Campbell (2012), Spatial Variation in the Optical Properties of Dissolved Organic Matter (DOM) in Lakes on the Canadian Precambrian Shield and Links to Watershed Characteristics *Aquat. Geochem, 18,* 21-44.

Murphy, K. R., G. M. Ruiz, W. T. M. Dunsmuir, and T. D. Waite (2006), Optimized parameters for fluorescence-based verification of ballast water exchange by ships, *Environ. Sci. Technol.,* 40, 2357–2362, doi:10.1021/ es0519381.

Murphy, K. R., C. A. Stedmon, T. D. Waite, and G. M. Ruiz (2007), Distinguishing between terrestrial and autochthonous organic matter sources in marine environments using fluorescence spectroscopy, *Mar. Chem.,* 108, 40–58.

Neff, J. C., J. C. Finlay, S. A. Zimov, S. P. Davydov, J. J. Carrasco, E. A. G. Schuur, and A. I. Davydova (2006), Seasonal changes in the age and structure of dissolved organic carbon in Siberian rivers and streams, *Geophys. Res. Lett., 33*.

O'Donnell, J. A., G. R. Aiken, E. S. Kane, and J. B. Jones (2010), Source water controls on the character and origin of dissolved organic matter in streams of the Yukon River basin, Alaska, *J. Geophys. Res., 115*(G3), G03025.

Ohno, T., and R. Bro (2006), Dissolved Organic Matter Characterization Using Multiway Spectral Decomposition of Fluorescence Landscapes, *Soil Sci. Soc. Am. J., 70*(6), 2028-2037.

Opsahl, S., R. Benner, and R. Amon (1999), Major flux of terrigenous dissolved organic matter through the Arctic Ocean, *Limnol. Oceanogr.,* 44(8), 2017–2023.

Osburn, C. L., D. W. O'Sullivan, and T. J. Boyd (2009), Increases in the longwave photobleaching of chromophoric dissolved organic matter in coastal waters, *Limnol. Oceanogr.,* 54(1), 145–159.

Peterson, B. J., R. M. Holmes, J. W. McClelland, C. J. Vorosmarty, I. A. Shiklomanov, R. B. Lammers, and S. Rahmstorf (2002), Increasing river discharge to the Arctic Ocean, *Science*, 298, 2171–2173, doi:10.1126/ science.1077445.

Peterson, M. L., S. Q. Lang, A. Aufdenkampe, and J. Hedges (2003), Dissolved organic carbon measurement using a modified high temperature combustion analyzer, *Mar. Chem.,* 81, 89–104, doi:10.1016/S0304- 4203(03)00011-2.

Pickart, R. S., and G. Stossmeister (2009), Outflow of Pacific water from the Chukchi Sea to the Arctic Ocean, *Chinese Journal of Polar Science*.

Pickart, R. S., M. A. Spall, G. W. K. Moore, T. J. Weingartner, R. A. Woodgate, K. Aagaard, and K. Shimada (2011), Upwelling in the Alaskan Beaufort Sea: Atmospheric forcing and local versus non-local response, *Progress in Oceanography, 88*, 78-100.

Polyakov, I. V., G. V. Alekseev, L. A. Timokhov, U. S. Bhatt, R. L. Colony, H. L. Simmons, D. Walsh, J. E. Walsh, and V. F. Zakharov (2004), Variability of the Intermediate Atlantic Water of the Arctic Ocean over the Last 100 Years, *Journal of Climate, 17*(23), 4485-4497.

Polyakov, I. V., G. V. Alekseev, R. V. Bekryaev, U. Bhatt, R. L. Colony, M. A. Johnson, V. P. Karklin, A. P. Makshtas, D. Walsh, and A. V. Yulin (2002), Observationally based assessment of polar amplification of global warming, *Geophys. Res. Lett., 29*(18).

Proshutinsky A., R. Krishfield, M.-L. Timmermans, J. Toole, E. Carmack, F. McLaughlin, W. J. Williams, S. Zimmermann, M. Itoh, K. Shimada (2009). Beaufort Gyre freshwater reservoir: State and variability from observations, *J. Geophys. Res.,* 114, C00A10, doi:10.1029

Qian, J., and K. Mopper (1996), Automated high-performance, high temperature combustion total organic carbon analyzer, *Anal. Chem.,* 68(18), 3090–3097, doi:10.1021/ac960370z.

Raymond, P. A., J. W. McClelland, R. M. Holmes, and A. V. Zhulidov (2007), Flux and age of dissolved organic carbon exported to the Arctic Ocean: A carbon isotopic study of the five largest Arctic rivers, *Global Biogeochem. Cycles,* 21, GB4011, doi:10.1029/2007GB002934.

Rudels, B. (2001), Arctic Basin Circulation, Academic, San Diego, Calif. Spencer, R. G. M., L. Bolton, and A. Baker (2007a), Freeze/thaw and pH effects on freshwater dissolved organic matter fluorescence and absorption properties from a number of U.K. locations, *Water Res.,* 41, 2941–2950, doi:10.1016/j.watres.2007.04.012.

Rudels, B., E. P. Jones, U. Schauer, and P. Eriksson (2004), Atlantic sources of the Arctic Ocean surface and halocline waters, *Polar Research, 23*(2), 181-208.

Rudels, B., Anderson, L. G., and Jones, E. P. (1996), Formation and evolution of the surface mixed layer and halocline of the Arctic Ocean, *J. Geophys. Res., 101*, 8807-8821.

Sierra, M. M. D., M. Giovanela, E. Parlanti, and E. J. Soriano-Sierra (2005), Fluorescence fingerprint of fulvic and humic acids from varied origins as viewed by single-scan and excitation/emission matrix techniques, *Chemosphere*, *58*(6), 715-733.

Spall, M. A., R. S. Pickart, P. S. Fratantoni, and A. J. Plueddemann (2008), Western Arctic Shelfbreak Eddies: Formation and Transport, *J. Phys. Oceanogr.*, *38*, 1644-1668.

Spencer, R. G. M., L. Bolton, and A. Baker (2007a), Freeze/thaw and pH effects on freshwater dissovled organic matter fluorescence and absorption properties from a number of UK locations, *Water Research*, *41*, 2941-2950.

Spencer, R. G. M., A. Baker, J. M. E. Ahad, G. L. Cowie, R. Ganeshram, R. C. Upstill-Goddard, and G. Uher (2007b), Discriminatory classification of natural and anthropogenic waters in two U.K. estuaries, *Sci. Total Environ.,* 373, 305–323, doi:10.1016/j.scitotenv.2006.10.052.

Spencer, R. G. M., G. R. Aiken, K. P. Wickland, R. G. Striegal, and P. J. Hernes (2008), Seasonal and spatial variability in dissolved organic matter quantity and composition from the Yukon River basin, Alaska, *Global Biogeochem. Cycles*, 22, GB4002, doi:10.1029/2008GB003231.

Spencer, R. G. M., G. R. Aiken, K. D. Butler, M. M. Dornblaser, R. G. Striegl, and P. Hernes (2009), Utilizing chromophoric dissolved organic matter measurements to derive export and reactivity of dissolved organic carbon exported to the Arctic Ocean: A case study of the Yukon River, Alaska, *Geophys. Res. Lett.,* 36, L06401, doi:10.1029/ 2008GL036831.

Stedmon, C. A., R. M. W. Amon, A. J. Rinehart, and S. A. Walker (2011), The supply and characteristics of colored dissolved organic matter (CDOM) in the Arctic Ocean: Pan Arctic trends and differences, *Mar. Chem., 124*(1–4), 108-118.

Stedmon, C. A., and R. Bro (2008), Characterizing dissolved organic matter fluorescence with parallel factor analysis: A tutorial, *Limnol. Oceanogr. Methods*, 6, 572–579.

Stedmon, C. A., S. Markager, L. Tranvik, L. Kronberg, T. Slätis, and W. Martinsen (2007), Photochemical production of ammonium and transformation of dissolved organic matter in the Baltic Sea, Mar. Chem., *104*(3-4), 227-240.

Stedmon, C. A., and S. Markager (2005a), Resolving the variability in dissolved organic matter fluorescence in temperate estuary and its catchment using PARAFAC analysis, *Limnol. Oceanogr.,* 50(2), 686 – 697.

Stedmon, C. A., and S. Markager (2005b), Tracing the production and degradation of autochthonous fractions of dissolved organic matter by fluorescence analysis, *Limnol. Oceanogr.,* 50(5), 1415–1426.

Stedmon, C. A., S. Marager, and R. Bro (2003), Tracing dissolved organic matter in aquatic environments using a new approach to fluorescence spectroscopy, *Mar. Chem.,* 82, 239–254, doi:10.1016/S0304- 4203(03)00072-0.

Stedmon, C. A., S. Markager, L. Tranvik, L. Kronberg, T. Slatis, and W. Martinsen (2007a), Photochemical production of ammonium and transformation of dissolved organic matter in the Baltic Sea, *Mar. Chem.,* 104, 227–240, doi:10.1016/j.marchem.2006.11.005.

Stedmon, C. A., D. N. Thomas, M. Granskog, H. Kaartokallio, S. Papadimitriou, and H. Kuosoa (2007b), Characteristics of dissolved organic matter in Baltic Sea ice: Allochthonous or autochthonous origins?, *Environ. Sci. Technol.,* 41(21), 7273–7279, doi:10.1021/ es071210f.

Stolbovi, V., G. Fisher, V. S. Ovenkin, and S. Rozhkova (1998), Soils of Russia-correlated with the revised legend of the FAO soil map of the world, IIASA Interim Report IR-97-070, Internaltional Institute for Applied Systems Analysis, Laxenburg, Austria.

Tarnocai, C., J. Canadell, E. Schuur, P. Kuhry, G. Mazhitova, and S. Zimov (2009), Soil organic carbon pools in the northern circumpolar permafrost region, *Global Biogeochemical Cycles*, *23*(2).

Twardowski, M. S., E. Boss, J. M. Sullivan, and P. L. Donaghay (2004), Modeling the spectral shape of absorption by chromophoric dissolved organic matter, *Mar. Chem., 89*(1–4), 69-88.

von Appen, W.-J., and R. S. Pickart (2012), Two Configurations of the Western Arctic Shelfbreak Current in Summer, *Journal of Physical Oceanography, 42*.

Walker, S. A., R. M. W. Amon, C. Stedmon, S. Duan, and P. Louchouarn (2009), The use of PARAFAC modeling to trace terrestrial dissolved organic matter and fingerprint water masses in coastal Canadian Arctic surface waters, *J. Geophys. Res., 114*(G00F06).

Watanabe, E. (2011), Beaufort shelf break eddies and shelf-basin exchange of Pacific summer water in the western Arctic Ocean detected by satellite and modeling analyses, *J. Geophys. Res.,, 116*.

Weishaar, J. L., G. R. Aiken, B. A. Bergamaschi, M. S. Fram, R. Fujii, and K. Mopper (2003), Evaluation of Specific Ultraviolet Absorbance as an Indicator of the Chemical Composition and Reactivity of Dissolved Organic Carbon, *Environmental Science & Technology*, *37*(20), 4702-4708.

Williams, C. J., J. B. Yavitt, R. Kelman Wieder, and N. L. Cleavitt (1998), Cupric oxide oxidation products of northern peat and peat-forming plants, *Can. J. Bot*, *76*, 51-62.

Woodgate, R. A., and K. Aagaard (2005), Revising the Bering Strait freshwater flux into the Arctic Ocean, *Geophys. Res. Lett.*, *32*.

Yamamoto-Kawai, M., F. A. McLaughlin, E. C. Carmack, S. Nishino, K. Shimada, and N. Kurita (2009), Surface freshening of the Canada Basin, 2003-2007: River runoff versus sea ice meltwater, *J. Geophys. Res., 114*.

Yamamoto-Kawai, M., N. Tanaka, and S. Pivovarov (2005), Freshwater and brine behaviors in the Arctic Ocean deduced from historical data of 18Oand alkalinity (1929–2002 A.D.), *J. Geophys. Res.,* 110, C10003, doi:10.1029/2004JC002793.

Yang, D., B. Ye, and A. Shiklomanov (2004), Discharge Characteristics and Changes over the Ob River Watershed in Siberia, *Journal of Hydrometeorology*, 595-610.

Yang, J. (2006), The Seasonal Variability of the Arctic Ocean Ekman Transport and Its Role in the Mixed Layer Heat and Salt Fluxes, *Journal of Climate*, *19*, 5366-5387.

Yao, X., Y. Zhang, G. Zhu, B. Qin, L. Feng, L. Cai, and G. Gao (2011), Resolving the variability of CDOM fluorescence to differentiate the sources and fate of DOM in Lake Taihu and its tributaries, *Chemosphere*, *82*(2), 145-155.